Ore Types of the Auriferous Lalor VMS Deposit, Snow Lake, Manitoba: Implications for Genesis and Post Depositional Processes

Shamus Duff

Thesis submitted to the
Faculty of Graduate and Postdoctoral Studies
in partial fulfillment of the requirements
for a Master of Science Degree in Earth Sciences

Department of Earth Sciences
Faculty of Science
University of Ottawa

Abstract

The Lalor deposit is a newly discovered Paleoproterozoic volcanogenic massive sulphide (VMS) deposit located at the east end of the Flin Flon-Snow Lake belt within the Snow Lake arc assemblage. Lalor is the largest of 11 VMS deposits in the Snow Lake arc assemblage, with combined resources and reserves of 25.3 Mt and average grades of 2.9 g/t Au, 25 g/t Ag, 5 wt% Zn and 0.79 wt% Cu, including 8.8 Mt at 4.6 g/t Au. Lalor and all other deposits in the Snow Lake arc assemblage have been affected by intense polyphase deformation and amphibolite facies metamorphism. As a result, both the original hydrothermal alteration assemblages and the ore mineral assemblages have been completely recrystallized. However, a variety of different ore types have been preserved, allowing the partial reconstruction of the hydrothermal system, including massive Fe-Zn sulphide lenses, discordant Cu-Au stringer zones, and distinctive precious metal-rich Au-Ag-Pb-Cu zones. The different ore types occur in a series of stratigraphically and structurally "stacked" ore lenses that partly overlap but still largely preserve the original architecture of the deposit.

The ore is distributed in 12 discrete lenses or zones of mineralization that are interpreted to be the result of several distinct and overlapping hydrothermal events. Type 1 Fe-Zn massive sulphide ore is the most common ore type in six ore lenses and consists of massive coarse-grained pyrite and sphalerite with trace galena in dominantly quartz-muscovite±kyanite-biotite schist (K alteration association). Type 2 Cu-Au mineralization consists of semi-massive and stockwork chalcopyrite and pyrrhotite in garnetiferous quartz-biotite±staurolite-amphibole-cordierite gneisses (footwall Mg-Fe alteration association). Despite extensive recrystallization and local remobilization, these two ore types are interpreted to represent the (metamorphosed) low- and high-temperature ore assemblages, respectively, of a typical volcanogenic massive

sulphide deposit. Type 3 Au-Ag-Pb-Cu-rich ore consists of stringer and disseminated sulphides and sulphosalts mainly hosted in chlorite-carbonate-actinolite schist (Mg-Ca and Ca alteration associations). Galena is an important indicator of Au mineralization and occurs in this ore type as fine-grained blebs in a matrix of chlorite, dolomite, calcite, anthophyllite, Ca-plagioclase, and calc-silicates (epidote, grossular, diopside, Ca-amphibole ± scapolite). Where abundant, the galena is associated with chalcopyrite, pyrite, pyrrhotite and minor to trace sphalerite, Ag-Sb-Pb sulphosalts, electrum and native gold. Type 4 low-sulphide ore contains ≤10 vol% disseminated pyrite in quartz-biotite-anthophyllite gneiss, with minor chlorite, staurolite, and coarse almandine garnet, and has variable Au grades. The sulphides and sulphosalts in ore types 3 and 4 are interpreted to be metamorphically remobilized from pre-existing disseminated mineralization.

The hydrothermal system developed during two main episodes of seafloor volcanism. Type 1 massive sulphides in the 10 and 11 lenses and in the 20, 30, 31, and 40 lenses were formed at the paleoseafloor. These lenses are underlain by Type 2 Cu-Au stockwork mineralization (27 Lens) and originally conformable zones of Type 3 Au-Ag-Pb mineralization (21, 24, 25, 26, and 28 lenses). The large Cu-Au stockwork zone (27 Lens) may have been the main feeder of the deposit and is partly continuous with disseminated Au-Ag-Pb-Cu galena-sulphosalts mineralization below the 20 base metal Lens. The Au-Ag-Pb-Cu mineralization is thought to have formed in the subseafloor from late-stage, lower-temperature hydrothermal fluids (ca. <300°C). In this model, significant Au was introduced first by high-temperature (>300°C) fluids responsible for the Type 2 Cu-Au mineralization and then by lower-temperature (possibly boiling) hydrothermal fluids responsible for Type 3 Ag-Au-Pb-Cu mineralization. Although all the ore types are extensively recrystallized and partly remobilized, their distribution strongly

supports primary hydrothermal Au enrichment at Lalor. The lead isotopic compositions of the ore galena show no evidence of post-magmatic disturbance that would be expected if Au had been introduced during deformation and metamorphism (e.g., as in the nearby New Britannia orogenic Au deposit), and the Au-rich assemblages are very similar to those that commonly occur in unmetamorphosed Au-rich volcanogenic massive sulphide deposits.

Acknowledgements

I would like to extend my gratitude to the financial and logistical support given by the Targeted Geoscience Initiative IV (TGI-IV) which made this project possible. Similarly, I would also like to thank to the geologists at HudBay, who not only helped tremendously with logistics but who provided excellent advice for this project. For their scientific guidance and supervision, I would like to thank Dr. Mark Hannington and Dr. Patrick Mercier-Langevin as well as Antoine Caté who was just as critical in making sure this project stayed on course. Lastly, best of luck to my colleagues at uOttawa who were always there to lend a hand to me inside and outside of the classroom.

Table of Contents

List of Figures

List of Tables

List of Appendices

Chapter 1: Introduction

The Lalor volcanogenic massive sulphide (VMS) deposit is located in Snow Lake, Manitoba, 200 km east of the Flin Flon and 777 deposits. The Snow Lake camp has been a prolific producer of base metals and Au since 1949, with more than 10 past-producing VMS deposits (Table 1) as well as the closed New Britannia (formerly Nor Acme) orogenic Au mine. Lalor is the largest VMS deposit to have been put into production in Snow Lake and the only currently operating mine in the area. The combined resources and reserves total 25.3 Mt with grades of 2.9 g/t Au, 25 g/t Ag, 5 wt% Zn and 0.79 wt% Cu (HudBay Minerals Inc., 2014), including 8.8 Mt at 4.6 g/t Au, making it the largest and richest VMS deposit of the Snow Lake camp (Mercier-Langevin et al., 2014). The Au grades are among the highest of any deposit in the Flin Flon-Snow Lake belt, rivalling those of the nearby Chisel North and Photo Lake auriferous VMS deposits (e.g., Galley et al., 2007). This paper describes the main ore lenses of the Lalor deposit and the spatial and paragenetic relationships of the different ore types, with the aim of better constraining the Au enrichment processes and their relative timing. This project was carried out as part of Targeted Geoscience Initiative 4: Contributions to the Understanding of Volcanogenic Massive Sulphide Deposit Genesis and Exploration Methods Development, under the direction of Dr. Patrick Mercier-Langevin of the Geological Survey of Canada, Québec, and Institut national de la recherche scientifique, Québec. A report was published in Duff et al. (2015).

1.1 Regional and Deposit Geology

The ten past-producing VMS mines in the Snow Lake district (Rod, Stall, Anderson, Ghost, Chisel, Chisel North, Photo Lake, Osborne Lake, Reed Lake and Spruce Point) and the currently operating Lalor Mine are located in the so-called Chisel basin of the Snow Lake arc assemblage (SLA), a NW-trending fold interference structure that dominates the local map pattern (Fig. 1). The Lalor deposit is in the lower portion of the Chisel sequence (termed Lower Chisel subsequence), together with the Chisel, Lost and Ghost Zn-Cu deposits and the Photo Lake auriferous VMS deposit (Fig. 2; Bailes and Galley, 1999; Bailes, 2009; Bailes et al., 2013; Caté et al., 2014; Engelbert et al., 2014a,b). The Lower Chisel subsequence consists of bimodal mafic and felsic volcanic rocks, dominated by mafic volcaniclastic rocks and aphyric basalts and the Powderhouse Dacite unit. These rocks are overlain by the Threehouse basalt (Galley et al., 2007), which marks the transition between the lower and upper parts of the Chisel sequence (Bailes and Galley, 1996; Engelbert, et al., 2014a,b). The Chisel and Chisel North deposits are spatially associated with rhyolite domes located close to the contact between the Upper and Lower Chisel subsequences (Galley et al., 1993; Bailes and Galley, 1996; Bailes, 2009). The Anderson sequence, which underlies the Chisel sequence and hosts the Stall, Rod, and Anderson deposits, consists dominantly of aphyric basalts and small felsic centers. In contrast to the deposits of the Chisel sequence, which are dominantly Zn-Cu deposits, the deposits of the Anderson sequence are distinctly Cu-rich (Bailes et al., 2013).

The Snow Lake arc assemblage is affected by at least four episodes of deformation associated with the Trans-Hudson orogeny (Kraus and Williams, 1999). The D_1 and D_2 events produced

tight, isoclinal, south-verging folds, shallowly dipping thrusts and the main foliation (Kraus and Williams, 1999; Bailes et al., 2013). These structures are refolded by north-northeast-trending F_3 folds and an associated S_3 crenulation cleavage (Martin, 1966; Kraus and Williams, 1999). The F_4 folds with east-trending axes locally overprint F_3 folds (Kraus and Williams, 1999). In the Lalor deposit, D_{1-2} and D_3 structures largely control the geometry of the ore lenses (Caté et al., 2014a). Volcanic units in the host succession are generally oriented parallel to the main S_{1-2} foliation and dip to the northeast (Caté et al., 2014a). The hanging-wall rocks are part of a separate volcanic succession in structural contact with the Lalor volcanic succession (Caté et al., 2014b) that dips steeply toward the northeast (Bailes, 2008, 2011).

The ore lenses of the Lalor deposit are located in the uppermost section of a volcanic succession that has been intensely hydrothermally altered (Lalor volcanic succession: Caté et al., 2014b). The hydrothermal alteration was metamorphosed to amphibolite facies during D_{1-2}, with syn- to late-D_2 peak conditions estimated at ca. 5 kbar and temperatures up to 550°C (Zaleski et al., 1991; Menard and Gordon, 1997; Lam et al., 2013, 2014; Tinkham, 2013). The metamorphic mineral assemblages have been correlated with whole-rock lithogeochemistry and define 5 distinct chemical associations (K-rich, K-Fe-Mg, Mg-Fe, Mg-Ca and Ca) described by Caté et al. (2013a, b, 2015).

1.2 Sampling and Analytical Methods

From June through August 2012, eleven exploration drill holes along section 5600N were logged and sampled in detail (Fig. 3). The drill core was logged in the interval starting 50 m above the

first sign of significant mineralization to the end of the hole. Samples were collected wherever strong mineralization was intersected, with the aim of encompassing the entire deposit and obtaining representative samples of all the different ore types. An additional ten exploration holes were logged along section 5300N. All logging and sampling was completed between May and August 2013. During this time, the mine opened and was in a pre-production phase, allowing the opportunity to map and sample underground in five areas between 795 and 865 m below surface. Results of the underground mapping and sampling are presented in Caté et al. (2014a, 2015).

Seventy drill-core samples were selected for detailed petrographic study and chemical analysis, including major metals, oxides and trace elements. Splits of each sample were crushed using a steel jaw crusher (in order of increasing Au content to minimize cross-contamination), then pulverized in a Cr-steel mill, both at the University of Ottawa. Pulverized samples were analyzed at Activation Laboratories in Ancaster, Ontario. SiO_2, Al_2O_3, Fe_2O_3, MnO, MgO, CaO, Na_2O, K_2O, TiO_2, P_2O_5, Sc, Be, V, Sr, and Ba were analyzed by peroxide fusion followed by dissolution and inductively couple plasma optical emission spectrometry (FUS-ICPOES). Silver, As, Bi, Ce, Co, Cr, Cu, Dy, Er, Eu, Ga, Gd, Ge, Hf, Ho, In, La, Lu, Mo, Nb, Nd, Ni, Pb, Pr, Rb, Sb, Sm, Sn, Tb, Tm, Ta, Tl, Th, U, W, Y, Yb, and Zr were analyzed by fusion followed by ICP mass spectrometry (FUS-ICPMS). Silver, Cd, Co, Cr, Cu, In, Li, Mn, Mo, Ni, Pb, and Zn were analyzed by 4-acid total dissolution followed by ICP mass spectrometry (TD-ICPMS). Tellurium, Se, As, Bi, and Sb were analyzed by hydride generation and ICPMS, and Hg was analyzed on a flow injection mercury system (Hg-FIMS). Gold and Ag were analyzed by fire assay with a graphite-furnace atomic absorption finish. Fluorine was analyzed by specific ion

electrode, and B was analyzed by prompt gamma neutron activation analysis (PGNAA). Total C, S and CO_2 were analyzed by combustion and infrared detection (IR). Loss on ignition was also determined by combustion. FeO was determined by titration.

Petrographic descriptions of the main ore types were supplemented by microanalysis of representative ore minerals and gangue by wavelength dispersive X-ray analysis (WDX) using a four-spectrometer Camebax MBX electron microprobe at the Earth Sciences Department of Carleton University, Ottawa. Microprobe analyses and mineral identifications were carried out by Dr. Ingrid Kjarsgaard as part of the TGI4 project on Lalor. Polished thin sections for analysis were provided to Dr. Kjarsgaard from the sampled drill holes following complete petrographic documentation. Sulphur isotope analyses were made on selected mineral separates of pyrite, chalcopyrite, pyrrhotite, sphalerite, and galena at the University of Ottawa's G.G. Hatch Stable Isotope Laboratory. Lead isotope ratios on galena were determined at Carleton University's Isotope Geochemistry and Geochronology Center (IGGC).

Ore mineral separates (pyrite, chalcopyrite, sphalerite and pyrrhotite) were analyzed for sulphur isotopic composition at the G.G. Hatch Laboratory at the University of Ottawa. Mineral separation was done by hand and samples were ground into a fine powder using an agate mortar and pestle. For analysis, samples were weighed into tin capsules with at least twice the sample weight of tungstic oxide. Calibrated internal standards are prepared with every batch of samples for normalization of the data. Samples were then loaded into a Vario el (Elementar, Germany) elemental analyser to be flash combusted at 1800°C. Released gases are carried by helium through the elemental analyzer to be cleaned, then separated by double "trap & purge". SO_2 gas

is then carried into the Delta XP isotope ratio mass spectrometer (Thermo Finnigan, Germany) for analysis. Analytical precision is ± 0.2‰. Values were reported relative to the Canon Diablo meteorite standard (Rees, 1978).

Lead isotope ratios on galena separates were analyzed at the Isotope Geochemistry and Geochronology Research Facility at Carleton University, Ottawa, on a Thermal Ionization Mass Spectrometry (TIMS; Finnigan Triton, Thermo Electron Corp). Single grains of galena were hand-picked under a binocular microscope. Galena separates were crushed and pulverized in an agate mortar, decomposed in a solution of nitric and hydrochloric acid and taken to incipient dryness. The products were loaded on a rhenium filament, and heated to 1300° to 1340°C in order to ionize the sample. Measured lead ratios include: $^{208}Pb/^{206}Pb$, $^{207}Pb/^{206}Pb$, $^{208}Pb/^{204}Pb$ $^{207}Pb/^{204}Pb$, and $^{206}Pb/^{204}Pb$. Instrument mass fractionation was corrected using NIST SRM 981. Analytical uncertainties for repeat analyses of standards in the lab are better than 0.01% (2σ). Errors of the ^{204}Pb isotopic ratios for galena including analytical errors and fractionation corrections are ± 0.13%.

Table 1: Grades and tonnage of historical VMS deposits of Snow Lake (after Bailes et al., 2013)

Mine	Tonnes	Au (g/t)	Ag (g/t)	Cu (wt.%)	Zn (wt%)
Chisel Sequence:					
Lalor Zn-Cu	18100000	0.64	25.24	0.64	8.97
Lalor Cu-Au	5400000	4.7	30.6	0.47	0.46
Chisel	7153532	1.76	44.76	0.54	10.6
Chisel North	2606212	0.58	21.43	0.21	9.49
Ghost and Lost	581438	1.2	39.09	1.34	8.6
Photo Lake	689885	4.9	29.38	4.58	6.35
Anderson Sequence:					
Stall	6381129	1.41	12.34	4.41	0.5
Rod	735219	1.71	16.11	6.63	2.9
Anderson	2510000	0.62	7.54	3.4	0.1
Other:					
Schist Lake	1846656	1.3	37.03	4.3	7.27
Osborne	2807471	0.27	4.11	3.14	1.5
Spruce Point	1865095	1.68	19.54	2.06	2.4
Reed Lake	2720000	0.62	7.63	4.5	0.89

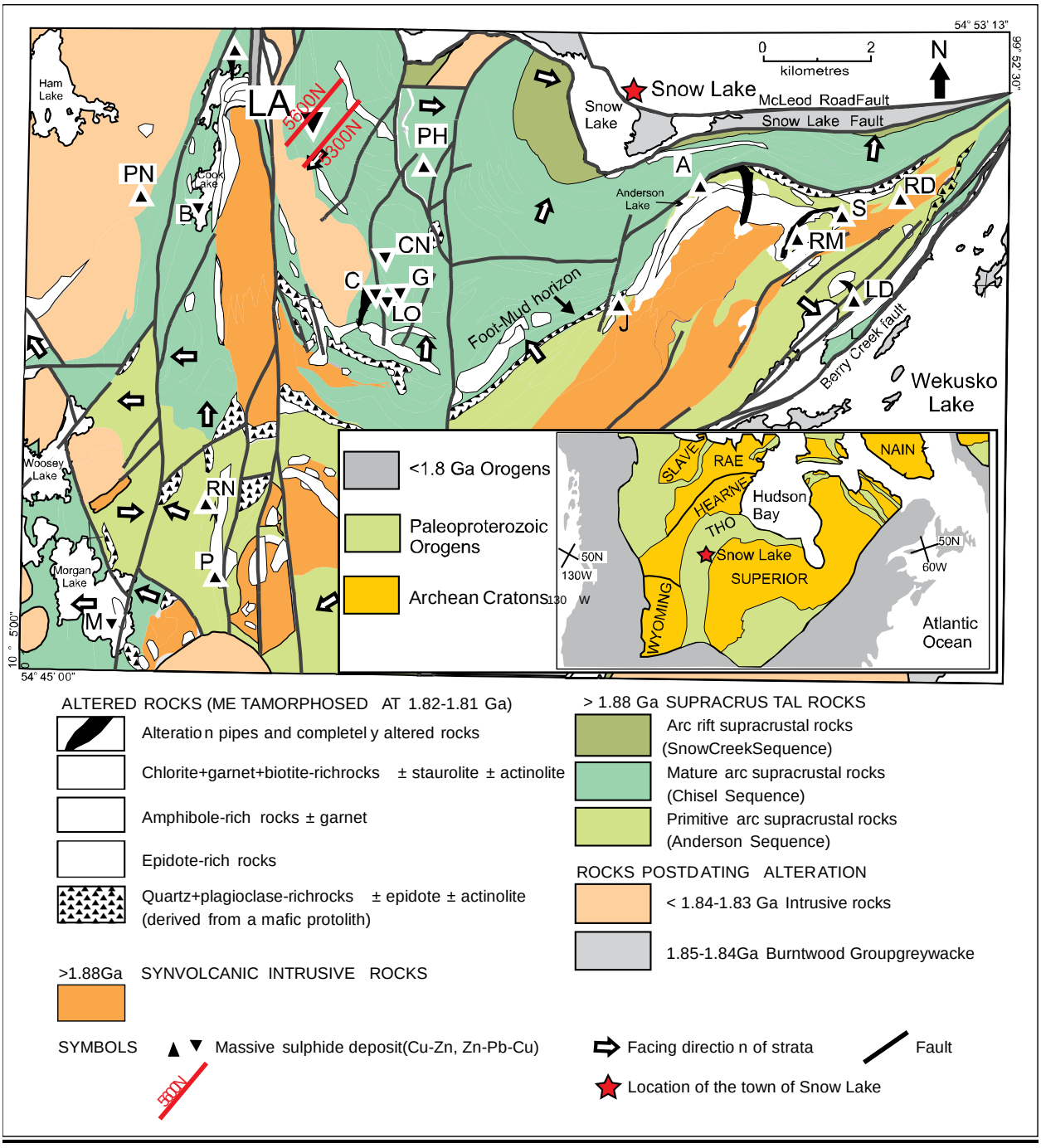

Figure 1: Regional Map of Snow Lake district with inset showing location of Snow Lake in Canada and red solid line showing study sections 5300N and 5600N. (Massive sulphide deposits are denoted by a two letter code. They are as follows: LA – Lalor, PH – Photo Lake, C – Chisel, CN – Chisel North, G - Ghost, LD – Linda, LO – Lost, M – Morgan Lake, P – Pot, Pn – Pen, RD – Rod, RM – Ram, RN – Raindrop, S – Stall.

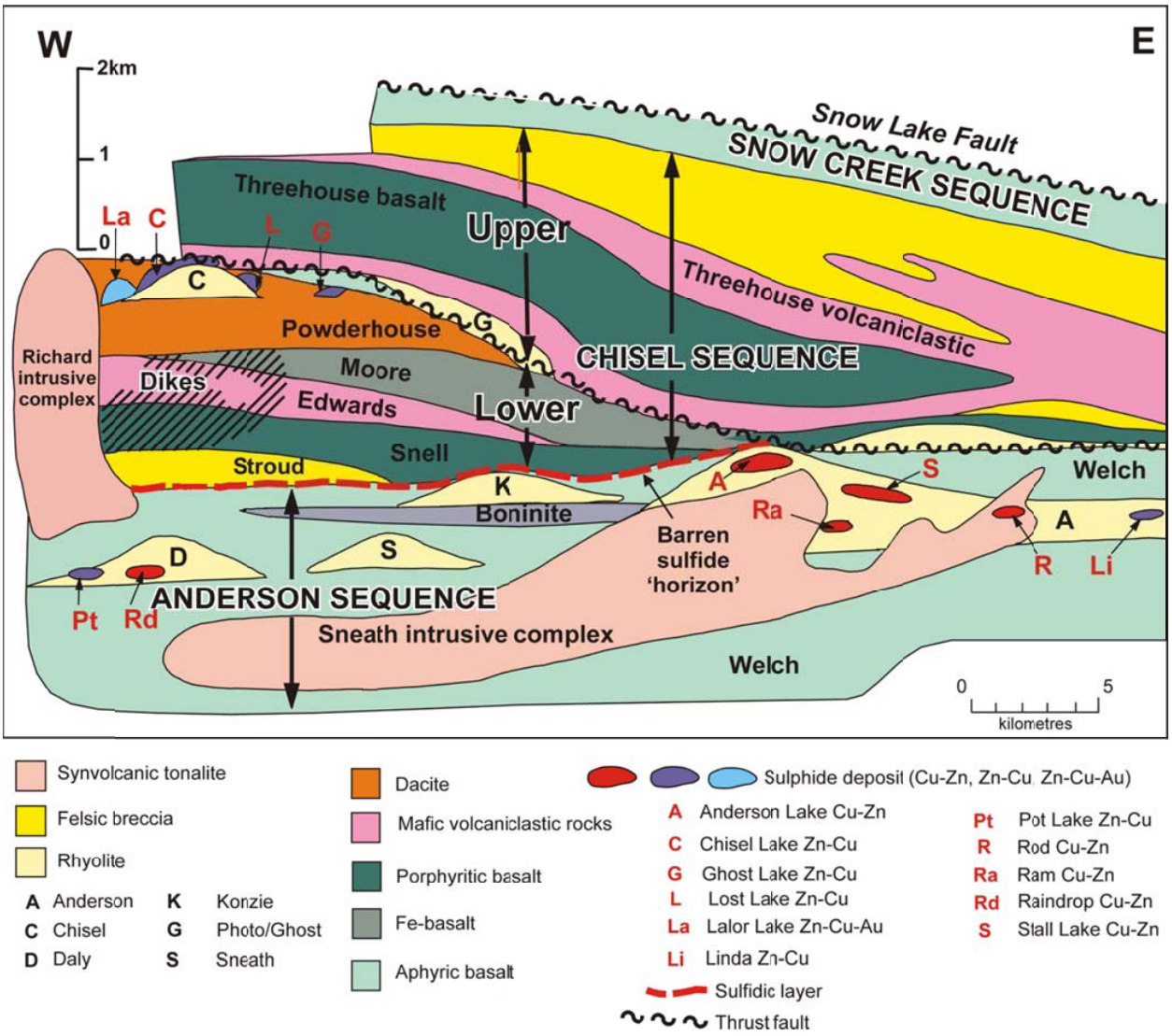

Figure 2: Schematic cross section of the Snow Lake Arc (from Bailes and Galley 1998), showing the positions of the Lalor, Chisel, Lost and Ghost Zn-Cu deposits and the Photo Lake Au-rich VMS deposit in the upper portion of the Chisel Sequence.

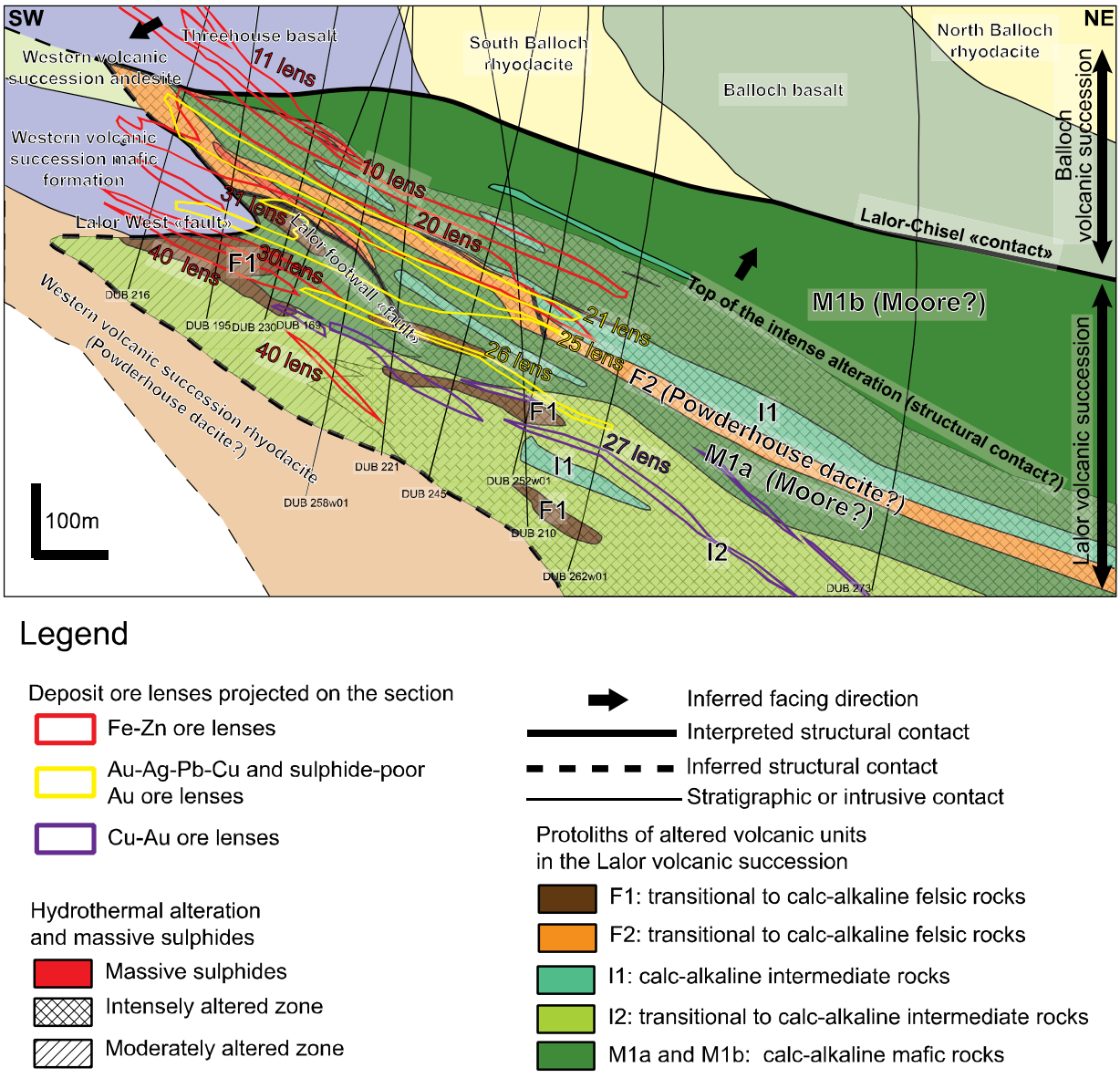

Figure 3: Cross section of the Lalor deposit at 5600N (looking northwest) from Caté et al. (2014). The distribution of the main Fe-Zn massive sulphide, Au-Ag-Pb-rich ore zones, and Au-Cu zones discussed in the text are also shown. 10 Lens is projected from section 5500N. Inferred lithologies are from Caté et al. (2014) and A.H. Bailes (Hudbay Minerals Inc. internal report, 2008).

Chapter 2: Distribution of the Ore Lenses

Unlike other deposits in the Snow Lake camp, the ore at Lalor is distributed among several different lenses. The currently defined resource has been divided into twelve ore lenses. Assay data for the main lenses considered in this study are shown in Table 2. Some of the ore lenses (main massive sulphide lenses, 10, 11, 20, 30, 31, and 40) are conformable with the host stratigraphy (dipping ~30°) and are structurally stacked. The longest dimensions of most of these lenses strike NW-SE; however, the 20 Lens, in the middle of the succession, strikes N-S, possibly indicating an intersecting fault control. Although the six main massive sulphide lenses are stacked, Bailes (2011) and Caté et al. (2014, 2015) suggest that there are fewer primary ore horizons, and numerous thrust faults and/or folds are likely responsible for the dismemberment and "stacking" of multiple sulphide zones. They recognized only two paleoseafloor horizons, one containing the 10 and 11 lenses and the other hosting the 20, 30, 31, and 40 lenses (Bailes et al., 2013; Caté et al., 2014). The lithogeochemically distinct rock types that host the massive sulphide lenses confirm that they formed during separate volcanic episodes (Caté et al., 2014, 2015). Discordant stockwork mineralization is spatially associated with the upper lenses (10 and 11) but has not been recognized in association with the lower lenses. Substantial Au enrichment is most closely associated with discordant Cu-Au stockwork mineralization in the 27 Lens and with broadly conformable disseminated Au-Ag-Pb-Cu mineralization in the 21, 24, 25, 26, and 28 lenses. The largest zone of Au-Ag-Pb-Cu mineralization is in the footwall of the 20 massive sulphide lens and is underlain by the discordant Cu-Au stockwork mineralization of the 27 Lens. Brief descriptions of the main massive sulphide ore lenses and their different host rocks are given below.

2.1 10 and 11 Lenses

The 11 and 10 lenses are structurally and stratigraphically the highest ore zones in the Lalor volcanic sequence. Both the 10 and 11 lenses consists of massive and semi-massive pyrite and sphalerite within quartz-muscovite-pyrite schist (K alteration association). Chloritic zones with stringer chalcopyrite mineralization occur only at the base of the 10 Lens. In most places, the contact between the hanging-wall rocks and the massive sulphides is sharp; locally there is a narrow transition from semi-massive pyrite-sphalerite into quartz-muscovite-pyrite schist. Wall rocks immediately above the 10 and 11 lenses are strongly pyritized, with abundant muscovite and kyanite. Locally (and generally only in the massive sulphide ore), kyanite comprises up to 25 vol.% of the rock as porphyroblasts up to 2 cm in size.

The contact between the massive sulphides and the underlying chloritic schist is generally gradational, with increasing chlorite and chalcopyrite content and decreasing pyrite and sphalerite in the footwall. Massive chlorite is common in the ore zones. Volcanic rocks in the footwall contain abundant quartz, biotite and chlorite, with coarse Mg-Fe amphibole (anthophyllite), kyanite, staurolite and garnet porphyroblasts (K-Mg-Fe and Mg-Fe alteration association). Garnet is most commonly almandine garnet, which varies from centimeter-sized up to massive 10-cm porphyroblasts. Although Cu-rich stockwork mineralization is well developed beneath the 10 Lens, the 11 Lens lacks a stringer zone and is thought to be a structurally dislocated portion of the 10 Lens.

2.2 20 Lens

The 20 Lens also consists of massive and semi-massive pyrite and sphalerite, but the hydrothermal alteration zoning in the immediate host rocks is more complex, owing to the presence of several different parent lithologies. In section 5300N, the hanging wall is a quartz-biotite-muscovite-kyanite assemblage (K alteration association), similar to the hanging wall of the 10 and 11 lenses and weakly altered intermediate rocks. Further north (section 5600N), the hanging wall is chlorite schist with abundant carbonate that is locally associated with Ca-rich (skarn-like) diopside, epidote, grossular and actinolite-tremolite alteration. Bright orange Ca-rich grossular is locally present in this alteration style. The footwall is dominantly chlorite-carbonate schist, but kyanite, muscovite, garnet, staurolite, anthophyllite and/or talc are present, representing complex transitions between the K, K-Mg-Fe, Mg-Fe, Mg-Ca and Ca associations.

2.3 30, 31 and 40 Lenses

The 31, 30 and 40 Lenses contain both massive and semi-massive sulphides, with carbonate, actinolite, and chlorite gangue minerals. The hanging wall and footwall of the 30 and 31 Lenses consist of alternating chlorite-carbonate and chlorite-actinolite/tremolite assemblages (Ca-Mg alteration association: Caté et al., 2015). Coarse magnetite crystals are also present in the hanging wall. The 40 Lens is the deepest zone of massive sulphides in the mine but is thought to have formed at the same stratigraphic horizon as the 30 and 31 lenses, owing to the presence of similar host rocks and alteration styles. Quartz, plagioclase and biotite with abundant garnet and minor anthophyllite are dominant about 15 m below the ore zone and are considered to represent

the metamorphic equivalent of moderately altered mafic, intermediate and felsic volcanic rocks in the footwall of the lenses (Caté et al., 2014).

2.4 Metal Zonation

The 10 Lens shows the expected VMS zonation with Fe-Zn in the upper portion of the lens and a discordant, although strongly transposed, Cu-Au stringer zone at the base (Figure 4). The 20 Lens lacks a Cu-Au stringer zone but is underlain (and possibly partly overprinted) by disseminated Au-Ag-Pb-Cu-rich mineralization. A large portion of the Au-rich 21 Lens cuts the western part of the 20 Lens (on section 5600N) and extends into the hanging wall. The 31 Lens is similarly cut by the Au-rich 25 Lens. For the most part, however, the Au-Ag-Pb-Cu-rich ore zones are broadly conformable. This conformable nature may indicate that heterogeneous permeability of the volcanic pile was a major control on mineralization. The large zone of semi-massive and stockwork-like chalcopyrite mineralization in the 27 Lens is stratigraphically the lowest occurrence of ore in the mine and may have been a central feeder zone for the entire deposit, in agreement with the high-temperature alteration in this part of the sequence (Caté et al., 2014; Mercier-Langevin et al., 2014). Although metamorphic remobilization of metals is apparent in all ore types, the scale of the remobilization is generally on the scale of a few meters and is restricted to the ore lenses, with the large-scale metal zonation remaining intact (see also Gagné et al., 2007).

Table 2: Average ore grades of different lenses discussed in the text (from Hudbay Minerals Inc.).

Lens	Ore Type	Au (g/t)	Ag (g/t)	Cu (wt. %)	Zn (wt. %)	Pb (wt. %)	Fe (wt. %)
Fe-Zn							
10	Type 1	2.12	23.58	0.79	11.48	0.25	25.28
11	Type 1	0.21	17.1	0.26	12.13	0.06	27.88
20	Type 1	2.49	31.16	0.91	8.37	0.32	19.59
31	Type 1	2.67	30.33	0.24	5.86	0.45	18.55
30	Type 1	1.67	28.25	0.3	5.36	0.56	17.06
40	Type 1	2.11	36.2	0.49	7.99	0.92	15.42
Au-Cu							
27	Type 2	8.38	22.63	4.45	0.29	0.02	8.63
Au-Ag-Pb							
21	Type 3	6.98	41.02	0.91	2.07	0.27	7.7
24	Type 3	7.13	32.13	0.3	1.42	0.4	4.74
25	Type 3	6.33	31.16	0.31	0.83	0.28	4.33
26	Type 3	6.31	38.07	0.67	0.48	0.38	6.42
28	Type 3	4.66	21.17	0.49	0.57	0.06	4.88

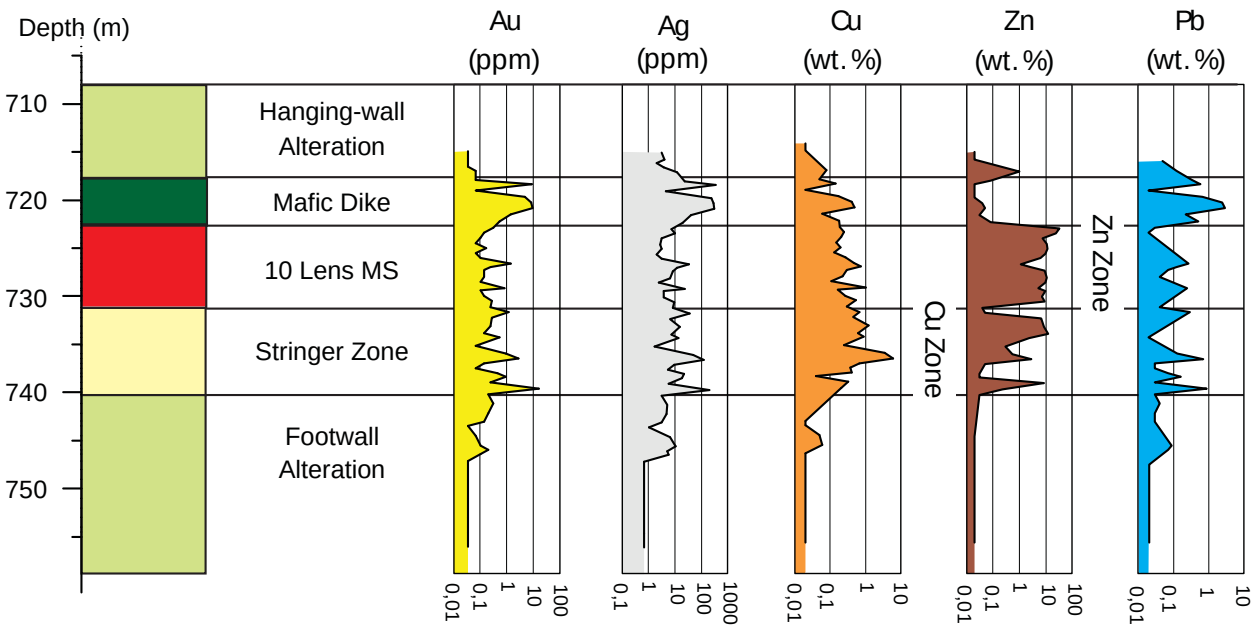

Figure 4: Down-hole log showing metal zonation in the 10 Lens massive sulfide zone, showing the expected VMS zonation with Fe-Zn in the upper portion of the lens and then Au-Cu stringer mineralization at the base. Note the anomalous Au-Ag enrichment within the mafic dyke.

Chapter 3: Ore Types of the Lalor Deposit

Four main ore types have been identified among the different ore lenses (Table 3). Some can be compared to mineralization typical of unmetamorphosed VMS deposits, but others may be hybrid ore types related to hydrothermal overprinting (i.e. two or more hydrothermal events affecting the same rocks) and the effects of metamorphic recrystallization and remobilization.

3.1 Type 1 Fe-Zn Massive Sulphide

Fe-Zn-rich massive sulphide (Fig. 5a, b) is volumetrically the most abundant ore type and dominates in six of the twelve delineated ore lenses. The 10 and 11 Fe-Zn lenses are contained mostly within quartz-muscovite-pyrite rocks of the K alteration association, and the 20, 30, 31 and 40 Fe-Zn lenses are mostly hosted by chlorite-carbonate-actinolite/tremolite schists of the Mg-Ca alteration association (Caté et al., 2015). Disseminated pyrite is abundant in the quartz-muscovite-altered rocks (Figure 5c). Although mostly intact bodies, slivers of the ore lenses, up to several meters across, occur in the adjacent wall rocks, displaced from the lenses by folding and transposition. Similarly, large enclaves of altered and foliated wallrocks are locally enclosed within massive sulphides (e.g., Bailes, 2011; Caté et al., 2014a). The sulphide mineralogy is generally the same in all of the lenses and is dominated by pyrite and sphalerite (10 to 70 vol.%); pyrrhotite and chalcopyrite are minor minerals (less than 10 vol.%). Galena is rare but present in fractures and tension gashes within fold hinges and especially where several mafic intrusions cut the upper massive sulphide lenses (10 and 11). The mafic dykes are folded, boudinaged, and S_2-foliated, suggesting that they were intruded before the main D_2 deformation, and remobilized

sulphides are common at their margins and in crosscutting fractures. A number of features clearly indicate the extent of recrystallization and annealing of the massive sulphides, including the presence of coarse-grained polycrystalline aggregates with well-developed triple junctions, large pyrite porphyroblasts (up to 5 cm), and *durchbewegung* texture (see below).

3.2 Type 2 Cu-Au-Rich Semi-Massive and Stockwork Mineralization

The Cu- and Au-rich semi-massive and stockwork mineralization is hosted in garnetiferous chlorite schist of the Mg-Fe alteration association immediately beneath the 10 Lens, and at depth in intensely altered quartz- and biotite-bearing rocks. Semi-massive (10-60 vol.%) chalcopyrite occurs in the immediate stratigraphic footwall of the 10 Lens, and disseminated and stringer mineralization (<10 vol.% chalcopyrite) grades outward into the surrounding wall rock. Masses of pyrrhotite are present locally within the chalcopyrite (Fig. 5d). In contrast, the strongly transposed, stockwork-like Cu-Au mineralization in the 27 Lens, much deeper in the footwall is not physically connected to massive sulphide ore higher up in the Lalor volcanic succession. The semi-massive chalcopyrite-pyrrhotite ore typically contains abundant quartz and biotite, and large (0.5-5 cm in size) garnet porphyroblasts are commonly surrounded by networks of remobilized chalcopyrite (Fig. 5e, f). Quartz flooding and veins of quartz with ankerite are also common. The adjacent wall rocks, which consist of the deep footwall, transposed high-temperature Mg-Fe alteration association (Mercier-Langevin et al., 2014; Caté et al., 2015) commonly contain quartz, cordierite and anthophyllite with minor chlorite, and locally porphyroblasts of staurolite and garnet. The anthophyllite forms arborescent growths (i.e. fern like) up to 5 cm in length, and the cordierite occurs as royal blue massive aggregates.

3.3 Type 3 Au-Ag-Pb-Cu-rich ore:

The main precious metal-rich ore consists mostly of disseminated sulphides and sulphosalts comprising up to 5 vol% galena (Fig. 5g) and 2 vol% chalcopyrite. The nature of the host rock varies but garnet- and amphibole-bearing rocks of the Mg-Fe chemical alteration association and chlorite-actinolite and Fe-dolomite schist of the Mg-Ca and Ca association (e.g., footwall of the 20 Lens), are the most common host. Pyrite, sphalerite, chalcopyrite and pyrrhotite are minor components that commonly occur as isolated grains in the cleavages of chlorite and in low-pressure zones between porphyroblasts of garnet. This style of mineralization is typically isolated from the main massive sulphide lenses and is best developed in the 21, 24, 25 West, 26 and 28 lenses. In general, galena is a strong indicators of Au grade in all of these lenses. The chlorite-carbonate-actinolite rocks locally include skarn-like assemblages with a variety of calc-silicates (epidote, grossular, diopside ± scapolite), corresponding to the Mg-Ca and Ca alteration associations of Caté et al. (2015).

3.4 Type 4 Low Sulphide Quartz-Pyrite Mineralization

Low-sulphide quartz-pyrite ore consists of quartz-biotite-anthophyllite rock with a distinctive gneissic or schistose texture. This ore type has locally high Au grades. Sulphide contents mostly rarely exceed 10 vol.% and correlate weakly with Au grade. Pyrite is dominant, but chalcopyrite, sphalerite and pyrrhotite are present locally in low-pressure zones between cleavages of the major phyllosilicate minerals and adjacent to porphyroblasts (Fig. 5h). Staurolite and anthophyllite are also present locally. Type 4 mineralization is spatially associated with Au-Ag-

Pb-Cu-rich galena-sulphosalts±chalcopyrite ore in several lenses (e.g., in the 21, 24 and 25 lenses) and occurs in the same broad zones of mineralization and locally grades into Au-Ag-Pb-Cu-rich ore over distances of a few meters.

Table 3: Principal ore types of the Lalor VMS deposit, Snow Lake.

Ore Type		Dominant Sulphides	Host Rock and Gangue Minerals
Type 1 (Fe-Zn)	Massive Sulphides	Coarse-grained pyrite, sphalerite, ±pyrrhotite, ±chalcopyrite, ±galena	Quartz-muscovite schist
Type 2 (Au-Cu)	Semi-massive and Stockwork	Semi-massive and stringer chalcopyrite, ±pyrrhotite	Garnetiferous quartz-biotite schist and gneiss; large garnet porphyroblasts, ±cordierite, ±anthophyllite, ±staurolite
Type 3 (Au-Ag-Pb)	Chlorite-Carbonate	Stringer and disseminated galena,±sulphosalts, ±pyrite, ±sphalerite, ±chalcopyrite, ±pyrrhotite	Chlorite-carbonate schist; mainly dolomite and calc-silicates (epidote, grossular, diopside)
Type 4 (Au)	Low-Sulphide	Disseminated and stringer pyrite, ±chalcopyrite, ±pyrrhotite, ±sphalerite	Quartz-biotite-chlorite schist; ±almandine garnet, ±anthophyllite, ±staurolite

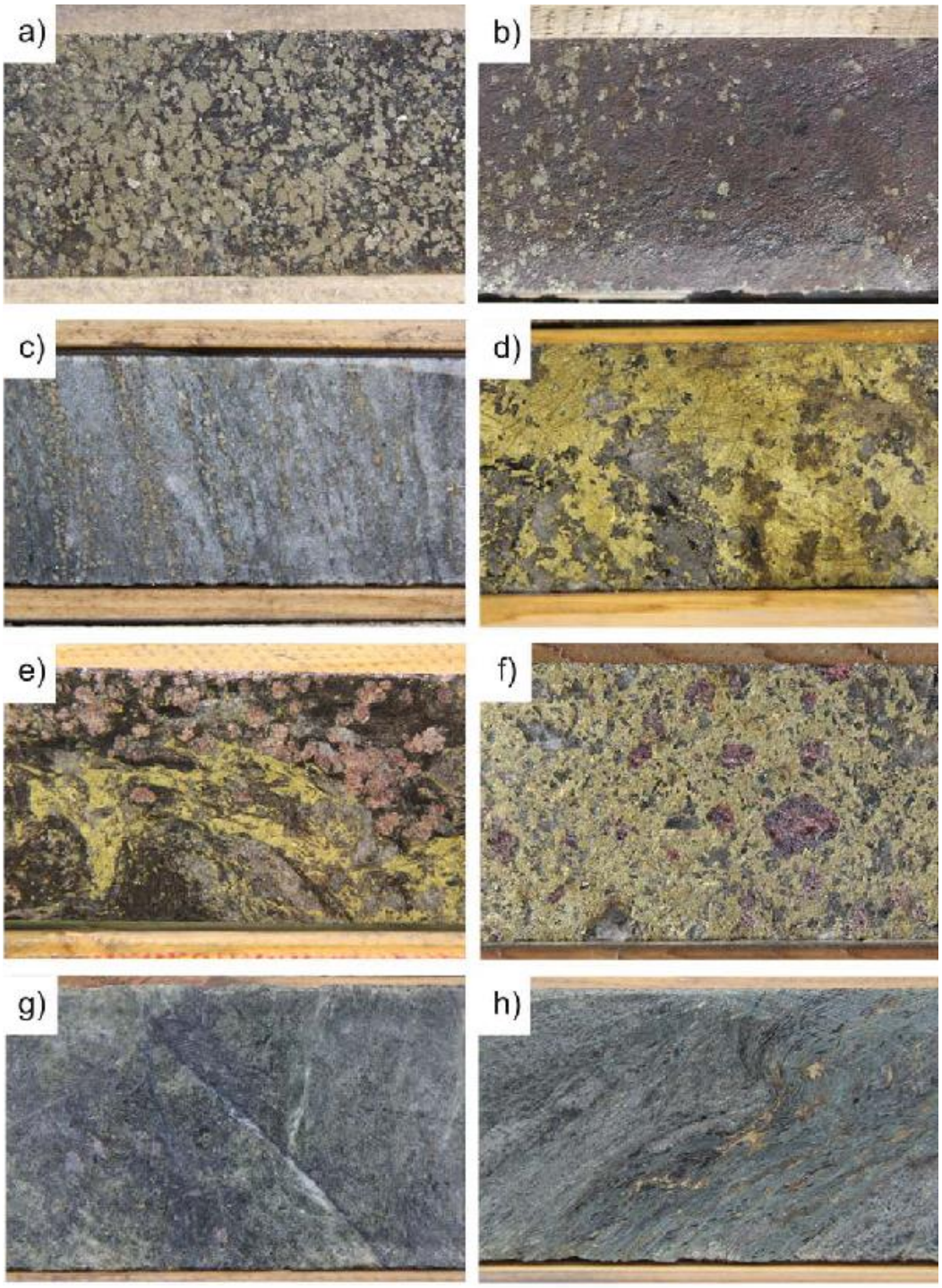
a)
b)
c)
d)
e)
f)
g)
h)

Figure 5: Photographs of representative ore types in NQ drill core (47.6 mm or 1-7/8 in diameter) from the Lalor deposit. a) Type 1 Fe-Zn-rich massive sulfide from 10 Lens (DUB174, 834.3-838.6 m), containing mostly euhedral pyrite with atoll structures in a matrix of Fe-rich sphalerite. b) Type 1 massive sphalerite ore from 10 Lens (DUB205, 788.0-805.0 m). c) Disseminated pyrite in the foliations of quartz-biotite schist from the hanging wall of the 31 Lens (DUB174, 872.0 m). d) Type 2 semi-massive chalcopyrite with pyrrhotite from the type locality in the 40 Lens (DUB263W05, 1270 m). e) Type 2 stockwork chalcopyrite mineralization with garnet porphyroblasts in a quartz-biotite matrix from the 40 Lens (DUB263W05). f) Type 2 massive chalcopyrite with large garnet porphyroblasts from the 40 Lens (DUB262W05, 1271.3 m). g) Type 3 Au-Ag-Pb mineralization in chlorite-carbonate schist, typical of the 21, 24, and 25 lenses (DUB210, 1038.8 m). The fine-grained, steel grey matrix is galena. H) Type 4 low sulfide ore with disseminated sulfides in quart-chlorite-biotite schist from the 25 Lens (DUB245; 995.8-1005.9 m).

Chapter 4: Ore Mineralogy and Mineral Chemistry

4.1 Pyrite

In the massive sulphide lenses, pyrite occurs as coarse-grained polycrystalline aggregates, in 2-5 cm patches with intergranular sphalerite. Elsewhere, pyrite occurs as isolated porphyroblasts in a homogenous sphalerite matrix. In many places, pyrite porphyroblasts show evidence of brittle deformation with fractures filled by sphalerite and other sulphides (Figure 6a, b). In other places, pyrite and sphalerite are clearly segregated into discontinuous gneissic bands. Classic *durchbewegung* texture is common, in which hard (6.0 - 6.5), brittle pyrite, and locally quartz nodules show evidence of rotation in a flowing matrix of softer (ductile) sphalerite (Fig. 7; Craig and Simpson, 1991). Most analyzed pyrite is nearly stoichiometric FeS_2. However, some pyrite contains up to 2 wt% Co, especially where intergrown with pyrrhotite. Some pyrite also contains up to 0.1 wt% Ni and up to 1 wt% As (Table 4).

4.2 Sphalerite:

Sphalerite in the massive sulphide lenses is coarsely crystalline 'blackjack', with high Fe contents (Table 4). Where it is most abundant, sphalerite is commonly associated with Fe-rich carbonate. Coarse grained polycrstalline aggregates with curved or straight grain boundaries are most common, but locally the sphalerite occurs in homogenous masses, typically with chalcopyrite inclusions distributed in a gridded network (e.g., chalcopyrite disease: Barton and Bethke, 1987) (Fig. 6a) or more commonly remobilized to grain boundaries (Fig. 6c). The average Fe content of sphalerite is 7.65 wt% (more than 15 mol.% FeS: Table 4) and is very homogeneous throughout most of the deposit. Cd contents are generally below 5 wt.% (average

2.3 wt.%). Hg is close to the detection limit but never exceeds 0.10 wt.%. In the 40 Lens, the sphalerite is orange in colour, which contrasts with the 'blackjack' sphalerite in the rest of the deposit, possibly resulting from metamorphic reactions, and indicating much lower Fe contents.

4.3 Chalcopyrite, Bornite, Cubanite

Disseminated chalcopyrite is present as isolated blebs and anhedral masses in the massive sulphide ores, and these generally increase in abundance toward the bottom of the lenses. In the Cu-Au stockwork zones, chalcopyrite occurs as discrete stringers within the main foliation of the altered host rocks, rimming large garnet porphyroblasts (Fig. 6d), and disseminated in the cleavages of the major gangue minerals. The chalcopyrite is nearly stoichiometric $CuFeS_2$ throughout the deposit (Table 4), although several grains of Ag-bearing chalcopyrite (up to 4 wt% Ag) were identified in association with Ag-sulphosalts. Traces of cubanite are present as exsolution lamellae in the chalcopyrite, typically as thin peach-coloured flames and locally as distinct crystallographically controlled bands intersecting at 60 and 120°. Bornite also occurs locally as inclusions in chalcopyrite and rarely with galena, electrum and sulphosalts in Type 3 Au-Ag-Pb-Cu-rich ore.

4.4 Pyrrhotite

Pyrrhotite is present in the massive sulphide ores, commonly as rims around pyrite or in pressure shadows. It is almost always closely associated with chalcopyrite, especially in the Type 2 semi-massive and stockwork chalcopyrite ore. Locally pyrrhotite is also present in late quartz veins,

commonly with gahnite. Fe and S are the only constituents of the pyrrhotite; no trace elements were detected in microprobe analyses (Table 4). One euhedral grain of Ag-pentlandite $(Ag,Fe,Ni)_9S_8$ was identified intergrown with pyrrhotite and cubanite.

4.5 Galena

Galena is most abundant in Type 3 Au-Ag-Pb-Cu-rich ore. It is a minor (< 5 vol.%) component of the massive sulphide ores where it occurs as coarse-grained aggregates in the 10 and 11 lenses and as finer-grained disseminations in the lower lenses (30, 31, 40). It occurs most commonly as anhedral to subhedral masses at grain boundaries of pyrite and sphalerite (Fig. 6f). However, (remobilized) galena also occurs as coarse cubes up to 1 cm in size in some late quartz veins. In the Au-Ag-Pb-Cu ore, fine-grained galena occurs within the mineral cleavages of the host chlorite-carbonate-actinolite schist, where it is commonly associated with microscopic grains of electrum and sulphosalts. Galena is rare in the low-sulphide Au-rich zones (Type 4), but where present shows the same general paragenesis with electrum and sulphosalts. Galena contains up to 4 wt% Se but is generally Ag-poor (<0.2 wt.%) and Te-poor (<0.1 wt%) (Table 4).

4.6 Pb-Sb-Sulphosalts

Numerous complex sulphosalts have been identified in the Type 3 Au-Ag-Pb-rich ore, together with galena, chalcopyrite and electrum. These include tetrahedrite $[(Cu,Fe)_{12}Sb_4S_{13}]$, bournonite $[PbCuSbS_3]$, boulangerite $[Pb_5Sb_4S_{11}]$, and meneghinite $[Pb_{13}CuSb_7S_{24}]$. These minerals typically occur as fine-grained, complex intergrowths with galena and, less commonly, with

chalcopyrite, freibergite (see below) and gold (Figure 6c). Only bournonite contains minor As (up to 4 wt%) , Se (up to 0.4 wt%), and Sn (up to 0.2 wt%) (Table 4).

4.7 Ag-sulphosalts

The major Ag minerals, other than electrum, are Ag-bearing tetrahedrite, freibergite [$(Ag,Cu,Fe)_{12}(Sb,As)_4S_{13}$], allargentum [$Ag_{1-x}Sb_x$], and sterryite [$Ag_2Pb_{10}(Sb,As)_{12}S_{29}$]. They occur mainly as Ag-rich inclusions in galena and less commonly as intergrowths with chalcopyrite. Silver-bearing tetrahedrite (Table 4) contains 1-7 wt% Ag, freibergite contains up to 37 wt% Ag, and some grains are notably tarnished. Lam et al. (2014) also identified aurostibite ($AuSb_2$), but this mineral was not found in the present study.

4.8 Ag-tellurides

Two Ag-bearing tellurides were identified by microprobe (Table 4). They are a Te-rich Ag-sulphide, possibly benleonardite [$Ag_8(Sb,As)Te_2S_3$], intergrown with electrum, and a hessite-like mineral, possibly stutzite [$Ag_{5-x}Te_3$], intergrown with chalcopyrite and sphalerite. Lam et al. (2014) also identified hessite [Ag_2Te] and altaite [PbTe], but these minerals were not encountered.

4.9 Gold and electrum

The main Au-bearing mineral in Type 2 Au-Cu mineralization and Type 3 Au-Ag-Pb-rich ore is electrum. Electrum commonly occurs at the grain boundaries and in microfractures of larger grains of galena, commonly together with various Sb- and Ag-bearing sulphosalts, as inclusions in pyrite or chalcopyrite, and rimming quartz inclusions in the sulphides. The grain sizes of the electrum range up to 0.1 mm, but much smaller grains are common. Both gold (<30 wt% Ag) and electrum (40-80 wt% Ag) compositions were found, but the Au:Ag ratio is variable and averages ~2:1 (Table 4). Significant Hg (average 3.41 wt%) and traces of Sb (0.38 wt%) are also present. Electrum is Hg-rich, although gold contains only 2.5 wt% Hg (average of 7 analyses) and electrum commonly contains 6-7 wt% Hg. Gold was not detected by microprobe in any of the other ore minerals (with the exception of allargentum which contained up to 7.4% Au).

4.10 Other trace minerals

Arsenopyrite [FeAsS], cobaltite [CoAsS], and gudmundite [FeSbS] were found in a number of different ore types. Fine-grained, euhedral arsenopyrite is locally associated with tetrahedrite, galena and electrum in the massive sulphide ores (Fig. 6c). Arsenopyrite contains up to 0.3 wt% Se but is otherwise free of trace elements (Table 4). Cobaltite and gudmundite occur together with pyrrhotite and chalcopyrite, and both contain up to 0.5 wt% Ni. Trace Bi occurs in some pyrite, pyrrhotite, and chalcopyrite grains (average 0.12 wt%; maximum 0.23 wt%), this is possibly the result pf the breakdown of tetrahedrite (however, peak overlap is a possibility as well).

Table 4: Geochemistry of major sulphide minerals within the Lalor deposit (Analyses by Dr, Ingrid Kjarsgaard)

Mineral	(n)	S	Fe	Co	Ni	Cu	Zn	Ga	As	Se	Ag	Cd	In	Sn	Sb	Te	Au	Hg	Pb	Bi	Total
Major and Minor Minerals:																					
Pyrite	27	53.70	47.29	0.27	0.02	0.01	0.02	0.01	0.11	0.02	0.02	0.02	0.01	0.01	<0.01	0.01	0.03	0.03	<0.01	0.12	101.71
FeS_2	min	52.23	45.61	<0.01	<0.01	<0.01	<0.01	<0.01	<0.01	<0.01	<0.01	<0.01	<0.01	<0.01	<0.01	<0.01	<0.01	<0.01	<0.01	<0.01	100.54
	max	55.18	48.07	2.08	0.12	0.09	0.09	0.07	1.40	0.05	0.09	0.07	0.04	0.05	<0.01	0.08	0.10	0.14	0.09	0.21	103.50
Pyrrhotite	30	38.80	60.97	0.01	0.02	0.02	0.02	0.02	0.01	0.02	0.02	0.01	<0.01	0.01	<0.01	0.01	0.03	0.01	0.06	0.09	100.13
FeS	min	37.39	59.90	<0.01	<0.01	<0.01	<0.01	<0.01	<0.01	<0.01	<0.01	<0.01	<0.01	<0.01	<0.01	<0.01	<0.01	<0.01	<0.01	<0.01	98.94
	max	40.00	62.00	0.05	0.13	0.14	0.09	0.09	0.05	0.09	0.11	0.07	0.05	0.05	<0.01	0.04	0.14	0.09	0.47	0.23	101.54
Sphalerite	19	32.24	7.65	0.01	0.01	0.54	55.97	0.18	0.01	0.02	0.01	2.32	<0.01	0.01	0.01	<0.01	0.04	0.02	0.05	0.07	99.17
ZnS	min	31.56	3.85	<0.01	<0.01	<0.01	52.00	0.04	<0.01	<0.01	<0.01	0.02	<0.01	<0.01	<0.01	<0.01	<0.01	<0.01	<0.01	<0.01	96.77
	max	32.82	9.24	0.03	0.07	3.57	60.14	0.32	0.03	0.06	0.06	5.10	0.05	0.06	0.07	0.01	0.16	0.09	0.35	0.17	100.94
Chalcopyrite	13	34.34	30.56	0.01	0.01	34.41	0.05	0.01	0.01	0.03	0.04	0.03	<0.01	0.01	0.01	0.01	0.02	0.01	0.09	0.07	99.72
$CuFeS_2$	min	33.91	29.84	<0.01	<0.01	34.04	<0.01	<0.01	<0.01	<0.01	<0.01	<0.01	<0.01	<0.01	<0.01	<0.01	<0.01	<0.01	<0.01	<0.01	98.21
	max	34.74	30.88	0.03	0.03	34.88	0.15	0.03	0.04	0.07	0.26	0.07	0.01	0.03	0.15	0.03	0.08	0.11	0.29	0.24	100.44
Cubanite	6	34.85	41.06	<0.01	0.02	23.30	<0.01	0.02	<0.01	0.02	0.09	0.01	0.01	0.01	<0.01	0.01	0.04	0.01	0.11	0.12	99.67
$CuFe_2S_3$	min	34.43	40.51	<0.01	<0.01	23.11	<0.01	<0.01	<0.01	<0.01	<0.01	<0.01	<0.01	<0.01	<0.01	<0.01	<0.01	<0.01	<0.01	0.07	98.40
	max	35.42	41.39	0.01	0.06	23.49	0.01	0.05	0.01	0.05	0.26	0.03	0.04	0.02	<0.01	0.04	0.23	0.04	0.38	0.20	100.51
Arsenopyrite	8	21.68	35.97	0.02	0.01	0.18	0.04	<0.01	42.63	0.27	0.02	0.01	<0.01	0.01	0.25	0.10	0.04	0.02	0.05	0.05	101.35
FeAsS	min	20.13	34.67	<0.01	<0.01	<0.01	0.01	<0.01	39.15	0.22	<0.01	<0.01	<0.01	<0.01	<0.01	0.01	<0.01	<0.01	<0.01	<0.01	98.97

	max	24.61	37.40	0.05	0.02	0.62	0.14	<0.01	45.47	0.31	0.06	0.07	0.03	0.04	1.73	0.23	0.11	0.11	0.19	0.14	101.98
Galena	12	13.59	0.03	0.01	<0.01	0.05	0.04	0.01	<0.01	0.38	0.05	0.04	<0.01	0.01	0.05	0.04	0.02	<0.01	85.30	0.06	99.71
PbS	min	13.19	<0.01	<0.01	<0.01	0.01	<0.01	<0.01	<0.01	0.05	<0.01	<0.01	<0.01	<0.01	<0.01	<0.01	<0.01	<0.01	84.49	<0.01	98.92
	max	13.92	0.18	0.03	0.01	0.18	0.10	0.04	0.03	0.60	0.22	0.13	0.03	0.04	0.15	0.12	0.09	0.04	86.03	0.30	100.66
Gold	7	0.06	0.79	0.01	0.01	0.09	<0.01	0.17	0.02	<0.01	22.99	0.01	<0.01	0.30	0.01	0.03	73.94	2.67	0.01	0.02	101.13
(Au,Ag)	min	<0.01	0.07	<0.01	<0.01	<0.01	<0.01	<0.01	<0.01	<0.01	12.10	<0.01	<0.01	<0.01	<0.01	<0.01	63.22	<0.01	<0.01	<0.01	100.26
	max	0.12	2.66	0.02	0.03	0.21	<0.01	0.61	0.07	0.01	29.19	0.08	<0.01	1.32	0.07	0.07	87.52	7.95	0.04	0.17	101.98
Electrum	11	0.05	0.17	0.01	0.01	0.11	0.02	<0.01	0.03	0.01	50.85	0.06	<0.01	0.13	0.62	0.09	43.83	3.88	0.05	0.01	99.92
(Au,Ag)	min	<0.01	<0.01	<0.01	<0.01	<0.01	<0.01	<0.01	<0.01	<0.01	40.21	<0.01	<0.01	<0.01	<0.01	0.06	16.86	0.09	<0.01	<0.01	98.21
	max	0.19	0.39	0.04	0.03	0.33	0.20	<0.01	0.28	0.02	78.55	0.30	<0.01	0.97	2.68	0.16	54.53	7.49	0.28	0.16	101.59
Tetrahedrite	7	25.53	6.38	<0.01	<0.01	37.77	0.76	<0.01	7.24	0.09	3.68	0.07	<0.01	0.06	19.17	<0.01	0.01	<0.01	0.01	0.05	100.85
$(Cu,Ag)_{12}(Sb,As)_4S_{13}$	min	24.38	6.01	<0.01	<0.01	34.19	0.32	<0.01	1.13	0.04	1.44	<0.01	<0.01	0.02	15.34	<0.01	<0.01	<0.01	<0.01	<0.01	99.62
	max	26.41	6.77	0.01	0.02	40.16	1.22	0.01	9.96	0.13	6.94	0.15	0.01	0.13	27.30	<0.01	0.05	0.01	0.08	0.15	101.78
Freibergite	13	22.60	5.73	0.01	0.01	23.04	0.67	<0.01	1.66	0.03	20.54	0.42	<0.01	0.07	24.86	<0.01	0.02	<0.01	0.07	0.04	99.77
$(Ag,Cu)_{12}(Sb,As)_4S_{13}$	min	18.58	5.05	<0.01	<0.01	12.85	0.25	<0.01	0.03	<0.01	12.39	0.12	<0.01	<0.01	14.26	<0.01	<0.01	<0.01	<0.01	<0.01	98.01
	max	24.99	7.22	0.04	0.04	30.34	1.16	<0.01	10.05	0.22	36.65	1.08	<0.01	0.12	28.18	<0.01	0.06	<0.01	0.35	0.15	101.22
Bournonite (As)	9	19.85	0.05	0.01	0.01	13.03	0.03	0.01	1.76	0.27	0.02	0.03	0.01	0.11	22.66	0.04	<0.01	<0.01	41.94	0.09	99.92
$PbCuSbS_3$	min	19.31	<0.01	<0.01	<0.01	12.52	<0.01	<0.01	0.09	0.11	<0.01	<0.01	<0.01	0.07	18.22	<0.01	<0.01	<0.01	41.29	<0.01	99.07
	max	20.32	0.20	0.03	0.05	13.61	0.10	0.05	4.78	0.43	0.07	0.10	0.03	0.14	25.13	0.14	0.01	<0.01	42.43	0.17	101.07
Boulangerite (As)	4	18.30	0.04	0.01	<0.01	0.05	0.02	<0.01	0.47	0.17	0.18	0.07	<0.01	0.12	25.13	<0.01	0.03	<0.01	54.23	0.09	98.92
$Pb_5Sb_4S_{11}$	min	18.20	<0.01	<0.01	<0.01	<0.01	<0.01	<0.01	0.02	<0.01	<0.01	<0.01	<0.01	0.09	24.27	<0.01	<0.01	<0.01	53.60	<0.01	98.32
	max	18.45	0.14	0.01	<0.01	0.20	0.06	<0.01	1.74	0.32	0.69	0.18	<0.01	0.15	26.00	<0.01	0.11	<0.01	54.85	0.27	99.18

Allargentum	4	2.00	0.02	0.01	<0.01	0.08	<0.01	<0.01	0.05	0.01	75.02	0.30	<0.01	0.01	17.99	0.05	4.65	0.13	0.07	0.02	100.40
$Ag_{1-x}Sb_x$	min	0.88	<0.01	<0.01	<0.01	<0.01	<0.01	<0.01	<0.01	<0.01	73.24	0.25	<0.01	<0.01	13.91	<0.01	1.76	<0.01	<0.01	<0.01	99.11
	max	3.19	0.04	0.02	<0.01	0.20	<0.01	<0.01	0.08	0.02	77.17	0.34	<0.01	0.03	20.11	0.10	7.35	0.35	0.14	0.05	102.10
Trace Minerals:																					
Ag-Chalcopyrite	2	32.45	28.96	<0.01	<0.01	32.19	0.03	0.05	0.03	0.03	3.71	0.02	<0.01	<0.01	<0.01	0.01	0.04	<0.01	0.19	0.05	97.75
$CuFeS_2$																					
Galena (Se)	3	12.51	0.53	0.02	<0.01	0.01	0.04	0.01	<0.01	2.45	0.06	0.02	<0.01	0.09	0.03	0.04	0.04	<0.01	83.89	<0.01	99.75
Pb(S,Se)																					
Cobaltite	1	19.96	4.97	29.46	0.46	<0.01	<0.01	<0.01	43.32	0.30	<0.01	<0.01	<0.01	0.05	1.07	<0.01	0.04	<0.01	0.10	0.14	99.86
CoAsS																					
Gudmundite	2	15.14	26.78	<0.01	0.16	0.05	<0.01	0.05	0.27	0.01	0.01	<0.01	<0.01	0.25	58.50	0.09	0.03	<0.01	0.08	0.01	101.42
FeSbS																					
Meneghinite	2	17.86	<0.01	0.01	0.01	1.29	0.03	<0.01	0.06	0.18	0.05	<0.01	<0.01	0.06	19.77	0.01	0.02	<0.01	61.35	0.07	100.77
$Pb_{13}CuSb_7S_{24}$																					
Sterryite	2	18.94	0.08	0.01	<0.01	0.36	0.07	0.02	0.11	0.19	3.62	<0.01	<0.01	0.15	26.86	<0.01	0.07	<0.01	49.69	0.02	100.19
$Ag_2Pb_{10}(Sb,As)_{12}S_{29}$																					
Ag-Pentlandite	1	31.88	38.15	0.08	15.72	1.70	<0.01	<0.01	0.04	0.03	12.64	<0.01	<0.01	<0.01	<0.01	0.03	<0.01	<0.01	<0.01	0.05	100.31
$(Ag,Fe,Ni)_9S_8$																					
Benleonardite	1	6.07	0.04	<0.01	0.01	<0.01	<0.01	<0.01	0.01	0.39	63.30	0.23	<0.01	0.05	7.38	23.60	0.01	<0.01	<0.01	0.10	101.20
$Ag_8(Sb,As)Te_2S_3$																					
Stützite(?)	1	1.23	1.80	<0.01	<0.01	0.15	0.03	<0.01	<0.01	0.02	57.83	0.28	<0.01	0.68	<0.01	31.76	0.06	0.10	1.31	<0.01	95.25
Ag_5Te_3																					

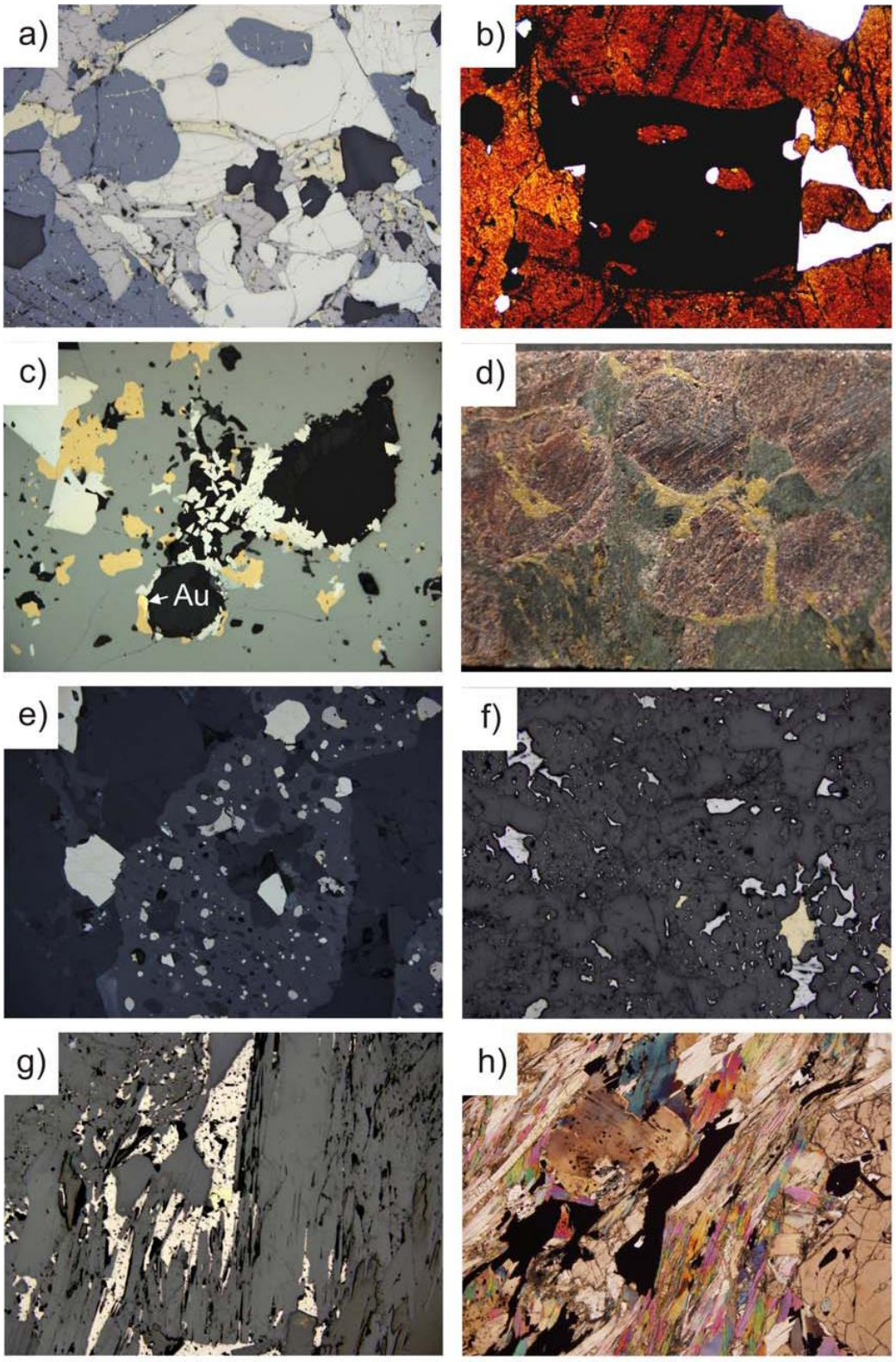
a)
b)
c)
Au
d)
e)
f)
g)
h)

Figure 6: Photomicrographs of representative ore textures in the main ore types of the Lalor deposit. a) Type 1 Fe-Zn massive sulfide with large, fractured poikiloblastic pyrite grain infilled by pyrrhotite and chalcopyrite, in a matrix of dark grey sphalerite (sample 515, reflected PPL, FOV=4.4 mm). b) Type 1 Fe-Zn massive sulfide with large poikiloblastic pyrite in a matrix of massive sphalerite (sample 514, transmitted light, FOV=4.4 mm). c) Disseminated pyrite, chalcopyrite and arsenopyrite rimming quartz inclusions in massive sphalerite. A gold grain can be seen adjacent to chalcopyrite at the rim of a rounded quartz inclusion (sample 507, reflected PPL, FOV=1 mm). d) Close-up of Type 2 semi-massive Au-Cu ore in drill core showing chalcopyrite rimming and as inclusions in large garnet porphyroblasts (DUB262W05, 1271.3 m). e) Typical poikiloblastic garnet with inclusions of pyrite, pyrrhotite, and chalcopyrite (sample 601, reflected PPL, FOV=1 mm). f) Typical fine-grained disseminated galena in quartz with lesser pyrite (sample 507, reflected PPL, FOV=1.1 cm). g) Pyrite and pyrrhotite in cleavages within quartz chlorite-biotite hosting Type 2 Au-Cu ore (sample 584, reflected PPL, FOV=4.4 mm). h) Typical texture of sulfides in cleavages within quartz-muscovite-garnet schist (sample 522,transmitted light, FOV=4.4 mm).

Figure 7: Photograph of classic *durchbewegung* texture (Craig and Simpson, 1991) in type 1 Fe-Zn-rich massive sulfide ore (DUB195, 809.7 m). The texture shows rounded nodule of hard pyrite and quartz in a matrix of softer sphalerite. NQ drill core (47.6 mm or 1-7/8 in diameter).

Chapter 5: Ore Geochemistry

Table 5 lists the average bulk geochemical compositions of the different ore types determined for the 70 samples analyzed in this study. The samples of massive sulphide ore average 11.7 wt% Fe and 12.3 wt% Zn, corresponding to 25 wt% FeS_2 and 18 wt% ZnS. Zinc shows a strong correlation with Cd (r=0.97), Hg (r=0.61), In (r=0.56) and Sb (r=0.48). Fe shows a positive correlation with Co (r=0.41) and Ni (r=0.48), but not with Zn. The pyrite-rich ores and sphalerite-rich ores clearly represent geochemically distinct assemblages, despite their occurrence together in the massive sulphide lenses.

Copper, which is present mainly in the semi-massive chalcopyrite ore, shows a moderately strong correlation with Se (r=0.48) and As (r=0.63), and to a lesser extent with Sn (r=0.39) and In (r=0.27). Sn and In are common trace constituents of Cu-rich ores in other VMS deposits (e.g. Hannington et al 1999), typically in the chalcopyrite-like minerals stannite and roquesite, but these were not identified in the present study.

Gold shows the strongest correlation with Ag (r= 0.98) and Te (r= 0.80), but the Au and Ag are distributed bimodally, with equally high contents in the Pb-rich ores and Au-Cu ores, so the statistical correlations with Pb and Cu in the bulk ore are weak. Although galena is the most common visual indicator for precious-metal enrichment in the chlorite-carbonate-actinolite-altered zones, Pb has a very poor correlation with Au and Ag at the hand-specimen scale. The strong correlation of Ag with Au reflects the high Ag content of the electrum and the association of electrum with Ag-rich sulphosalts, especially in the precious metal-rich chlorite-carbonate-

actinolite-altered zones. The correlation with Te suggests the presence of an unidentified Au-bearing telluride.

In order to better understand the variance of the data and to reduce it into categories, a principal component analysis was performed. The principal component analysis (Figure 8) confirms that the bulk geochemical compositions of the ores include a significant mafic volcanic component (TiO_2, Al_2O_3, Na_2O, P_2O_5, Sc, Th, Y, Cr, V), a felsic element component (Al_2O_3, Hf, Nb, Ta, Zr, and LREE), a phyllosilicate component (K_2O, Al_2O_3, Ba, Cs, Li, F, and Ga), a chloritic component (MgO, Al_2O_3, Mn), and a carbonate or calc-silicate component (CO_2, CaO, MgO, MnO, and Sr). CaO and CO_2 contents strongly correlate with Pb in the precious metal-rich Au-Ag-Pb-Cu-rich ores hosted in chlorite-carbonate-actinolite altered rocks, as well as with U, Th, Y, and HREE. The latter elemental suite may reflect an association with secondary minerals (e.g., xenotime) that are the product of metamorphic remobilization. CaO is also weakly correlated with Sr, Mn and MgO (present in dolomite but also in co-existing chlorite, actinolite, and tremolite).

Table 5. Average bulk compositions of selected ore types of the Lalor VMS deposit.

Element	Unit	Massive Sulphide n = 26	Semi-Massive Chalcopyrite n = 9	Chlorite Carbonate n = 26	Low Sulphide High Au n = 10
SiO_2	%	19.63	57.67	39.71	46.94
Al_2O_3		5.08	8.52	7.25	9.17
Fe_2O_3		13.25	2.08	2.90	4.32
FeO		15.1	13.4	8.0	14.1
MgO		3.30	7.48	9.94	8.23
MnO		0.20	0.12	0.25	0.29
CaO		3.05	1.81	10.52	1.45
Na_2O		0.16	0.07	0.08	0.11
K_2O		0.32	0.30	0.16	0.41
TiO_2		0.19	0.25	0.15	0.31
P_2O_5		0.06	0.16	0.06	0.16
CO_2		0.78	0.11	3.45	0.25
Total C		0.23	0.04	0.98	0.08
Total S		25.7	6.11	7.87	7.08
LOI		0.52	0.07	2.21	0.17
Cu		2.37	1.42	1.06	4.13
Zn		12.32	0.42	4.57	1.88
Pb		0.15	0.04	0.84	0.04
Total		102.41	100.07	100.00	99.12
Au	ppm	10.5	44.0	147	11.4
Ag		51	124	365	66.4
As		356	102	38.0	57.5
Sb		93	2.2	8.6	2.4
Cd		307	17.1	107	49.2
Hg		83.12	1.01	14.84	5.53
Tl		0.21	0.20	0.74	0.15
Sn		14	3	9	16
In		0.6	0.2	0.2	0.4
W		26	2.4	1.1	4.4
Ga		10	11	12	14
Ge		1.6	0.8	1.2	1.1
Co		96	88	38	70
Ni		20	9	6	15
Se		122	74	121	77
Bi		1.2	0.4	5.8	2.8
Te		14.0	65.2	63.8	20.8
Mo		5	2	3	4
V		54	63	22	179
U		1.75	0.78	1.29	0.92
Th		1.10	1.67	1.41	2.10
Ba		37	37	31	78
Sr		30	12	38	16
Cs		0.1	0.2	0.1	0.2
F		250	860	510	600
B		1	2	1	<1
Be		<1	<1	<1	<1
Li		9	22	8	11
Hf		0.6	1.0	1.3	1.1
Ta		0.13	0.15	0.15	0.15
Zr		24	38	44	45
Nb		2.2	3.3	3.1	3.4
Sc		10	14	9	24
Y		5.0	10.5	16.7	11.5
∑REE		42.4	67.3	85.5	95.8

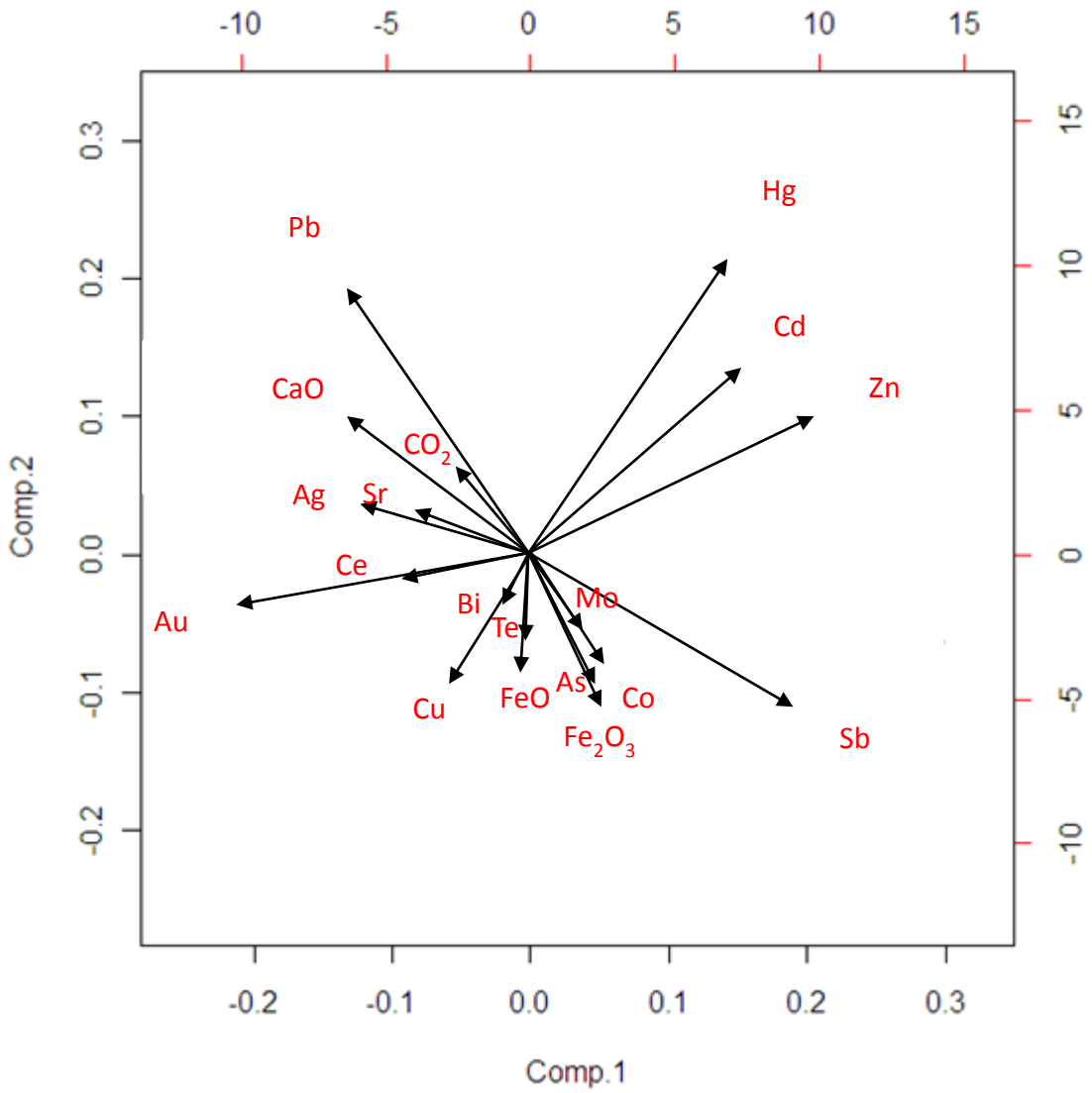

Figure 8: Bi-plot of principal components based on 19 elements showing groupings based on PCA 1 and PCA 2. Elements in proximity to each other are considered to be influenced by the same components where distance is inversely related to how strongly elements are controlled by the same component.

Chapter 6: Sulphur and Lead Isotopes

Sulphur isotope compositions of pyrite, sphalerite, pyrrhotite and chalcopyrite show a limited range from $\delta^{34}S$ 0.41 to 2.84 ‰ with no significant difference between minerals (Figure 9). This narrow range is typical of sulphides that have been extensively recrystallized during metamorphism (e.g., Shanks 2001; Fig. 8). Although it has been shown that many sulphide minerals can retain their isotopic compositions through metamorphism (e.g., Corriveau and Spry, 2014), it is common for highly metamorphosed massive sulphide deposits to have a very narrow range of values, reflecting probable loss of light sulphur during recrystallization (Crowe, 1994; Cook and Hoefs, 1997). In contrast, shear zone-hosted orogenic gold deposits in the Flin Flon-Snow Lake belt have generally higher $\delta^{34}S$ values (2.8 to 5.5‰: Fedorowich et al., 1991; Ansdell and Kyser, 2006), consistent with hydrothermal fluids in the shear zones interacting with a wide range of Proterozoic metamorphic and igneous rocks. The data also contrast with the $\delta^{34}S$ values of barren sulphide occurrences outside the Flin Flon-Snow Lake belt in rocks of similar age and metamorphic grade (e.g., Polito et al., 2007).

Lead isotope ratios were measured on six galena separates from the Au-Ag-Pb-rich ore associated with chlorite-carbonate-altered rocks and three galena separates from the massive sulphides in the 10 and 11 lenses (See Appendix E). All samples exhibit a tight cluster of $^{206}Pb/^{204}Pb$, $^{207}Pb/^{204}Pb$ and $^{208}Pb/^{204}Pb$ ratios, averaging 15.400, 15.122, and 34.895, respectively, with no difference between the ore types. These data compare closely to the Pb isotope ratios of galena separates from Chisel and Chisel North (15.432, 15.161 and 35.058: Thorpe, 2008) at low $^{206}Pb/^{204}Pb$ and $^{207}Pb/^{204}Pb$ (Figure 10). The similarity of Pb isotope

compositions of galena in the Au-Ag-Pb-rich galena-sulphosalts±chalcopyrite ore and in the massive sulphides strongly suggests a common Pb source and negates a late-stage post-magmatic event as the origin of the Au-Ag-Pb-rich mineralization. A post-magmatic event (e.g. a syn-metamorphic event) would have been expected to introduce distinctly different, and likely more radiogenic, Pb (cf. Sangster, 1972, 1978; Thorpe, 2008), similar to that in the nearby New Britannia (Nor Acme), Rex, Herb Lake, Bingo, and Ferro Au mines of the Snow Lake camp (Figure 10).

Lalor ore galenas are the least radiogenic of the VMS deposits in the region but generally fall on the Pb-isotope linear array of the Flin Flon-Snow Lake mineral belt (cf. Sangster 1972, 1978). The linear array of data on the Pb-Pb plot is similar to that inferred for crust-mantle mixing in other Precambrian greenstone terranes (e.g., Thorpe, 1999) and reflects contributions of both older crustal components and mantle sources. The most radiogenic end-members represent the signatures of material derived from the crust.

Table 6: Sulphur isotope compositions of ore minerals from the Lalor massive sulphide deposit.

Sample	Lens	Ore Type	δ34S (‰)	Mineral
517-Py	10	1	2.58	Pyrite
518-Py	10	1	2.22	Pyrite
521-Py	10	1	2.27	Pyrite
545-Py	10	1	1.65	Pyrite
632-Py	10	1	2.61	Pyrite
635-Py	10	1	2.84	Pyrite
637-Py	10	1	2.06	Pyrite
643-Py	10	1	1.87	Pyrite
651-Py	10	1	1.88	Pyrite
666-Py	10	1	1.29	Pyrite
545-Sp	10	1	0.93	Sphalerite
667-Sp	10	1	0.41	Sphalerite
664-Cp	10	1	1.36	Chalcopyrite
516-Po	10	1	1.41	Pyrrhotite
651-Po	10	1	1.83	Pyrrhotite
664-Po	10	1	1.17	Pyrrhotite
549-Cp	10	3	1.03	Chalcopyrite
658-Py	10	3	0.85	Pyrite
665-Cp	10	4	1.08	Chalcopyrite
665-Po	10	4	1.22	Pyrrhotite
536-Py	21	1	1.51	Pyrite
595-Py	21	1	2.59	Pyrite
596-Py	21	1	1.86	Pyrite
536-Sp	21	1	1.72	Sphalerite
559-Py	21	3	2.40	Pyrite
611-Py	21	3	2.45	Pyrite
559-Sp	21	3	1.60	Sphalerite
598-Py	21/20	1	1.80	Pyrite

599-Py	21/20	1	2.19	Pyrite
598-Sp	21/20	1	1.36	Sphalerite
618-Py	21/25	1	2.13	Pyrite
608-Py	21/20	3	2.20	Pyrite
619-Py	25	N/A	2.79	Pyrite
562-Py	25	1	2.33	Pyrite
587-Py	25	1-3	1.52	Pyrite
524-Py	25	3	2.66	Pyrite
586-Py	25	3	2.42	Pyrite
575-Py	25/26	3	0.56	Pyrite
538-Cp	27	2	2.34	Chalcopyrite
539-Cp	27	2	1.84	Chalcopyrite
540-Py	27	2	1.28	Pyrite
578-Py	27	2	1.68	Pyrite
538-Po	27	2	2.27	Pyrrhotite
603-Cp	N/A	2	1.40	Chalcopyrite
631-Py	N/A	2	1.96	Pyrite
628-Cp	N/A	4	2.45	Chalcopyrite
628-Py	N/A	4	2.30	Pyrite
581-Py	Vein	N/A	0.96	Pyrite
586-Sp	N/A	N/A	2.07	Sphalerite

Table 7. Pb isotope ratios of galena from different ore types of the Lalor massive sulphide deposit.

Sample	Description	Location (Ore Type)	$^{206}Pb/^{204}Pb$	$^{207}Pb/^{204}Pb$	$^{208}Pb/^{204}Pb$
SD-524	Euhedral grains with minor pyrite and pyrrhotite in a matrix of quartz and chlorite (DUB252W01, 1016.8 m)	25 Lens (Type 3)	15.403	15.120	34.899
SD-581	12 cm thick vein of pyrrhotite, pyrite and galena with minor chalcopyrite in quartz- biotite-actinolite/tremolite-garnet (DUB258W01, 803.7 m)	N/A (vein)	15.402	15.128	34.892
SD-611	Vein of sphalerite and galena with minor chalcopyrite in quartz-muscovite-gahnite-biotite (DUB169, 900.5 m)	21 Lens (Type 3)	15.399	15.113	34.888
SD-652	Coarse pyrite and sphalerite with lesser galena in actinolite-tremolite and epidote (DUB211, 909.2 m)	10 Lens (Type 3)	15.398	15.125	34.898
SD-654	Coarse pyrite and galena with interstitial sphalerite in carbonates (DUB174, 877.8 m)	31 Lens (Type 1)	15.396	15.122	34.885
SD-655	Galena adjacent to quartz vein in a massive pyrite (underground, 825 mL)	10 Lens (N/A)	15.394	15.116	34.868
SD-662	Thick (50 cm) galena vein cutting stringer zone sulphides (underground, 810 mL)	10 Lens (vein)	15.396	15.122	34.891
SD-663	Quartz vein with galena concentrated in a fold hinge (underground, 865 mL)	20 Lens (vein)	15.412	15.132	34.936

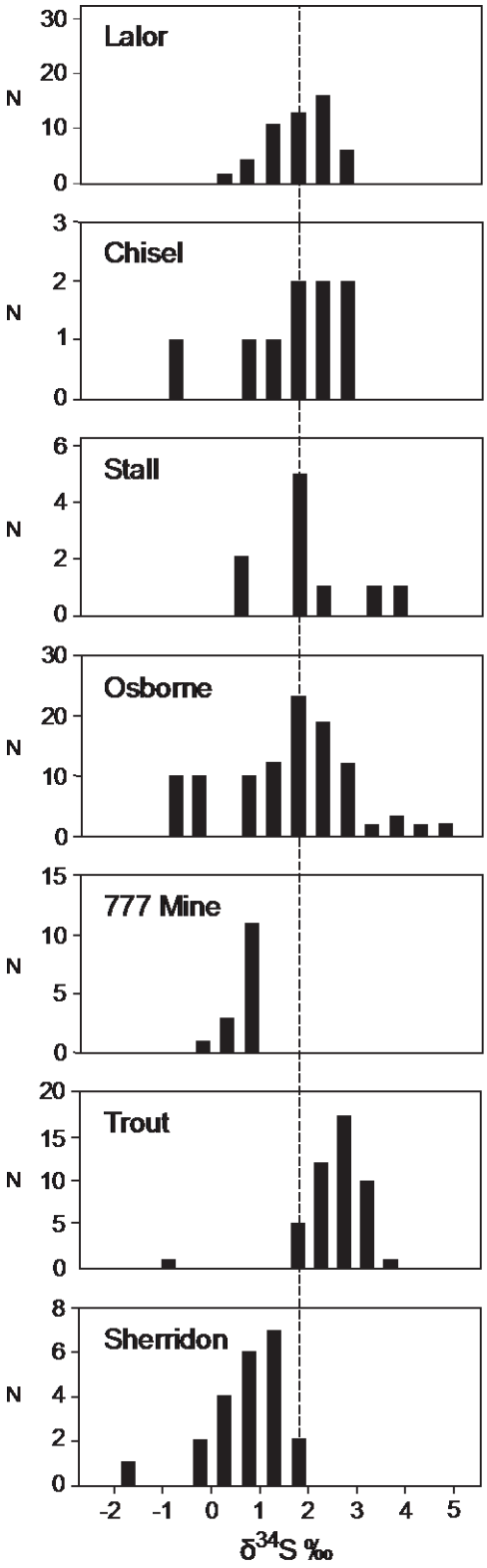
Lalor
Chisel
Stall
Osborne
777 Mine
Trout
Sherridon
N
30
20
10
0
3
2
1
6
4
15
5
8
-2
-1
0
1
2
3
4
5
δ34S ‰

Figure 9: Histogram of sulfur isotope data from the Lalor massive sulfide deposit (Table 6), comparing the average value for Lalor sulfides (dashed line) with the distribution of $\delta^{34}S$ values for Chisel Lake and Stall in the Snow Lake camp (J.M. Franklin, unpublished data) and for the 777 Mine and Trout Lake Mine in Flin Flon (Polito et al., 2007). Data for the Sherridon sediment-hosted massive sulfide deposit are from (Sangster, 1973). Sulfide δ34S values for Lalor range from 0.4 to 2.8 per mil (av. +1.8 per mil), similar to all other Paleoproterozoic VMS deposits in the region. Somewhat more variable compositions are evident at 777 and Trout Lake, at Osborne Lake northeast of Snow Lake, and at Sherridon; the lower δ34S values at Sherridon may possibly reflect the influence of reduced sediments in the mine sequence.

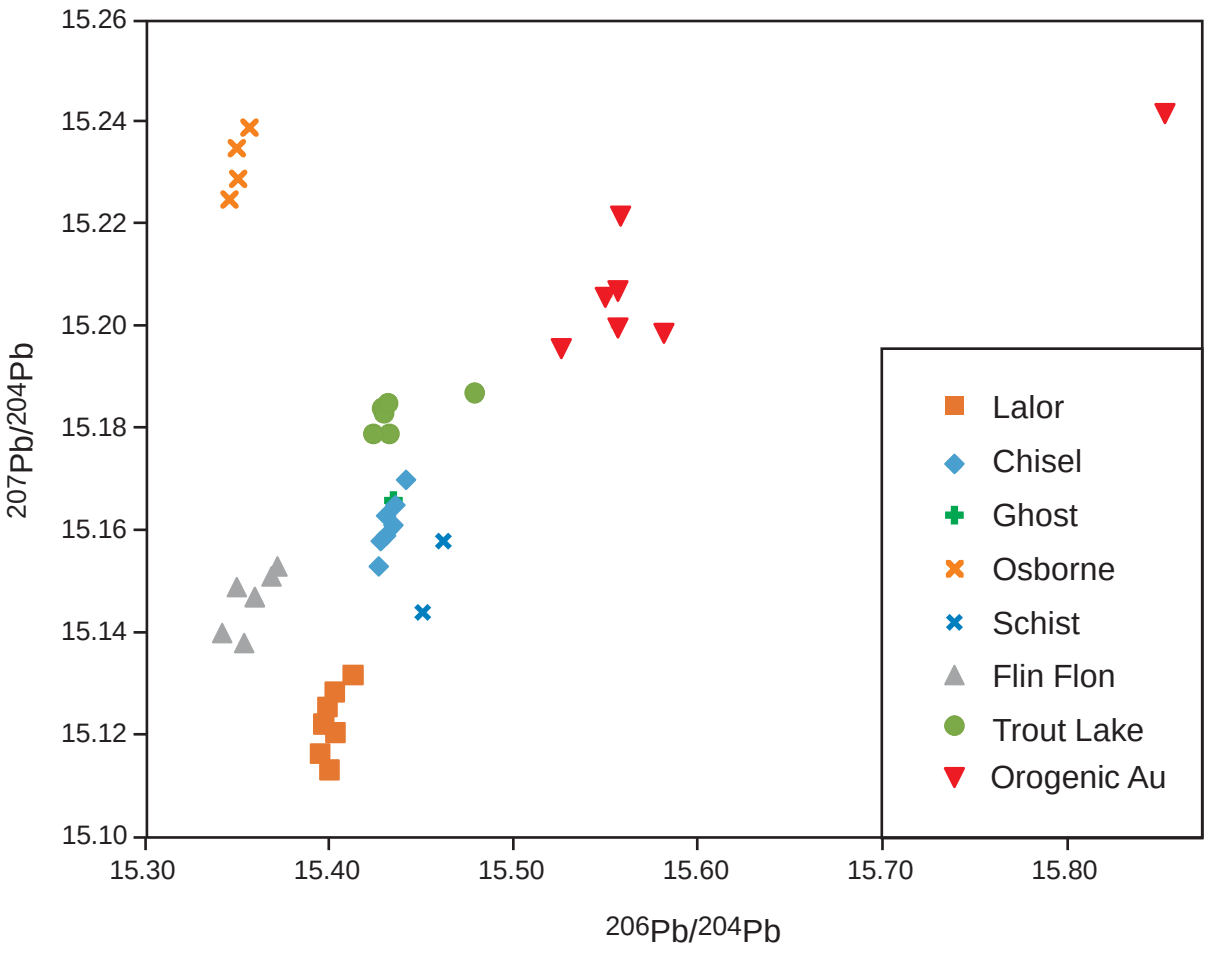
15.26
15.24
15.22
15.20
15.18
15.16
15.14
15.12
15.10
15.30
15.40
15.50
15.60
15.70
15.80
207Pb/204Pb
206Pb/204Pb
Lalor
Chisel
Ghost
Osborne
Schist
Flin Flon
Trout Lake
Orogenic Au

Figure 10: $^{207}Pb/^{204}Pb$ versus $^{206}Pb/^{204}Pb$ ratios for galena from selected VMS deposits and orogenic gold deposits in the Flin Flon-Snow Lake belt. Data are from Thorpe (2008) and J.M. Franklin (unpublished), and Galley and Franklin (1989). The samples were collected by D. Sangster, J.M. Franklin, A. Galley, M. Fedikow, and R. Healy, and the analyses were performed in a number of different laboratories, including at the University of Alberta (G.L. Cumming, 1982), Geospec Consultants Limited, and at the Geological Survey of Canada. Data for late post-magmatic mineralization (including orogenic gold deposits: Nor Acme, Bingo, Ferro, Herb lake, Rex Mine, and Threehouse) are from Galley and Franklin (1989). Data for Lalor are from this study. The ore Pb from Lalor is the least radiogenic of the VMS deposits in the region but generally falls on a Pb-isotope linear array including the Lalor, Ghost and Chisel deposits. Galena lead isotope signatures for the younger gold mines of the Snow Lake camp (Nor Acme, Rex, Herb Lake, Bingo, and Ferro) form a distinctly separate secondary array.

Chapter 7: Summary and Discussion

Four major ore types are recognized in the twelve ore lenses at Lalor, including Fe-Zn-rich massive sulphides, Au-Cu rich semi-massive and stockwork-like chalcopyrite in chloritic rocks (dominated by chlorite-biotite-staurolite-anthophyllite-cordierite ± kyanite/sillimanite), Au-Ag-Pb-rich disseminated sulphides and sulphosalts in chlorite-carbonate-actinolite (dominated by chlorite-calcite ± diopside ± epidote ± talc), and pyritic quartz-biotite rock. In the Fe-Zn-rich massive sulphides, Au is interstitial to pyrite and sphalerite in coarsely recrystallized polycrystalline aggregates, commonly with sulphosalts and chalcopyrite. In semi-massive and stockwork-like Au-Cu mineralization Au is closely associated with chalcopyrite, and in chlorite-carbonate-actinolite ± calc-silicate rocks Au is associated with disseminated polymetallic sulphides, especially galena, and related Ag-Sb-Pb-sulphosalts.

All ores have been extensively recrystallized during syn-D_2 amphibolite facies metamorphism. The stoichiometric compositions of the major Cu-Fe-sulphides (pyrite, pyrrhotite, chalcopyrite), the very uniform composition of sphalerite, the low trace element contents in galena, and the abundance of minor and trace sulphosalts and other minerals are typical of massive sulphide ores that have been extensively recrystallized (e.g., Chen and Petruk, 1980; Petruk and Schnarr, 1981; Petruk and Wilson, 1993); Craig and Vokes, 1993; Huston et al., 1995). In such ores, trace elements in the major ore minerals are expelled during recrystallization to form minor phases that commonly occur at the margins of the grains or at triple-junction contacts. The presence of mercurian electrum probably reflects the loss of Hg from primary sphalerite during metamorphism and its collection by electrum (cf. Healy and Petruk, 1988), a major source of Hg

in all of the deposits of the belt (e.g., Healy and Petruk, 1990). Certain minerals, such as tetrahedrite, retain their high Ag contents despite the metamorphism. In some metamorphosed ore deposits, pyrite decomposition liberates sulphur that may play a role in remobilization of Au (e.g., as $Au(HS)_2^-$ in metamorphic hydrothermal fluids derived from dehydration reactions), and high fS_2 conditions caused by pyrite breakdown have been documented at several highly metamorphosed massive sulphide deposits such as Osborne Lake, Montauban and Geco (Bristol and Froese 1989; Tomkins 2007; Tomkins et al., 2006). However, strong buffering by iron silicates or oxides may limit this process, and the uniformly high FeS contents of sphalerite at Lalor suggest that fS_2 remained low during metamorphism (e.g., Craig and Vokes, 1993). Thus, although the soft and ductile minerals like galena, various sulphosalts, electrum and gold were mechanically remobilized into fractures and cleavages, metamorphic reactions that might have dissolved (and transported) Au likely did not occur.

The ore lenses also preserve an apparent primary metal enrichment. Zn-rich massive sulphide ores are Cd-, Hg-, Sb-, and As-rich, whereas the Cu-rich semi-massive sulphide and stockwork ores (normalized to 100% sulphides) are enriched in Co, Ni, Mo, Se, Te±Bi. The Pb-rich ores are enriched in Au, Ag, As, Se and Te compared to the other ore types. In general, Au shows a generally poor correlation with all other trace elements, except Ag. As in other deposits of the Chisel Sequence, high Au grades occur in both Cu- and Zn-rich ores in different lenses, and this most likely reflects primary differences in the conditions of Au mineralization (e.g., including both high-temperature Cu-Au mineralization and lower-temperature Zn-Au mineralization: cf. Huston et al., 2000).

The unusual stratigraphic position of the Pb-rich ores relative to the other ore lenses at Lalor raises the possibility that they are not part of the VMS system but were emplaced during a much later metamorphic event. However, the tight clustering of the Pb isotope data along the Flin Flon-Snow Lake linear array suggests that the Pb and the closely associated Au were cogenetic with the massive sulphides. As noted by Sangster (1978), the fact that the Pb isotopes from the various VMS deposits cluster and do not lie on secondary isochrons, like the Au deposits, suggests that the Pb (and by inference other metals) in each deposit have a discrete uniform composition and do not show any multi-stage post-magmatic history. The presence of "low-temperature" disseminated galena-rich ores stratigraphically below the main massive sulphide lenses suggests that they formed as a late-stage synvolcanic hydrothermal overprint, possibly in response to subseafloor boiling. Galley et al. (1993) and Gibson et al. (2014) similarly interpret the Chisel, Lost, and Ghost deposits as having formed within a shallow marine basin in which boiling of the hydrothermal fluid likely occurred, and Engelbert et al. (2014b) proposes boiling as the probable mechanism of formation of the high-grade Au ores at Photo Lake. Such low-temperature, disseminated style ore assemblages at Lalor are also much more sensitive to metamorphism and remobilization, perhaps explaining why part of the Au-Ag-Pb ore is spatially associated with highly-strained rocks, brittle amphibolitic assemblages, and weakly altered mafic dykes (Caté et al., 2015).

The ores at Lalor are geochemically and mineralogically similar to the other deposits of the Chisel Sequence (Chisel, Chisel North, Lost, and Ghost). Gold is significantly enriched in all of the deposits compared to the Anderson Sequence (Stall, Rod, and Anderson). Silver, As, Cd, Hg, and Sn contents (normalized to 100% sulphides) are also higher than in typical Snow Lake

concentrates (Hannington and Jonasson, unpublished; Table 6). Notably, the Co, Se, Ni, and Te abundances in the Lalor ore-related minerals are significantly higher than those in the Chisel ores. Trace Co and Ni occur in pyrrhotite and pyrite, and cobaltite, gudmundite, and Se-bearing arsenopyrite are present in the massive sulphides. These differences may reflect the dominantly mafic host rocks and the lack of rhyolite at Lalor compared to Chisel. The most Au-rich deposits of the Chisel Sequence show a close association with felsic volcanic rocks and local rhyolite domes (Galley et al., 1993; Gibson et al., 2014). Similarly, the Au-rich Photo Lake deposit has been interpreted to occur within a thick section of coherent rhyolite (Engelbert et al., 2014a). Although the Lalor deposit is thought to be situated at a similar stratigraphic position as Chisel and Chisel North (Bailes et al., 2013), detailed studies suggest some differences between the footwall successions (Bailes et al., 2013; Caté et al., 2013a,b, 2015), including a minor proportion of felsic volcanic rocks in the Lalor volcanic (footwall) succession. Moreover, mafic magmatism was clearly ongoing during the mineralizing event at Lalor, as evidenced by the presence of dykes with compositions similar to the Threehouse basalt. These observations indicate that Au enrichment in the camp is not limited to deposits with mainly rhyolite in the immediate footwall.

Table 8. Trace element contents of different ore types from Lalor (normalized to 100% sulphides) compared to Snow Lake mineral concentrates.

Deposit	Concentrate/Ore	(n)	Cu wt.%	Fe	Zn	Pb	Au ppm	Ag	As	Sb	Co	Se	Ni	Cd	Mo	Te	Bi	Hg	Tl	Ga	In	Sn
Lalor	Fe-Zn	23	5.08	17.0	24.9	0.34	4.39	110	768	181	208	273	48	648	11	30	1	180	0.3	19	2	24
Lalor	Cu-Au	6	29.1	20.4	7.93	0.19	86.15	362	91	15	342	533	77	219	18	142	15	24	0.8	65	3	75
Lalor	Au-Ag-Pb	15	7.69	13.3	24.4	10.1	38.21	563	314	38	294	778	41	625	17	140	8	82	0.9	88	2	80
Lalor	Low-sulphide	5	16.0	15.0	3.16	0.49	66.61	401	464	3	901	824	90	155	16	117	4	12	0.5	64	2	23
Snow Lake	Cu Concentrate	3	19.5	34.6	2.16	0.03	5.91	93	655	367	381	225	21	57	29	63	29	16	0.6	12	30	16
Stall/Rod	Cu Concentrate	3	19.6	34.4	1.36	0.02	6.16	37	472	49	297	255	16	40	22	52	41	10	0.2	7	29	12
Chisel	Cu Concentrate	3	19.7	22.2	9.73	6.21	21.00	1800	2042	3379	38	293	24	250	28	46	55	73	4.7	5	9	26
Snow Lake	Zn Concentrate	3	0.71	9.61	53.7	0.02	0.52	30	353	78	17	116	<10	1300	2	4	2	120	0.5	11	8	9
Chisel	Zn Concentrate	4	0.22	8.42	54.5	0.2	0.22	27	585	56	20	83	10	1300	2	3	2	120	0.4	10	6	8
Chisel	Pb Concentrate	3	1.21	6.86	6.29	61.4	8.03	956	2229	8436	8	589	24	120	8	120	200	130	26	2	1	6

Lalor data are calculated from samples in Table 5, after normalizing to 100% metals+Fe+S. Type 1 includes only samples with Me+Fe+S >30 wt.%; Au, Ag, and Te concentrations in the calculations were cut off at 30 ppm Au, 300 ppm Ag, and 150 ppm Te. Data for mill concentrates from other Snow Lake deposits are from Hannington and Jonasson, 1986, unpublished data.

References

Ansdell, K.M., and Kyser, K.T., 2006, Mesothermal gold mineralization in a Proterozoic greenstone belt, western Flin Flon Domain, Saskatchewan, Canada: Economic Geology, v. 87, p. 1496-1524.

Bailes, A. H., 2008, Geological setting of the Lalor and Photo Lake VMS deposits, Hudbay Internal Report, Bailes Geoscience, 45 p.

Bailes, A.H., 2009, Geological and Geochemical Investigation of Altered Rocks Hosting the Lalor VMS Deposit: Unpublished Report for HudBay Minerals Inc., 96 p.

Bailes A.H., 2011, A review of structural features associated with VMS deposits in the Chisel-Lalor-Photo lakes area: Unpublished Report for HudBay Minerals Inc., 31 p.

Bailes, A.H., and Galley, A.G., 1999, Evolution of the Paleoproterozoic Snow Lake arc assemblage and geodynamic setting for associated volcanic-hosted massive sulphide deposits, Flin Flon Belt, Manitoba, Canada: Canadian Journal of Earth Sciences, v. 36, no. 11, p. 1789–1805, doi:10.1139/e98-111.

Bailes, A.H., and Galley, A.G., 1996, Setting of Paleoproterozoic volcanic-hosted massive sulphide deposits, Snow Lake, in G.F. Bonham-Carter, A.G. Galley and G.E.M. Hall, eds.,

EXTECH I: A Multidisciplinary Approach to Massive Sulphide Research in the Rusty Lake and Snow Lake Greenstone Belts, Manitoba: Geological Survey of Canada, Bulletin 426, p.105-138.

Bailes, A., Rubingh, K., Gagné, S., Taylor, C., Galley, A., Bernaeur, S., and Simms, D., 2013, Volcanological and structural setting of Paleoproterozoic VMS and Gold deposits at Snow Lake, Manitoba: Geological Association of Canada–Mineralogical Association of Canada Joint Annual Meeting, Field Trip Guidebook FT-A2, Manitoba Geological Survey Open File OF2013-3, 63 p.

Barton, P.B., and Bethke, P.M. Jr., 1987, Chalcopyrite disease in sphalerite: Pathology and epidemiology: Amercian Mineralogist, v. 72, p. 451-467.

Bristol, C.C., and Froese, E., 1989, Highly metamorphosed altered rocks associated with the Osborne Lake volcanogenic massive sulfide deposit, Snow Lake area, Manitoba: Canadian Mineralogist, v. 27, p. 593-600.

Caté, A., Mercier-Langevin, P., Ross, P.-S., Duff, S., Hannington, M., Dubé, B., and Gagné, S., 2015. Geology and gold enrichment processes at the Paleoproterozoic Lalor auriferous volcanogenic massive sulphide deposit, Snow Lake, Manitoba, *In:* Targeted Geoscience Initiative 4: Contributions to the Understanding of Volcanogenic Massive Sulphide Genesis and Exploration Methods Development, (eds) J.M. Peter and P. Mercier-Langevin; Geological Survey of Canada: Open File xxxx, p. xx-xx.

Caté, A., Mercier-Langevin, P., Ross, P.-S., Duff, S., Hannington, M., Dubé, B., and Gagné, S., 2013a, The Paleoproterozoic Lalor VMS deposit, Snow Lake, Manitoba: preliminary observations on the nature and architecture of the gold- and base metal-rich ore and alteration zones: Geological Survey of Canada, Open File 7483, 19 p.

Caté, A., Mercier-Langevin, P., Ross, P.-S., Duff, S., Hannington, M., Dubé, B., and Gagné, S., 2013b, Preliminary observations on the geological environment of the Paleoproterozoic auriferous volcanogenic massive sulphide deposit of Lalor, Snow Lake, Manitoba: Geological Survey of Canada, Open File 7372, 13 p.

Caté, A., Mercier-Langevin, P., Ross, P.-S., and Simms, D., 2014a. GS-8 Structural controls on geometry and ore distribution in the Lalor auriferous VMS deposit, Snow Lake, west-central Manitoba (part of NTS 63K16): preliminary results from underground mapping; Manitoba Mineral Resources, Manitoba Geological Survey, Report of Activities 2014, p. 104-115.

Caté, A., Mercier-Langevin, P., Ross, P.-S., Duff, S., Hannington, M., Gagné, S., and Dubé, 2014b. Insights on the chemostratigraphy of the volcanic and intrusive rocks of the Lalor auriferous volcanogenic massive-sulphide deposit host succession, Snow Lake, Manitoba; Geological Survey of Canada, Current Research 2014-6, 20 p.

Chen, T.T., and Petruk, W., 1980, Mineralogy and characteristics that affect recoveries of metals and trace elements from the ore at Heath Steele Mines, New Brunswick: Canadian Institute of Mining and Metallurgy Bulletin v. 73, p. 167-178.

Cook, N.J., Hoefs, J., 1997, Sulphur isotope characteristics of metamorphosed Cu-(Zn) volcanogenic massive sulfide deposits in the Norwegian Caledonides: Chemical Geology, v.135, p. 307-324.

Corriveau, L., and Spry, P.G., 2014, Metamorphosed hydrothermal ore deposits, in Scott, S.D., ed., Geochemistry of Mineral Resources, Treatise on Geochemistry, Elsevier, New York, v. 12.

Craig, J.R., and Simpson, C., 1991, Rotational fabrics in pyrite from Ducktown, Tennessee: Economic Geology, v. 86, p. 1737-46.

Craig, J.R., and Vokes, F.M., 1993, The metamorphism of pyrite and pyritic ores: an overview: Mineralogical Magazine, v. 57, p. 3-18.

Crowe D.E., 1994, Preservation of original hydrothermal $\delta^{34}S$ values in greenschist to upper amphibolite volcanogenic massive sulfide deposits: Geology, v. 22, p. 873-876.

Duff, S., Hannington, M.D., Caté, A., Mercier-Langevin, and Kjarsgaard, I.M., 2015. Major ore types of the Paleoproterozoic Lalor auriferous volcanogenic massive sulphide deposit, Snow Lake, Manitoba, In: Targeted Geoscience Initiative 4: Contributions to the Understanding of Volcanogenic Massive Sulphide Deposit Genesis and Exploration Methods Development, (ed.) J.M. Peter and P. Mercier-Langevin; Geological Survey of Canada, Open File 7853, p. 147–170.

Engelbert, M.S., Friesen, V., Gibson, H., and Lafrance, B., 2014a, Volcanic reconstruction of the productive VMS ore interval in the Paleoproterozoic Chisel sequence, Snow Lake, Manitoba: Geological Association of Canada–Mineralogical Association of Canada, Joint Annual Meeting, Fredericton, May 20–22, 2014, Program with Abstracts, p. 83–84.

Engelbert, M.S., Gibson, H.L., Lafrance, B., 2014b, Geologic Setting, Mineralogy, and Geochemistry of the Paleoproterozoic Photo Lake VMS Deposit, Snow Lake, Manitoba, PDAC-SEG Student Minerals Colloquium, March 3, (poster presentation).

Fedorowich, J., Stauffer, M., and Kerrich, R., 1991, Structural setting and fluid characteristics of the Proterozoic Tartan Lake gold deposit, Trans-Hudson Orogen, northern Manitoba: Economic Geology, v. 86, p. 1434–1467.

Froese, E., and Gasparrini, E., 1975, Metamorphic zones in the Snow Lake area, Manitoba: Canadian Mineralogist, v. 13, p. 162–167.

Gagné, S., Beaumont-Smith, C.J., Williams-Jones, A.E., and Hynes, A., 2007, Investigation of a Pb-Ag-Au–rich hangingwall in lens 4 of the Chisel North mine, Snow Lake, Manitoba (NTS 63K16): preliminary results; in Report of Activities 2007, Manitoba Science, Technology, Energy and Mines, Manitoba Geological Survey, p. 43–50.

Galley, A. G., Syme, R., and Bailes, A. H., 2007, Metallogeny of the Paleoproterozoic Flin Flon Belt, Manitoba and Saskatchewan, *in* Goodfellow, W. D., ed., Mineral Deposits of Canada: A

synthesis of major deposit types, district metallogeny, the evolution of geological provinces, and exploration methods. Special Publication 5, Geological Association of Canada, Mineral Deposits Division, p. 509-531.

Galley, A.G., Bailes, A.H., and Kitzler, G., 1993, Geological setting and hydrothermal evolution of the Chisel Lake and North Chisel Zn–Pb–Cu–Ag–Au massive sulphide deposits, Snow Lake, Manitoba: Exploration and Mining Geology, v. 2, p. 271–295.

Gibson, H., Engelbert, M.S., Lafrance, B., Friesen, V., DeWolfe, M., Tinkham, D.K., and Bailes, A.H., 2014, Reconstruction of the ore interval and environment for the Paleoproterozoic Lost and Ghost Lake VMS deposits, Snow Lake, Manitoba: Geological Association of Canada–Mineralogical Association of Canada, Joint Annual Meeting, Fredericton, May 20–22, 2014, Program with Abstracts, p. 102.

Hannington, M.D., Barrie, C.T., and Bleeker, W., 1999, The Giant Kidd Creek volcanogenic massive sulfide deposit, western Abitibi Subprovince, Canada: Economic Geology Monograph 10, p.1-30

Healy, R.E., and Petruk, W., 1988, Mineralogical characteristics that affect metal recoveries from Cu, Zn, Pb and Ag ores of Manitoba: An Investigation of the mineralogy of the Trout Lake deposit: Canada Centre for Minerals and Energy Technology, Investigative Report IR 88-61, p. 181

Healy, R.E., and Petruk W., 1990, Petrology of Au-Ag-Hg alloys and 'invisible' gold in the Trout Lake massive sulfide deposit, Flin Flon, Manitoba: Canadian Mineralogist, v.28, p.189-206.

Huston, D.L., Sie, S.H., Suter, G.F., Cooke, D.R., and Both, R.A., 1995, Trace elements in sulfide minerals from eastern Australian volcanic-hosted massive sulfide deposits: Part I. Proton microprobe analyses of pyrite, chalcopyrite, and sphalerite, and Part II. Selenium levels in pyrite: comparison with $\delta^{34}S$ values and implications for the source of sulfur in volcanogenic hydrothermal systems: Economic Geology, v. 90, p. 1167-1196.

Huston, D.L., 2000, Gold in volcanic-hosted massive sulfide deposits: Distribution, genesis and exploration: Reviews in Economic Geology v. 13, p. 401-426.

Kraus, J., and Williams, P.F., 1999, Structural development of the Snow Lake allochthon and its role in the evolution of the southeastern Trans-Hudson Orogen in Manitoba, central Canada: Canadian Journal of Earth Sciences, v. 36, p. 1881–1899.

Lam, J., Tinkham, D.K., and Gibson, H. 2013: Identification of metamorphic assemblages and textures associated with gold mineralization at the Lalor deposit, Snow Lake, Manitoba; Geological Association of Canada–Mineralogical Association of Canada, Joint Annual Meeting, Winnipeg, May 22–24, 2013, Program with Abstracts, p. 127.

Lam, J., Tinkham, D.K., and Gibson, H., 2014, Characterization of gold occurrences with respect to metamorphism at the Lalor deposit, Snow Lake, Manitoba: Geological Association of

Canada–Mineralogical Association of Canada, Joint Annual Meeting, Fredericton, May 20–22, 2014, Program with Abstracts, p. 150–151.

Martin, P. 1966: Structural analysis of Chisel Lake orebody; Canadian Mining and Metallurgical Bulletin, v. 69, p. 208–214.

Menard, T., and Gordon, T.M., 1997, Metamorphic P-T paths from the eastern Flin Flon belt and Kisseynew domain, Snow Lake, Manitoba; Canadian Mineralogist, v. 35, p. 1093–1115.

Mercier-Langevin P., Hannington, M.D., Dubé B., Bécu V., 2011, The gold content of volcanogenic massive sulfide deposits: Mineralium Deposita, v. 46, p. 509–539.

Mercier-Langevin, P., Caté, A., and Ross, P.-S., 2014, Whole-rock oxygen isotope mapping, Lalor auriferous VMS deposit footwall alteration zones, Snow Lake, west-central Manitoba (NTS 63K16), Report of activities 2014, Manitoba Mineral Resources, Manitoba Geological Survey, p. 94-103.

Petruk, W., and Schnarr, J.R., 1981, An evaluation of the recovery of free and unliberated mineral grains, metals and trace elements in the concentrator of Brunswick Mining and Smelting Corp. Ltd.: Canadian Institute of Mining and Metallurgical Bulletin, v. 74, p. 132-159.

Petruk, W., and Wilson, J.M., 1993, Silver and gold in some Canadian volcanogenic base metal deposits, in Y.T. Maurice (ed.), Proc. 8th Quadrennial IAGOD Symposium, Ottawa, Schweizerbart'sche, Stuttgart, p. 105-117.

Polito P., Kyser, K., Lawie, D., Cook, S., Oates, C., 2007, Application of sulphur isotopes to discriminate Cu-Zn VHMS mineralization from barren Fe sulphide mineralization in the greenschist to granulite facies Flin-Flon - Snow Lake - Hargrave River region: Geochemistry, Exploration, Analysis, Environment, v. 7, p. 129-138.

Sangster D.F., 1972, Isotopic Studies of Ore-Leads in the Hanson Lake - Flin Flon - Snow Lake Mineral Belt, Saskatchewan and Manitoba: Canadian Journal of Earth Sciences, v. 9, p. 500-513.

Sangster, D.F., 1978, Isotopic studies of ore-leads of the circum-Kisseynew volcanic belt of Manitoba and Saskatchewan: Canadian Journal of Earth Sciences, v.15, p. 1112-1121.

Shanks, W.C., 2001, Stable Isotopes in Seafloor Hydrothermal Systems: Vent fluids, hydrothermal deposits, hydrothermal alteration, and microbial processes: Reviews in Mineralogy and Geochemistry, v. 43, p. 468-525.

Tinkham, D.K. 2013, A model for metamorphic devolatilization in the Lalor deposit alteration system, Snow Lake, Manitoba; Geological Association of Canada–Mineralogical Association of Canada, Joint Annual Meeting, Winnipeg, May 22–24, 2013, Program with Abstracts, p. 187.

Thorpe, R.I., 1999, The lead isotope linear array for volcanogenic massive sulfide deposits of the Abitibi and Wawa subprovinces, Canadian Shield: Economic Geology Monograph 10, p. 555-576.

Thorpe, R.I., 2008. Release of lead isotope data in 4 databases: Canadian, western Superior, foreign, and whole rock and feldspar: Geological Survey of Canada Open File Report 5664, 42 p.

Tomkins, A.G., 2007, Three mechanisms of ore re-mobilisation during amphibolite facies metamorphism at the Montauban Zn–Pb–Au–Ag deposit: Mineralium Deposita, v. 42, p. 627-637.

Tomkins, A.G., Frost, R.B., Pattison, D.R.M., 2006, Arsenopyrite melting during metamorphism of sulfide ore deposits: Canadian Mineralogist, v. 44, p. 1045-1062.

Zaleski, E., Froese, E. and Gordon, T. M. 1991: Metamorphic petrology of Fe-Zn-Mg-Al alteration at the Linda volcanogenic massive sulfide deposit, Snow Lake, Manitoba; Canadian Mineralogist, v. 29, no. 4, p. 995–1017.

APPENDIX A

Whole Rock Geochemistry

Appendix A: Whole rock geochemistry

Analysis	Unit	D.L.	Analysis Method	SD-LAL-501 (Type 3)	SD-LAL-503 (Type 3)	SD-LAL-505 (Type 3)	SD-LAL-507 (Type 3)	SD-LAL-508 (Type 3)
SiO2	%	0.01	FUS-ICP	13.9	36.19	45.23	52.88	52.07
Al2O3		0.01	FUS-ICP	6.03	11.42	10.24	13.21	1.15
FeO		0.1	TITR	29.6	4.8	3.8	2.2	3.1
Fe2O3		0.01	FUS-ICP	3.01	3.13	2.52	0.43	0.35
MnO		0.001	FUS-ICP	0.2	0.277	0.188	0.286	0.579
MgO		0.01	FUS-ICP	10.14	19.39	12.76	7.94	15.71
CaO		0.01	FUS-ICP	4.23	8.98	14.65	14.07	23.04
Na2O		0.01	FUS-ICP	0.05	0.17	0.1	0.09	0.04
K2O		0.01	FUS-ICP	0.02	0.08	0.04	0.06	< 0.01
TiO2		0.001	FUS-ICP	0.115	0.142	0.168	0.278	0.145
P2O5		0.01	FUS-ICP	0.02	0.12	0.02	0.08	< 0.01
LOI		N/A	FUS-ICP	1.21	0.85	0.26	0.235	0.835
C-Total		0.01	IR	0.57	0.45	0.15	0.15	0.41
CO2		0.01	IR	1.85	1.25	0.37	0.32	1.26
Total S		0.01	IR	22.4	3.65	2.93	1.15	0.54
F	ppm	0.01	FUS-ISE	< 0.01	0.17	< 0.01	0.01	0.01
Total	%	N/A	N/A	93.35	90.90	93.43	93.38	99.23
Au	ppm	0.03/0.005	FA-GRA/FA-AA	0.639	8	8.44	8.65	3.58
Ag		1/3	TD-MS/FA-GRA	16	65.5	259	186	184
As		0.1	AR-MS	42.6	6.3	1.8	3	13
B		1	PGNAA	< 1	< 1	< 1	< 1	< 1
Ba		3	FUS-ICP	< 3	10	8	11	< 3
Be		1	FUS-ICP	< 1	2	< 1	1	1
Bi		0.02	AR-MS	0.4	0.59	< 0.02	0.05	3.83
Cd		0.2	TD-MS	180	73.5	17.9	7.7	3.5
Co		0.5	TD-MS	35.6	67	26.6	2.6	2.5
Cr		1	TD-MS	7	< 1	6	< 1	3
Cs		0.1	FUS-MS	< 0.1	< 0.1	< 0.1	< 0.1	< 0.1
Cu		10/0.5/50	FUS-MS/TD-MS/FUS-Na2O2	3320	> 10000	8065	3760	242.5
Ga		1	FUS-MS	9	17	25	14	3
Ge		0.5	FUS-MS	0.7	1.1	1.6	0.5	1.1
Hf		0.1	FUS-MS	1.3	2.4	1.8	2.2	1
Hg		0.005	Hg-FIMS/ICP-OES	31.300	12.400	3.780	6.510	1.490
In		0.1	FUS-MS	0.2	0.5	0.1	< 0.1	< 0.1
Li		1	TD-MS	3	6	2	4	5
Mo		2/1	FUS-MS/TD-MS	3.5	2	1.5	0.5	0.5
Nb		0.2	FUS-MS	2.6	6	4	5.4	3.2
Ni		1	TD-MS	18	6	10	4	4
Pb		100/2	FUS-Na2O2/TD-MS	1840	4130	54700	51100	29600
Sb		0.02	AR-MS	119	0.08	0.19	0.16	< 0.02
Sc		1	FUS-ICP	8	14	10	13	11
Se		1	NP-MS	145	46	229	171	148
Sn		1	FUS-MS	4	16	26	6	< 1
Sr		2	FUS-ICP	16	32	50	77	14
Ta		0.01	FUS-MS	0.18	0.29	0.16	0.24	0.18
Th		0.05	FUS-MS	0.92	2.36	1.6	1.96	2.81
U		0.01	FUS-MS	0.54	2.63	3.89	2.59	0.64
V		5	FUS-ICP	6	7	7	9	6
W		0.5	FUS-MS	4.4	2.5	1	1.5	< 0.5
Y		0.5	FUS-MS	14.3	35	33	30.4	15.8
Zn		0.5/100	TD-MS/FUS-Na2O2	87800	25400	996	278	663
Zr		1	FUS-MS	42	79	57	74	35

Appendix A: Whole rock geochemistry (cont.)

Analysis	Unit	SD-LAL-509 (Type 3)	SD-LAL-512 (Type 1)	SD-LAL-513 (Type 1)	SD-LAL-514 (Type 1)	SD-LAL-515 (Type 1)	SD-LAL-518 (Type 1)	SD-LAL-520 (Type 1)	SD-LAL-522 (Type ?)
SiO2	%	47.84	3.63	4.04	2.47	2	12.95	8.76	51.13
Al2O3		11.54	0.43	0.31	0.13	0.11	0.61	1.83	8.88
FeO		2.6	25.6	16.7	16.7	18.5	21.8	11.7	11.4
Fe2O3		0.8	7.66	32.77	9.94	8.25	3.82	39.69	8.68
MnO		0.256	0.088	0.034	0.115	0.095	0.181	0.023	0.298
MgO		11.95	0.28	0.17	0.1	0.05	0.22	0.14	8.14
CaO		18.56	1.77	0.18	6.46	0.21	0.13	0.12	0.69
Na2O		0.09	0.02	0.02	< 0.01	< 0.01	0.05	0.02	0.18
K2O		0.03	0.02	0.01	< 0.01	< 0.01	0.07	0.02	0.54
TiO2		0.214	0.012	0.019	0.003	0.001	0.016	0.064	0.379
P2O5		< 0.01	< 0.01	< 0.01	0.01	< 0.01	< 0.01	< 0.01	0.13
LOI		0.135	0.82	0.095	3.645	0.09	0.055	0.01	0.15
C-Total		0.11	0.41	0.06	1.61	0.06	0.06	0.01	0.09
CO2		0.16	1.23	0.13	5.68	0.12	< 0.01	0.01	0.21
Total S		0.9	38.8	47	34	39.2	36.8	44.3	8.45
F	ppm	0.12	< 0.01	< 0.01	< 0.01	< 0.01	< 0.01	< 0.01	< 0.01
Total	%	95.19	80.77	101.54	80.86	68.69	76.76	106.70	99.35
Au	ppm	189	2.34	2.84	2.51	3.08	0.131	1.75	2.02
Ag		837	96	89	89	68	7	43	22
As		94.8	32.1	26.7	106	335	30.6	57.3	163
B		< 1	< 1	< 1	< 1	< 1	4	< 1	5
Ba		4	5	< 3	< 3	< 3	6	19	26
Be		< 1	< 1	< 1	< 1	< 1	< 1	< 1	< 1
Bi		0.1	0.12	0.15	0.5	0.47	1.18	0.42	9.19
Cd		11.3	509	166	551	683	421	18.8	12.1
Co		1.9	162	142	134	84.6	132	172	23.6
Cr		< 1	< 1	7	< 1	< 1	3	< 1	2
Cs		< 0.1	< 0.1	< 0.1	< 0.1	< 0.1	< 0.1	< 0.1	0.4
Cu		6790	13700	27400	41000	44800	937	37700	12700
Ga		13	8	3	8	13	17	6	16
Ge		0.8	4.1	3.1	2.2	4.4	2	0.9	1.3
Hf		1.8	< 0.1	< 0.1	< 0.1	0.2	0.1	0.2	1.2
Hg		2.570	54.000	25.400	75.400	91.100	434.000	5.610	0.606
In		< 0.1	0.5	0.2	0.8	0.8	0.1	0.2	0.1
Li		3	1	1	< 1	< 1	3	1	38
Mo		0.5	10.5	15	7.5	6	6.5	4.5	3
Nb		5.9	< 0.2	0.4	0.4	< 0.2	< 0.2	0.6	4.3
Ni		4	19	8	6	5	9	3	6
Pb		8760	2810	59	72	88	55	126	161
Sb		0.09	15.8	29.8	481	500	266	135	6.37
Sc		11	1	< 1	< 1	< 1	1	2	18
Se		129	58	107	91	103	37	175	66
Sn		2	14	18	43	76	7	26	3
Sr		54	8	3	12	2	4	4	15
Ta		0.24	0.02	0.03	0.02	0.03	0.02	0.06	0.22
Th		1.44	0.12	0.1	0.05	< 0.05	0.18	0.41	2.31
U		0.95	1.17	2.24	1.33	0.54	1.68	0.66	1.16
V		12	< 5	< 5	< 5	< 5	7	7	46
W		< 0.5	1.1	1.2	1.8	0.8	< 0.5	1.7	3.9
Y		21	1.1	< 0.5	1.3	< 0.5	< 0.5	1.2	9.8
Zn		152	209000	67400	238000	302000	254000	12800	1860
Zr		64	2	2	< 1	7	4	9	47

Appendix A: Whole rock geochemistry (cont.)

Analysis	Unit	SD-LAL-523 (Type 3)	SD-LAL-524 (Type 3)	SD-LAL-525 (Type 3)	SD-LAL-526 (Type 3)	SD-LAL-527 (Type 3)	SD-LAL-529 (Type 4)	SD-LAL-531 (Type 3)	SD-LAL-535 (Type 3)
SiO2	%	20.94	44.77	76.87	12.32	8.95	76.1	61.54	13.9
Al2O3		12.65	9.44	1.02	7.36	5.02	6.23	13.89	8.34
FeO		2.8	3.2	1.8	4.7	6.5	3.5	2.2	3.2
Fe2O3		9.74	< 0.01	0.01	0.41	8.27	0.59	1.42	3.16
MnO		0.151	0.14	0.084	0.326	0.154	0.228	0.284	0.221
MgO		21.94	9.09	6.6	18.53	12.84	4.69	6.52	11.45
CaO		10.02	16.22	8.33	20.92	9.6	1.62	8.22	29.18
Na2O		0.04	0.11	0.04	0.01	0.03	0.07	0.22	0.06
K2O		0.01	0.05	< 0.01	0.01	0.01	0.34	0.78	0.02
TiO2		0.593	0.053	0.015	0.133	0.219	0.113	0.237	0.396
P2O5		0.28	< 0.01	0.01	0.02	0.19	< 0.01	0.08	0.2
LOI		4.165	0.435	0.25	14.975	8.21	0.04	0.04	14.05
C-Total		1.84	0.2	0.12	6.45	3.62	0.03	0.02	6.1
CO2		6.49	0.67	0.38	23.5	12.8	< 0.01	0.06	22
Total S		7.13	2.57	0.59	2.96	15.1	1.32	0.87	3.36
F	ppm	< 0.01	< 0.01	0.03	0.1	< 0.01	0.09	0.1	0.12
Total	%	98.79	86.95	96.12	112.62	91.51	94.87	96.38	115.64
Au	ppm	2.09	5.66	44.1	1.06	4.57	3.78	104	1.56
Ag		36	593	245	26	161	45.5	670	27
As		10.6	3	1.5	2	16.5	21.5	87.4	34.1
B		< 1	< 1	< 1	< 1	3	2	< 1	< 1
Ba		< 3	8	< 3	< 3	< 3	64	155	4
Be		< 1	2	1	< 1	< 1	< 1	< 1	< 1
Bi		0.17	0.15	0.17	0.25	1.84	5.8	100	3.95
Cd		4.4	25.7	6.8	63.9	250	4.1	7.1	16.8
Co		26.5	3.5	2.1	108	192	34.1	3.6	47.9
Cr		2	< 1	7	< 1	< 1	5	< 1	< 1
Cs		< 0.1	< 0.1	< 0.1	< 0.1	< 0.1	0.2	0.3	< 0.1
Cu		2455	418	693	2115	65200	5485	4500	3230
Ga		22	10	2	9	8	10	15	11
Ge		0.9	0.8	1.3	0.7	0.6	1.1	1	0.6
Hf		1.1	0.6	0.2	1.9	0.6	1.3	2.3	1.1
Hg		1.240	4.010	3.360	9.520	46.400	2.700	4.390	3.710
In		0.1	< 0.1	< 0.1	0.3	0.9	0.1	< 0.1	0.1
Li		3	14	9	2	2	26	5	8
Mo		< 2	0.5	< 2	1.5	5	4	2	2
Nb		5.8	1.4	< 0.2	3.8	2.3	2.4	4.5	5.1
Ni		6	6	5	6	10	4	3	5
Pb		3300	5030	2520	2520	1490	198	5030	2520
Sb		0.84	2.23	0.23	0.19	0.1	23.3	15.8	3.51
Sc		24	7	4	9	15	7	12	19
Se		72	697	203	58	59	23	60	55
Sn		5	3	1	3	5	1	3	6
Sr		35	99	11	44	23	21	47	76
Ta		0.25	0.04	0.05	0.19	0.1	0.18	0.3	0.2
Th		2.9	1.8	0.33	1.73	1.33	1.04	1.69	2.27
U		2.06	0.38	0.09	1.1	0.59	0.76	1.07	1.06
V		202	19	12	9	35	9	7	61
W		1.2	< 0.5	< 0.5	1.5	1.5	< 0.5	1.9	1
Y		20.3	9.5	3.4	21.4	17.8	12.1	21.3	20.3
Zn		2010	1920	510	27100	95100	1510	781	5410
Zr		50	20	8	66	25	48	78	52

Appendix A: Whole rock geochemistry (cont.)

Analysis	Unit	SD-LAL-541 (Type 2)	SD-LAL-544 (Type 2)	SD-LAL-547 (Type 4)	SD-LAL-556 (Type 1)	SD-LAL-558 (Type 2)	SD-LAL-560 (Type 3)	SD-LAL-563 (Type 2)	SD-LAL-564 (Type 2)
SiO2	%	57.67	32.86	21.11	43.12	59.14	41.54	44.82	77.09
Al2O3		3.3	3.37	7.18	14.02	5.79	5.47	14.19	6.32
FeO		11.2	12.6	7.8	11.2	9.1	4.1	16.8	4.5
Fe2O3		4.82	13.79	8.43	3.81	6.19	1.99	< 0.01	0.62
MnO		0.136	0.207	0.219	0.137	0.204	0.742	0.289	0.089
MgO		4.85	4.62	5.61	10.27	5.87	17.99	14.93	7.69
CaO		2.18	12.05	7.6	10.76	0.97	16.5	0.59	0.23
Na2O		0.17	0.08	0.14	0.23	0.08	0.11	0.09	0.08
K2O		0.29	0.05	0.07	0.66	0.86	0.03	0.21	0.38
TiO2		0.004	0.008	0.309	0.707	0.096	0.126	0.467	0.083
P2O5		0.01	< 0.01	0.07	0.23	0.05	0.02	0.22	0.01
LOI		0.675	0.04	0.05	0.35	0.055	2.485	0.225	0.035
C-Total		0.3	0.02	0.02	0.005	0.02	1.12	0.1	0.01
CO2		1.05	0.06	0.08	0.005	0.09	3.85	0.35	0.06
Total S		8.05	14.7	16.6	1.48	6.91	2.06	3.41	0.6
F	ppm	< 0.01	< 0.01	< 0.01	0.08	< 0.01	< 0.01	0.24	0.19
Total	%	94.71	94.46	75.29	96.98	95.43	98.13	96.69	97.80
Au	ppm	11.5	212	3.2	0.404	3.3	3.56	3.12	8
Ag		49	149	181	6	107	117	14	35
As		15.3	236	16.7	188	1	20.9	171	250
B		< 1	< 1	< 1	2	< 1	< 1	< 1	< 1
Ba		62	9	7	92	141	4	10	26
Be		< 1	4	< 1	< 1	< 1	3	< 1	< 1
Bi		2.6	0.18	0.18	< 0.02	0.1	0.22	< 0.02	0.09
Cd		15	29.3	251	0.5	58.6	7.2	13.8	11.6
Co		43.8	146	19.8	52.1	19.4	7.3	55.4	5
Cr		< 1	< 1	4	3	5	< 1	7	4
Cs		0.1	< 0.1	< 0.1	0.2	0.4	< 0.1	0.2	0.2
Cu		73000	108000	73700	367	52900	3030	2920	2535
Ga		8	9	11	17	10	8	17	9
Ge		0.9	2.7	3.2	0.9	1.5	0.8	0.9	0.7
Hf		< 0.1	< 0.1	1.5	1.1	0.3	1.3	1.1	1.4
Hg			2.370	52.500	0.117	0.849	1.680	0.062	0.160
In		0.5	0.5	1	< 0.1	0.4	< 0.1	< 0.1	< 0.1
Li		6	2	4	23	12	7	45	27
Mo		2.5	3	23	0.5	< 2	4.5	2	0.5
Nb		0.7	< 0.2	5.9	5.2	< 0.2	3	8.5	2.5
Ni		3	4	9	8	4	5	7	3
Pb		67	234	3120	29	337	5000	61	67
Sb		0.37	1.69	0.08	2.32	0.1	5.57	0.48	0.64
Sc		2	2	15	42	7	10	22	8
Se		142	141	68	5	45	163	34	2
Sn		5	3	106	< 1	5	4	1	< 1
Sr		14	100	52	27	37	35	5	5
Ta		0.03	0.04	0.24	0.27	0.07	0.12	0.24	0.16
Th		< 0.05	< 0.05	4.27	2.92	0.25	1.31	3	1
U		0.03	0.05	2.17	1.32	0.12	0.89	0.86	0.63
V		6	10	86	385	45	< 5	174	< 5
W		0.8	105	28	< 0.5	< 0.5	0.9	10.4	< 0.5
Y		1.3	1.9	9.2	14	3.6	20.6	8.5	14.7
Zn		3170	6370	98400	267	3720	755	11300	1140
Zr		< 1	1	67	50	10	47	43	54

Appendix A: Whole rock geochemistry (cont.)

Analysis	Unit	SD-LAL-565 (Type 3/4)	SD-LAL-567 (Type 2)	SD-LAL-568 (Type 3)	SD-LAL-569 (Type 3)	SD-LAL-570 (Type 3)	SD-LAL-572 (Type 2)	SD-LAL-576 (Type ?)	SD-LAL-580 (Type 2)
SiO2	%	36.99	50.33	37.19	13.09	72.14	55	64.36	42.46
Al2O3		17.43	5.46	0.31	4.8	7.67	15.31	9.28	10.61
FeO		12.3	22	10.3	26.2	4.6	10.7	3.3	19.8
Fe2O3		3.1	0.53	10.59	2.93	2.46	1.38	0.84	3.08
MnO		0.538	0.119	0.445	0.169	0.107	0.181	0.047	0.199
MgO		15.95	4.73	12.21	4.22	6.1	11.98	5.75	9.76
CaO		0.3	0.24	15.49	1.96	1.29	1.26	1.44	1.42
Na2O		0.14	0.04	0.03	0.05	0.05	0.08	0.14	0.09
K2O		2	0.06	< 0.01	0.04	0.41	< 0.01	1.29	0.47
TiO2		0.293	0.136	0.083	0.087	0.153	0.746	0.179	0.51
P2O5		0.01	0.04	0.09	0.02	0.04	0.69	< 0.01	0.34
LOI		0.06	0.065	0.155	0.12	0.11	0.065	0.7	0.02
C-Total		0.02	0.04	< 0.01	< 0.01	0.04	0.07	0.33	0.02
CO2		0.1	0.09	0.26	0.19	0.18	0.06	1.07	0.02
Total S		0.67	11.5	11.9	24.4	2.21	0.32	2.25	10.4
F	ppm	0.35	< 0.01	< 0.01	< 0.01	0.15	0.17	0.16	< 0.01
Total	%	89.90	95.38	99.05	78.28	97.56	97.84	90.98	99.20
Au	ppm	3.38	31.6	3	1.11	0.837	6	1.34	0.36
Ag		22	140	51	73	37	5	13	19
As		14.3	377	11.6	12.1	10	48.7	48.2	1.1
B		< 1	< 1	< 1	< 1	< 1	3	< 1	< 1
Ba		327	9	< 3	< 3	162	< 3	87	82
Be		< 1	< 1	< 1	< 1	1	< 1	< 1	< 1
Bi		1.75	0.09	0.18	7.57	0.28	0.07	23	0.19
Cd		24.4	83.8	66.3	366	5.1	2	225	18.1
Co		78.2	127	4.4	2.5	5.9	29	15.8	500
Cr		4	6	< 1	< 1	1	< 1	3	< 1
Cs		0.9	< 0.1	< 0.1	< 0.1	0.3	< 0.1	0.4	0.4
Cu		3430	46500	26200	41900	4355	95.5	1840	19500
Ga		29	8	3	9	10	17	11	13
Ge		1.4	0.7	1.1	0.5	1	1	0.8	1
Hf		4.2	0.4	0.9	0.9	1.4	2	3	1.2
Hg		0.045	0.717	8.880	12.600	0.386	0.135	1.060	0.068
In		0.1	0.5	0.4	0.3	0.1	< 0.1	< 0.1	0.1
Li		28	9	14	5	35	37	13	16
Mo		< 2	2.5	16.5	2.5	2.5	< 2	2	3
Nb		9.3	0.8	2.4	2.2	3	8.8	7.1	3.8
Ni		4	13	5	7	3	3	4	13
Pb		223	59	559	11500	3930	38	173	85
Sb		0.85	1.25	0.86	0.29	8.28	4	0.15	0.18
Sc		17	10	9	4	9	31	9	30
Se		8	119	134	92	21	2	13	154
Sn		3	8	60	37	2	2	2	2
Sr		15	4	10	14	15	7	31	25
Ta		0.17	0.04	0.1	0.07	0.15	0.45	0.37	0.19
Th		3.83	0.22	1.33	0.66	1.29	5.75	2.57	2.44
U		1.96	0.12	0.64	0.67	1.37	2.29	1.27	0.67
V		21	50	12	< 5	< 5	157	< 5	163
W		< 0.5	1.4	1	2.9	0.6	< 0.5	0.9	7.1
Y		34.2	4.7	11.5	10.9	13.4	17.3	28.1	14
Zn		49100	9500	22200	148000	6230	608	52900	4200
Zr		144	12	31	31	51	97	102	52

Appendix A: Whole rock geochemistry (cont.)

Analysis	Unit	SD-LAL-582	SD-LAL-584	SD-LAL-585	SD-LAL-586	SD-LAL-587	SD-LAL-588	SD-LAL-592	SD-LAL-595
		(Type 1/3)	(Type 3)	(Type 3)	(Type 3)	(Type 3)	(Type 1)	(Type 1)	(Type 1)
SiO2	%	21.62	72.69	32.25	50.56	1.22	18.68	36.35	6.01
Al2O3		2.56	3.12	6.93	6.99	0.62	7.31	11.15	1.88
FeO		22.5	8.2	10.1	5	17.1	28.9	10.7	16.7
Fe2O3		0.24	0.78	1.31	< 0.01	10.79	19.42	2.03	25.99
MnO		0.26	0.212	0.165	0.148	0.115	0.144	0.057	0.08
MgO		1.11	3.72	4.3	6.05	1.62	2.58	12.04	1.25
CaO		6.84	2.88	8.3	5.7	14.71	1.01	4.6	2.26
Na2O		0.08	0.09	0.02	0.06	< 0.01	0.68	0.19	0.02
K2O		< 0.01	0.09	0.01	0.01	< 0.01	1.98	0.09	0.02
TiO2		0.062	0.009	0.03	0.074	0.012	0.352	0.223	0.059
P2O5		0.02	< 0.01	0.12	0.14	0.01	0.06	0.23	0.03
LOI		0.02	0.05	0.06	0.035	8.24	0.025	0.05	0.09
C-Total		0.01	0.01	0.005	0.01	3.68	0.02	0.01	0.005
CO2		0.03	0.09	0.06	0.06	12.8	0.03	0.09	0.09
Total S		23.2	4.08	13.8	8.74	31.5	25.1	9.03	39.2
F	ppm	< 0.01	< 0.01	< 0.01	< 0.01	< 0.01	< 0.01	< 0.01	< 0.01
Total	%	78.55	96.02	77.46	83.58	102.42	106.29	86.84	93.68
Au	ppm	0.177	3380	22.8	1.64	0.784	0.928	2.17	26.8
Ag		45	5500	57	12	8	22	27	168
As		40.5	198	9.9	10.8	132	148	211	224
B		1	2	2	< 1	< 1	2	1	< 1
Ba		9	8	< 3	< 3	< 3	186	5	< 3
Be		< 1	< 1	< 1	< 1	< 1	< 1	< 1	< 1
Bi		3.52	0.19	8.07	0.21	0.11	0.03	< 0.02	< 0.02
Cd		327	8.9	370	266	274	57.7	223	144
Co		9.9	7.2	78.6	13.8	189	72.7	16.3	98.8
Cr		< 1	3	< 1	2	< 1	7	< 1	1
Cs		< 0.1	< 0.1	< 0.1	< 0.1	< 0.1	0.4	< 0.1	< 0.1
Cu		1135	11700	6200	573.5	1870	877.5	3055	82700
Ga		5	6	20	15	8	9	13	7
Ge		< 0.5	1.4	1.7	1.5	5.9	0.6	1.3	3.7
Hf		0.3	< 0.1	0.5	1.2	0.1	0.9	2.3	0.2
Hg		131.000	16.400	17.800	18.500	24.400	12.800	16.100	23.300
In		0.3	0.1	0.4	0.3	0.3	0.1	1.5	0.3
Li		1	3	1	2	< 1	18	19	2
Mo		11	2	4	3	4	5.5	1.5	15
Nb		1.2	< 0.2	0.6	2.5	0.4	3.3	5.8	0.7
Ni		20	6	5	3	3	225	3	10
Pb		5000	5000	2590	3240	529	4780	1040	5000
Sb		0.27	2.13	0.87	0.51	6.02	1.43	0.44	1.63
Sc		6	2	4	9	< 1	21	4	5
Se		128	167	48	46	60	83	91	110
Sn		2	9	21	4	8	2	2	85
Sr		147	11	44	27	28	36	33	15
Ta		0.04	0.02	< 0.01	0.36	0.06	0.17	0.32	0.02
Th		0.75	0.08	0.47	1.11	0.2	2.31	1.95	0.24
U		2.25	0.11	2.18	2.69	1.43	5.87	1.1	1.69
V		34	17	21	37	< 5	128	< 5	20
W		0.8	< 0.5	0.9	1	< 0.5	< 0.5	2.6	< 0.5
Y		3.9	2	22.3	21.3	0.8	9.6	7.7	1.6
Zn		152000	2900	162000	129000	149000	27900	62400	63300
Zr		15	1	17	46	4	40	78	7

Appendix A: Whole rock geochemistry (cont.)

Analysis	Unit	SD-LAL-597	SD-LAL-598	SD-LAL-601	SD-LAL-604	SD-LAL-611	SD-LAL-612	SD-LAL-613	SD-LAL-615
		(Type 1)	(Type 1)	(Type ?)	(Type 3)	(Type 3)	(Type 3)	(Type 4)	(Type 4)
SiO2	%	23.91	17.23	42.3	35.65	51.67	37.88	62.67	46.07
Al2O3		2.84	1.68	13.09	13.62	4.83	10.12	6.33	8.17
FeO		< 0.1	4.8	13.5	13	5.4	8.4	4.2	22.7
Fe2O3		20.43	18.85	8	9.7	0.05	7.33	5.56	2.32
MnO		0.195	0.134	0.617	0.377	0.081	0.223	0.043	0.09
MgO		0.8	0.59	3.26	11.64	6.55	9.19	7.46	3.31
CaO		2.68	1.31	3.09	0.89	1.22	10.71	2.89	6.89
Na2O		0.3	0.03	0.18	0.05	0.06	0.26	0.14	0.07
K2O		0.02	0.01	4.27	0.36	0.03	0.08	0.08	0.02
TiO2		0.074	0.044	0.788	0.609	0.099	0.128	0.052	0.021
P2O5		0.03	0.02	0.56	0.49	0.03	0.09	0.06	0.03
LOI		0.28	0.025	0.045	0.035	0.285	0.275	0.15	0.03
C-Total		0.13	0.03	0.02	0.04	0.13	0.13	0.07	0.005
CO2		0.43	0.02	0.07	0.03	0.44	0.42	0.23	0.03
Total S		21.8	33.2	10.3	7.31	7.68	8.84	5.44	12.8
F	ppm	< 0.01	< 0.01	0.19	< 0.01	< 0.01	< 0.01	< 0.01	< 0.01
Total	%	73.92	77.97	100.09	93.80	78.56	94.08	95.38	102.56
Au	ppm	0.436	0.456	0.183	11.5	0.465	31	318	13
Ag		20	80	8	22.5	25	188	742	58
As		18.6	63.5	2.1	2.9	25.7	163	14.7	1.3
B		< 1	< 1	< 1	< 1	< 1	3	9	< 1
Ba		12	< 3	232	75	< 3	5	5	< 3
Be		< 1	< 1	< 1	< 1	< 1	< 1	< 1	< 1
Bi		0.45	0.13	0.58	0.56	9.94	0.28	0.45	0.05
Cd		755	438	37.4	5.3	377	24.3	12.1	1.7
Co		8.8	36.8	26.5	74.6	14	19.3	9.7	38.4
Cr		6	< 1	< 1	10	5	3	2	2
Cs		< 0.1	< 0.1	0.7	0.2	< 0.1	< 0.1	< 0.1	< 0.1
Cu		900.5	274.5	477.5	60500	1580	58400	33800	7285
Ga		7	11	17	18	9	13	9	12
Ge		0.9	0.9	0.5	0.8	0.8	0.9	0.9	0.8
Hf		0.4	0.2	1.4	1	1.1	1.1	0.5	< 0.1
Hg		45.200	303.000	9.680	0.408	18.100	2.570	5.540	0.379
In		1.4	0.2	< 0.1	0.4	0.1	0.4	0.6	0.2
Li		2	2	38	12	11	12	14	6
Mo		2.5	12.5	< 2	2	2.5	2.5	0.5	3
Nb		2	0.6	6.5	4.3	2.1	2.1	0.8	< 0.2
Ni		7	5	3	18	2	5	3	28
Pb		1500	5000	171	16	5000	3560	1230	167
Sb		1.07	17.2	0.09	1.26	1.99	28.8	0.12	0.11
Sc		6	4	42	57	4	7	8	3
Se		204	97	5	149	72	119	176	135
Sn		3	6	3	6	2	7	5	2
Sr		63	5	30	8	9	27	22	22
Ta		0.26	0.07	0.31	0.22	0.17	0.12	0.08	< 0.01
Th		1.64	0.25	4.47	3.15	0.71	0.83	0.5	0.11
U		6.74	0.65	1.54	1.1	0.44	0.5	0.18	0.95
V		58	24	320	441	5	< 5	< 5	< 5
W		< 0.5	< 0.5	4.4	< 0.5	0.9	1	1.1	< 0.5
Y		7.6	2.2	16.3	25.9	11.2	7.5	17.4	3.3
Zn		212000	234000	19200	742	111000	7400	4180	827
Zr		19	6	69	43	31	37	17	1

Appendix A: Whole rock geochemistry (cont.)

Analysis	Unit	SD-LAL-616	SD-LAL-617	SD-LAL-618	SD-LAL-626	SD-LAL-629	SD-LAL-633	SD-LAL-634	SD-LAL-635
		(Type 2)	(Type 2)	(Type 1)	(Type 4)	(Type 4)	(Type 1)	(Type 1)	(Type 1)
SiO2	%	78.74	61.87	2.65	36.67	49.94	15.54	23.12	8.47
Al2O3		6.6	3.66	0.63	5.45	15.02	7.68	8.59	7.03
FeO		4.6	14.9	8.5	28.2	13.7	30.8	15.2	8.7
Fe2O3		1.41	3.8	0.96	3.21	0.59	2.35	1.53	3.49
MnO		0.079	0.029	0.147	0.206	0.214	0.046	1.158	0.322
MgO		4.31	3.15	0.52	6.38	15.19	0.35	3.87	4.37
CaO		1.59	1.2	13.31	0.21	0.89	3.03	2.23	2.44
Na2O		0.05	0.03	< 0.01	0.08	0.06	0.97	0.18	0.13
K2O		1.19	0.27	< 0.01	0.19	< 0.01	0.99	0.68	0.05
TiO2		0.146	0.047	0.007	0.195	0.767	0.464	0.415	0.3
P2O5		0.02	0.01	0.01	0.07	0.4	0.17	0.04	0.07
LOI		0.05	0.05	6.075	0.155	0.085	0.105	0.15	0.15
C-Total		0.005	0.01	2.82	0.08	0.1	< 0.01	0.07	< 0.01
CO2		< 0.01	0.09	9.33	0.23	0.07	0.16	0.23	0.25
Total S		1.05	9.49	28.2	14.8	0.18	25.9	20.5	23.7
F	ppm	0.15	< 0.01	< 0.01	< 0.01	0.12	< 0.01	< 0.01	< 0.01
Total	%	99.88	99.16	97.06	96.44	97.25	99.86	88.46	93.27
Au	ppm	6.51	9.25	1.19	14.9	0.438	0.187	0.809	0.521
Ag		6	100	75	92	7	33	29	13
As		50.1	4.9	121	94.8	16.6	265	16.9	37.7
B		< 1	3	2	< 1	< 1	< 1	< 1	< 1
Ba		163	38	< 3	69	< 3	228	54	4
Be		< 1	< 1	< 1	< 1	< 1	< 1	< 1	< 1
Bi		0.09	2.3	2.22	15.7	6.27	0.66	0.21	0.14
Cd		0.2	10.2	667	41.6	1.8	303	336	1000
Co		11.5	14.9	226	208	42.7	75.6	121	101
Cr		5	1	4	14	10	< 1	5	4
Cs		0.5	0.1	< 0.1	0.1	< 0.1	< 0.1	0.5	< 0.1
Cu		835	14300	3075	66400	1240	5170	8375	156.5
Ga		9	6	12	8	18	7	14	12
Ge		0.7	0.7	4.6	0.6	0.9	1.6	1.1	0.7
Hf		1.2	0.7	< 0.1	0.4	1.4	1	1.5	1.1
Hg		0.052	1.950	32.700	0.314	0.054	98.200	189	593.000
In		< 0.1	0.1	0.4	1	< 0.1	1.2	0.5	0.9
Li		35	10	1	3	11	5	20	10
Mo		2	3	5.5	3	2	3.5	3.5	0.5
Nb		2.9	1.1	0.2	1.1	6.4	4	5.3	4.9
Ni		2	12	4	68	12	12	8	2
Pb		113	1900	5000	107	10	221	260	48
Sb		12.2	0.53	500	19.1	0.33	363	8.95	8.23
Sc		8	3	< 1	16	56	22	14	18
Se		13	28	50	143	3	58	115	55
Sn		1	1	25	19	< 1	3	5	6
Sr		15	7	20	5	10	132	17	17
Ta		0.11	0.06	0.06	0.03	0.28	0.27	0.3	0.28
Th		1.27	0.73	0.05	0.81	4.37	2.56	3.37	2.78
U		0.78	0.58	2.14	0.58	1.67	1.72	1.6	1.35
V		5	6	19	71	472	61	59	88
W		< 0.5	< 0.5	471	9.3	3.1	10.5	13.3	13
Y		6.8	7.5	0.8	6.6	12.8	8.4	6.3	11.3
Zn		352	5510	239000	3130	443	113000	1E+05	338000
Zr		46	22	1	16	71	41	61	47

Appendix A: Whole rock geochemistry (cont.)

Analysis	Unit	SD-LAL-636	SD-LAL-637	SD-LAL-638	SD-LAL-639	SD-LAL-640	SD-LAL-642	SD-LAL-647
		(Type 1)	(Type 1)	(Type 1)	(Type 1)	(Type 1)	(Type 1)	(Type 3)
SiO2	%	13.63	16.05	46.23	6.42	54.49	13.95	66.76
Al2O3		13.1	5.9	16.05	1.64	11.29	0.12	6.77
FeO		28.3	10.6	9.1	< 0.1	7	29	8.4
Fe2O3		11.85	36.21	6.45	17.1	3.58	24.94	3.31
MnO		0.374	0.042	0.376	0.13	0.4	0.024	0.13
MgO		2.74	1.95	14.37	1.67	11.43	0.06	3.7
CaO		4.63	0.61	0.2	0.29	0.64	0.48	0.2
Na2O		0.26	0.15	0.17	0.02	0.07	< 0.01	0.08
K2O		0.48	0.8	1.54	0.03	0.01	< 0.01	0.3
TiO2		0.39	0.136	0.555	0.039	0.476	0.002	0.106
P2O5		0.2	0.01	< 0.01	0.02	0.12	< 0.01	0.08
LOI		0.1	0.035	0.265	0.03	0.825	0.1	0.42
C-Total		0.03	0.01	0.13	0.005	0.34	0.06	0.19
CO2		0.17	0.06	0.4	0.03	1.31	0.14	0.65
Total S		25.7	39.6	3.6	28.2	1.28	32	3.4
F	ppm	< 0.01	< 0.01	0.24	< 0.01	0.22	< 0.01	< 0.01
Total	%	104.86	112.31	99.98	96.42	98.23	107.38	96.36
Au	ppm	1.51	0.121	0.687	3.76	0.272	0.386	33
Ag		54	12	6	13.5	4	62	35.5
As		5.4	12.1	38.8	15.5	20.2	1380	0.8
B		< 1	< 1	< 1	1	3	< 1	< 1
Ba		46	105	131	< 3	6	< 3	86
Be		< 1	< 1	< 1	< 1	< 1	< 1	< 1
Bi		0.02	0.2	0.07	2.33	8.61	0.75	0.6
Cd		11.8	3	1.3	1170	2.7	126	6.9
Co		384	14.1	40.5	93.1	19.4	12.6	45.1
Cr		9	5	18	3	30	4	6
Cs		0.3	0.2	0.8	< 0.1	< 0.1	< 0.1	0.1
Cu		19000	138.5	1295	3145	684.5	19400	30600
Ga		15	8	20	8	17	< 1	15
Ge		0.6	< 0.5	1	0.6	0.7	0.9	< 0.5
Hf		0.6	1.3	1.7	0.1	1	< 0.1	0.9
Hg		14.400	3.050	0.330	5.130	0.079	4.920	0.112
In		0.3	< 0.1	< 0.1	4.2	< 0.1	< 0.1	0.2
Li		15	13	34	2	5	< 1	7
Mo		2.5	15	0.5	0.5	2	2.5	< 2
Nb		3	3.6	7.9	0.3	2.7	< 0.2	0.7
Ni		20	19	4	6	5	103	3
Pb		232	1340	197	213	21	5000	64
Sb		1.01	29.8	22.2	0.36	0.38	12.6	0.1
Sc		32	8	28	3	28	< 1	9
Se		74	321	11	27	5	78	73
Sn		4	1	4	6	3	< 1	2
Sr		56	34	11	2	4	3	8
Ta		0.09	0.25	0.35	0.05	0.13	< 0.01	0.21
Th		1.48	2.93	0.82	0.12	0.79	< 0.05	1.16
U		1.11	7.91	0.49	0.12	0.38	0.23	0.45
V		194	12	110	14	107	< 5	143
W		13	1	3.1	1.9	20.4	< 0.5	0.7
Y		6	3.8	9	6.7	11.6	< 0.5	3.5
Zn		29100	1500	5440	408000	49700	65000	18600
Zr		25	57	64	5	39	< 1	34

Appendix A: Whole rock geochemistry (cont.)

Analysis	Unit	SD-LAL-648 (Type 1)	SD-LAL-649 (Type 2)
SiO2	%	25.02	55.15
Al2O3		2.82	11.68
FeO		14.9	15.5
Fe2O3		20.54	3.3
MnO		0.234	0.732
MgO		2.04	8.34
CaO		0.34	1.01
Na2O		0.18	0.24
K2O		0.14	< 0.01
TiO2		0.006	0.595
P2O5		0.02	0.33
LOI		0.025	0.09
C-Total		0.01	0.005
CO2		0.04	0.09
Total S		22.1	1.33
F	ppm	< 0.01	0.09
Total	%	89.12	98.47
Au	ppm	5.72	0.732
Ag		83.5	8
As		5480	36
B		2	2
Ba		14	< 3
Be		< 1	< 1
Bi		0.07	0.09
Cd		37.2	3.1
Co		124	40.8
Cr		< 1	15
Cs		< 0.1	< 0.1
Cu		180000	4785
Ga		6	15
Ge		0.9	0.9
Hf		< 0.1	1.1
Hg		0.285	0.031
In		1.6	0.1
Li		7	22
Mo		0.5	2
Nb		0.4	5
Ni		6	11
Pb		292	24
Sb		0.42	0.74
Sc		3	48
Se		894	21
Sn		13	2
Sr		6	11
Ta		0.05	0.19
Th		0.37	2.96
U		0.05	0.99
V		9	453
W		< 0.5	< 0.5
Y		2.9	12.7
Zn		7020	743
Zr		1	49

Appendix A: Whole Rock Geochemistry (cont.)

Analysis	Unit	D.L.	Analysis Method	SD-LAL-501	SD-LAL-503	SD-LAL-505	SD-LAL-507	SD-LAL-508
La	ppm	0.05	FUS-MS	8.09	54.1	16.1	24.8	24.7
Ce		0.05	FUS-MS	16.6	103	33.2	53	52.1
Pr		0.01	FUS-MS	1.87	12.1	3.83	5.83	5.97
Nd		0.05	FUS-MS	7.4	49.8	14.7	24.6	23.1
Sm		0.01	FUS-MS	1.75	10.1	3.46	5.35	4.73
Eu		0.005	FUS-MS	0.292	2.35	0.501	1.03	0.767
Gd		0.01	FUS-MS	1.81	8.71	4	5.43	4.08
Tb		0.01	FUS-MS	0.36	1.28	0.8	0.88	0.57
Dy		0.01	FUS-MS	2.44	6.7	5.33	5.25	3.32
Ho		0.01	FUS-MS	0.55	1.34	1.18	1.11	0.63
Er		0.01	FUS-MS	1.73	3.78	3.59	3.31	1.76
Tm		0.005	FUS-MS	0.272	0.54	0.557	0.495	0.244
Yb		0.01	FUS-MS	1.91	3.42	4.07	3.4	1.6
Lu		0.002	FUS-MS	0.322	0.547	0.75	0.63	0.263
Tl		0.05	FUS-MS	0.19	0.07	0.17	0.12	0.15

Appendix A: Whole Rock Geochemistry (cont.)

Analysis	Unit	SD-LAL-509	SD-LAL-512	SD-LAL-513	SD-LAL-514	SD-LAL-515	SD-LAL-518	SD-LAL-520	SD-LAL-522
La	ppm	13	1.57	0.35	1.58	0.45	0.68	10.5	17.3
Ce		26.9	3.4	0.71	3.24	1.16	1.47	24.2	38.4
Pr		3.24	0.38	0.09	0.37	0.14	0.16	2.81	4.3
Nd		13	1.49	0.37	1.58	0.53	0.69	10.7	16.6
Sm		3.06	0.3	0.13	0.32	0.12	0.11	1.63	2.91
Eu		0.301	0.109	0.024	0.15	0.041	0.058	0.22	0.453
Gd		3.45	0.24	0.11	0.29	0.08	0.09	0.84	1.97
Tb		0.58	0.04	0.02	0.04	0.01	0.02	0.1	0.31
Dy		3.83	0.2	0.1	0.23	0.08	0.1	0.41	1.81
Ho		0.8	0.04	0.02	0.04	0.01	0.02	0.06	0.38
Er		2.41	0.11	0.05	0.11	0.04	0.05	0.15	1.14
Tm		0.364	0.018	0.006	0.015	0.005	0.007	0.019	0.168
Yb		2.37	0.12	0.04	0.09	0.04	0.05	0.11	1.16
Lu		0.38	0.022	0.007	0.015	0.008	0.01	0.015	0.198
Tl		< 0.05	< 0.05	< 0.05	< 0.05	< 0.05	< 0.05	< 0.05	0.19

Appendix A: Whole Rock Geochemistry (cont.)

Analysis	Unit	SD-LAL-523	SD-LAL-524	SD-LAL-525	SD-LAL-526	SD-LAL-527	SD-LAL-529	SD-LAL-531	SD-LAL-535
La	ppm	17.3	10.9	2.46	22.3	17.3	11	12.4	19.1
Ce		46.3	21.5	4.86	47.2	39.9	22.8	27.7	42.9
Pr		6.4	2.31	0.54	5.24	4.65	2.56	3.28	5.27
Nd		25.4	8.93	1.89	21.8	19.8	10.2	13	19.2
Sm		5.24	1.79	0.53	4.33	4.24	2.31	2.99	3.74
Eu		0.651	0.42	0.133	0.495	0.623	0.844	0.482	1.18
Gd		4.71	1.76	0.61	4.12	3.94	2.1	3.41	3.74
Tb		0.68	0.28	0.11	0.63	0.58	0.37	0.58	0.59
Dy		3.94	1.64	0.7	3.71	3.15	2.3	3.78	3.63
Ho		0.76	0.33	0.15	0.73	0.6	0.49	0.83	0.73
Er		2.07	0.96	0.42	2.13	1.66	1.44	2.45	2.08
Tm		0.287	0.14	0.063	0.309	0.239	0.228	0.351	0.306
Yb		1.8	0.94	0.42	2.06	1.56	1.6	2.36	1.92
Lu		0.296	0.163	0.071	0.345	0.257	0.277	0.373	0.31
Tl		< 0.05	0.13	0.31	< 0.05	< 0.05	7.72	7.14	< 0.05

Appendix A: Whole Rock Geochemistry (cont.)

Analysis	Unit	SD-LAL-541	SD-LAL-544	SD-LAL-547	SD-LAL-556	SD-LAL-558	SD-LAL-560	SD-LAL-563	SD-LAL-564
La	ppm	0.44	0.87	34.8	30.8	0.76	6.29	8.55	5.36
Ce		1.06	1.37	76.4	67.1	2.05	14.9	20.6	11.4
Pr		0.14	0.14	8.3	7.82	0.28	2.01	2.52	1.28
Nd		0.67	0.54	32.4	30.3	1.37	7.73	11.8	4.93
Sm		0.23	0.24	5.46	5.61	0.48	2	2.22	1.1
Eu		0.065	0.197	0.59	1.34	0.122	0.989	0.376	0.212
Gd		0.27	0.24	3.52	4.28	0.48	2.76	1.93	1.3
Tb		0.04	0.05	0.43	0.56	0.1	0.56	0.27	0.29
Dy		0.22	0.29	2.04	3.12	0.71	3.93	1.65	2.21
Ho		0.04	0.06	0.34	0.56	0.15	0.81	0.34	0.56
Er		0.13	0.18	0.94	1.52	0.43	2.35	1.11	2
Tm		0.018	0.029	0.134	0.222	0.064	0.33	0.189	0.331
Yb		0.12	0.2	0.83	1.5	0.43	2.11	1.33	2.38
Lu		0.021	0.034	0.139	0.254	0.075	0.352	0.217	0.415
Tl		0.15	0.06	< 0.05	1.05	0.25	< 0.05	< 0.05	0.07

Appendix A: Whole Rock Geochemistry (cont.)

Analysis	Unit	SD-LAL-565	SD-LAL-567	SD-LAL-568	SD-LAL-569	SD-LAL-570	SD-LAL-572	SD-LAL-576	SD-LAL-580
La	ppm	34.8	1.23	21.7	7.28	19.8	59.1	26.2	7.08
Ce		72.4	2.97	49.6	15.7	43.4	133	57.7	17.3
Pr		9.15	0.39	6.12	1.77	4.9	15.7	6.74	2.19
Nd		33.8	1.55	21.9	7.08	19.3	60	26.7	8.73
Sm		7.07	0.47	4.32	1.52	3.8	10.6	5.49	2.19
Eu		0.817	0.087	0.814	0.288	0.615	1.69	0.763	0.426
Gd		6.43	0.65	3.24	1.53	3.19	6.84	4.81	2.2
Tb		1	0.13	0.43	0.27	0.51	0.87	0.85	0.4
Dy		6.3	0.81	2.4	1.74	2.89	4.19	5.22	2.52
Ho		1.35	0.17	0.47	0.37	0.57	0.7	1.06	0.53
Er		4.36	0.55	1.36	1.16	1.61	1.77	3.22	1.63
Tm		0.708	0.087	0.203	0.183	0.234	0.238	0.507	0.264
Yb		5.14	0.59	1.35	1.26	1.51	1.4	3.54	1.91
Lu		0.91	0.097	0.228	0.216	0.255	0.207	0.601	0.332
Tl		0.52	< 0.05	< 0.05	< 0.05	1.83	0.14	0.5	0.07

Appendix A: Whole Rock Geochemistry (cont.)

Analysis	Unit	SD-LAL-582	SD-LAL-584	SD-LAL-585	SD-LAL-586	SD-LAL-587	SD-LAL-588	SD-LAL-592	SD-LAL-595
La	ppm	8.66	0.78	19.8	25.5	2.32	11.2	3.89	3.19
Ce		17.8	1.65	48.2	59.7	5.16	26.9	8.83	7.06
Pr		2.09	0.19	6.58	7.65	0.6	3.44	1.11	0.91
Nd		7.45	0.92	27.9	29.9	2.52	12.8	4.76	3.2
Sm		1.37	0.36	6.87	6.23	0.36	2.29	1.02	0.68
Eu		0.296	0.111	1.28	1.34	0.053	0.747	0.234	0.139
Gd		1.04	0.23	6.28	5.25	0.23	1.86	1.11	0.49
Tb		0.13	0.05	0.92	0.75	0.03	0.26	0.22	0.07
Dy		0.74	0.31	4.92	4.17	0.16	1.65	1.44	0.4
Ho		0.14	0.07	0.85	0.82	0.03	0.36	0.31	0.08
Er		0.4	0.23	2.05	2.37	0.09	1.13	0.95	0.23
Tm		0.056	0.036	0.261	0.349	0.014	0.186	0.15	0.033
Yb		0.35	0.24	1.65	2.46	0.11	1.32	1.06	0.21
Lu		0.055	0.039	0.276	0.416	0.022	0.238	0.179	0.033
Tl		< 0.05	0.51	< 0.05	< 0.05	0.09	0.69	0.08	< 0.05

Appendix A: Whole Rock Geochemistry (cont.)

Analysis	Unit	SD-LAL-597	SD-LAL-598	SD-LAL-601	SD-LAL-604	SD-LAL-611	SD-LAL-612	SD-LAL-613	SD-LAL-615
La	ppm	11.2	2.12	37.3	31	3.69	2.26	3.9	2.47
Ce		22	4.61	81.7	60.9	8.05	4.69	8.79	5.24
Pr		2.38	0.56	10.2	7.57	0.98	0.69	1.16	0.64
Nd		7.93	2.3	38.6	28.7	4.05	3.09	5.2	2.5
Sm		1.28	0.4	7.04	5.35	1	0.9	1.41	0.59
Eu		0.947	0.231	1.86	0.715	0.117	0.237	0.495	0.2
Gd		1.02	0.37	5.51	4.91	1.08	1.05	1.77	0.63
Tb		0.18	0.05	0.66	0.84	0.23	0.18	0.37	0.09
Dy		1.17	0.33	3.39	5.32	1.69	1.22	2.55	0.53
Ho		0.24	0.08	0.64	1.09	0.41	0.3	0.57	0.12
Er		0.74	0.25	1.88	3.19	1.44	1.02	1.79	0.41
Tm		0.111	0.046	0.285	0.456	0.245	0.17	0.289	0.071
Yb		0.73	0.43	1.91	2.9	1.7	1.22	1.95	0.54
Lu		0.118	0.097	0.32	0.432	0.3	0.211	0.335	0.096
Tl		< 0.05	< 0.05	4.16	0.46	< 0.05	0.06	< 0.05	< 0.05

Appendix A: Whole Rock Geochemistry (cont.)

Analysis	Unit	SD-LAL-616	SD-LAL-617	SD-LAL-618	SD-LAL-626	SD-LAL-629	SD-LAL-633	SD-LAL-634	SD-LAL-635
La	ppm	12	11.3	1.05	13	39.2	21.8	24.6	22.4
Ce		25.6	24.2	1.95	30.3	83.9	49.9	52.2	50.7
Pr		3.17	3.01	0.25	3.92	10.4	6.05	5.76	5.8
Nd		12	11.4	1.17	15.2	39	23.6	21.2	21.5
Sm		2.47	2.16	0.15	3.03	7.03	4.32	3.25	3.91
Eu		0.39	0.388	0.208	0.499	1.07	2.6	0.662	0.47
Gd		2.35	1.97	0.12	2.63	5.53	3.18	2.01	3.19
Tb		0.33	0.27	0.02	0.32	0.66	0.36	0.27	0.42
Dy		1.68	1.52	0.12	1.63	3.04	1.72	1.41	2.33
Ho		0.3	0.3	0.02	0.27	0.51	0.31	0.27	0.45
Er		0.84	0.87	0.07	0.71	1.3	0.87	0.78	1.26
Tm		0.118	0.126	0.011	0.1	0.171	0.123	0.11	0.189
Yb		0.79	0.84	0.07	0.65	1.03	0.79	0.66	1.32
Lu		0.143	0.15	0.013	0.107	0.17	0.133	0.1	0.228
Tl		1.25	0.22	< 0.05	< 0.05	< 0.05	0.28	0.12	< 0.05

Appendix A: Whole Rock Geochemistry (cont.)

Analysis	Unit	SD-LAL-636	SD-LAL-637	SD-LAL-638	SD-LAL-639	SD-LAL-640	SD-LAL-642	SD-LAL-647
La	ppm	20.2	5	3.03	3.27	6.06	0.77	9.13
Ce		42.1	11.5	6.68	7.88	13	1.48	20
Pr		5.16	1.32	0.87	0.99	1.67	0.18	2.32
Nd		18.2	4.92	3.42	4.14	6.72	0.69	9.09
Sm		3.15	0.85	0.73	0.91	1.72	0.14	1.62
Eu		0.659	0.5	0.084	0.102	0.145	0.063	0.197
Gd		2.25	0.89	0.9	1.08	1.96	0.14	1.17
Tb		0.27	0.15	0.2	0.2	0.36	0.02	0.15
Dy		1.56	0.85	1.51	1.25	2.19	0.07	0.76
Ho		0.27	0.16	0.35	0.24	0.45	0.01	0.15
Er		0.73	0.41	1.23	0.61	1.34	0.04	0.43
Tm		0.103	0.054	0.206	0.084	0.205	0.006	0.067
Yb		0.63	0.33	1.52	0.55	1.39	0.04	0.49
Lu		0.097	0.051	0.266	0.087	0.243	0.005	0.092
Tl		0.05	1.32	1.01	0.12	< 0.05	< 0.05	< 0.05

Appendix A: Whole Rock Geochemistry (cont.)

Analysis	Unit	SD-LAL-648	SD-LAL-649
La	ppm	3.72	22.9
Ce		7.52	51.2
Pr		0.76	6.57
Nd		2.62	25.2
Sm		0.29	4.72
Eu		0.105	0.769
Gd		0.32	3.76
Tb		0.06	0.49
Dy		0.45	2.75
Ho		0.1	0.54
Er		0.31	1.52
Tm		0.047	0.226
Yb		0.28	1.47
Lu		0.04	0.237
Tl		< 0.05	< 0.05

APPENDIX B

Pearson Correlation Matrix

Appendix B: Pearson Correlation Matrix

	Zn	Pb	As	Sb	Au	Ag	Cd	MnO	Hg	Ba	Sr	Cu	FeO	Fe2O3	Tl	Sn	In	W	Co	Ni	Se	Bi	Mo	V	Cr	Cs	K2O	CO2	Mn	CaO
Zn	**1.00**																													
Pb	-0.12	**1.00**																												
As	-0.06	-0.06	**1.00**																											
Sb	**0.48**	-0.09	0.00	**1.00**																										
Au	-0.10	0.02	0.00	-0.05	**1.00**																									
Ag	-0.13	0.08	0.00	-0.06	**0.98**	**1.00**																								
Cd	**0.97**	-0.11	-0.05	**0.42**	-0.10	-0.12	**1.00**																							
MnO	-0.12	0.07	-0.05	-0.18	-0.02	-0.02	-0.11	**1.00**																						
Hg	**0.61**	-0.08	-0.05	0.23	-0.04	-0.05	**0.56**	0.10	**1.00**																					
Ba	-0.23	-0.14	-0.07	-0.01	-0.07	-0.08	-0.23	0.13	-0.12	**1.00**																				
Sr	-0.06	0.22	-0.11	0.00	-0.05	-0.01	-0.03	0.00	-0.01	0.11	**1.00**																			
Cu	-0.11	-0.12	**0.62**	0.02	0.00	-0.01	-0.09	-0.11	-0.12	-0.12	-0.08	**1.00**																		
FeO	0.10	**-0.23**	0.14	**0.25**	-0.07	-0.12	0.02	-0.07	0.11	0.11	-0.01	0.19	**1.00**																	
Fe2O3	0.11	-0.14	**0.24**	0.03	-0.09	-0.11	0.10	**-0.25**	-0.01	-0.03	-0.14	**0.32**	0.17	**1.00**																
Tl	-0.19	-0.05	-0.06	-0.06	0.01	0.05	-0.18	0.09	-0.10	0.43	0.02	-0.15	-0.19	-0.09	**1.00**															
Sn	**0.27**	0.05	0.02	**0.33**	-0.02	0.00	0.23	-0.09	0.04	-0.22	-0.09	**0.39**	0.11	**0.24**	-0.14	**1.00**														
In	**0.56**	-0.15	**0.24**	0.12	-0.06	-0.08	0.65	-0.11	0.10	-0.12	0.00	**0.28**	-0.03	0.19	-0.15	0.16	**1.00**													
W	0.21	0.00	-0.01	**0.48**	-0.02	-0.03	**0.24**	-0.03	0.01	-0.08	0.04	0.02	-0.03	-0.07	-0.05	0.10	0.02	**1.00**												
Co	0.17	-0.20	0.06	0.22	-0.10	-0.13	0.14	0.00	0.10	-0.01	-0.06	0.23	**0.41**	0.18	-0.16	0.06	0.14	0.26	**1.00**											
Ni	-0.06	0.00	0.07	-0.05	-0.04	-0.05	-0.07	-0.10	-0.05	0.20	0.00	-0.02	**0.48**	**0.25**	-0.03	-0.06	-0.05	-0.04	0.07	**1.00**										
Se	-0.16	0.14	**0.66**	-0.06	0.06	0.13	-0.12	-0.05	-0.08	-0.18	0.17	**0.49**	-0.03	**0.24**	-0.13	0.03	0.14	-0.06	0.02	-0.01	**1.00**									
Bi	-0.08	0.00	-0.04	-0.05	-0.01	0.06	-0.06	0.01	-0.07	0.20	0.06	-0.07	-0.14	-0.14	**0.59**	-0.06	-0.07	-0.02	-0.10	-0.03	-0.09	**1.00**								
Mo	0.23	-0.10	-0.09	0.14	-0.07	-0.07	0.17	-0.12	0.17	-0.15	0.03	0.17	0.19	**0.45**	-0.07	**0.66**	0.01	0.06	0.07	0.07	-0.01	-0.08	**1.00**							
V	-0.22	-0.17	-0.09	-0.15	-0.07	-0.11	-0.21	0.30	-0.08	0.16	-0.08	-0.09	0.13	-0.08	0.04	-0.15	-0.14	-0.05	0.10	0.07	-0.20	-0.07	-0.17	**1.00**						
Cr	-0.14	-0.09	-0.09	-0.11	-0.04	-0.07	-0.16	0.23	-0.09	0.06	**-0.26**	-0.11	0.09	-0.03	-0.03	-0.14	-0.10	0.02	0.00	0.15	-0.16	-0.01	-0.11	0.38	**1.00**					
Cs	-0.23	-0.16	-0.09	-0.15	-0.08	-0.10	-0.23	0.36	-0.11	0.80	-0.09	-0.17	0.02	-0.06	0.34	-0.21	-0.21	-0.07	0.07	0.09	-0.22	0.11	-0.19	0.17	0.17	**1.00**				
K2O	-0.19	-0.13	-0.05	-0.07	-0.05	-0.08	-0.19	0.25	-0.10	**0.82**	0.04	-0.15	0.09	0.01	0.42	-0.19	-0.15	-0.07	-0.05	0.22	-0.18	0.10	-0.14	0.25	0.06	0.82	**1.00**			
CO2	0.04	-0.03	-0.06	0.11	-0.05	-0.06	0.03	0.01	-0.06	-0.19	0.14	-0.08	-0.17	-0.09	-0.11	-0.04	-0.03	0.19	0.17	-0.08	-0.10	-0.04	-0.05	-0.09	-0.16	-0.17	-0.16	**1.00**		
Mn	-0.08	0.05	-0.06	-0.16	-0.03	-0.03	-0.06	1.00	0.13	0.12	-0.01	-0.12	-0.06	-0.24	0.06	-0.09	-0.08	-0.02	0.00	-0.10	-0.06	0.00	-0.11	**0.29**	0.23	0.35	0.23	0.01	**1.00**	
CaO	-0.16	**0.41**	-0.13	-0.04	-0.03	0.04	-0.14	0.17	-0.14	**-0.28**	**0.45**	-0.13	**-0.37**	**-0.26**	-0.08	0.03	-0.15	0.16	-0.09	-0.16	0.12	0.01	-0.05	-0.16	**-0.31**	**-0.30**	**-0.24**	**0.61**	0.16	**1.00**

Values at ±0.24 are significant at the 0.05 level. Based on 70 observations

APPENDIX C

Sample list

Sample ID	Hand Sample Description	Interval (m)	DDH ID
501	Euhedral pyrrhotite, pyrite and sphalerite in a chlorite matrix with small patches of quartz.	1019.9	DUB210 (5600N)


Lithology				
Carbonate-Chlorite Schist				
Min. Style and Lens(es)				
Type 3 – Lens 21				
Au	**Ag**	**Cu**	**Zn**	**Pb**
0.55	22.29	0.42	5.04	0.49

Sample ID	Hand Sample Description	Interval (m)	DDH ID
502	Disseminated pyrrhotite and pyrite concentrated on the cleavages of a chlorite, biotite/amphibole matrix.	1021.8	DUB210 (5600N)


Lithology				
Carbonate-Chlorite Schist				
Min. Style and Lens(es)				
Type 3 – Lens 21				
Au	**Ag**	**Cu**	**Zn**	**Pb**
0.24	2.06	0.14	0.91	0.05

Sample ID	Hand Sample Description	Interval (m)	DDH ID
503	Pyrrhotite and pyrite concentrated in a local fracture. Some euhedral sphalerite can be seen proximal to the fracture. The matrix outside the fracture is mostly amphibole with some chlorite.	1024.5	DUB210 (5600N)


Lithology				
Carbonate-Chlorite Schist				
Min. Style and Lens(es)				
Type 3 – Between lenses 21 and 25				
Au	**Ag**	**Cu**	**Zn**	**Pb**
6.69	126.9	0.96	1.54	1.81

Sample ID	Hand Sample Description	Interval (m)	DDH ID
504	Pyrite with minor pyrrhotite and sphalerite in a chlorite quartz matrix.	1029.0	DUB210 (5600N)


Lithology				
Carbonate-Chlorite Schist				
Min. Style and Lens(es)				
Type 3 – Lens 25				
Au	**Ag**	**Cu**	**Zn**	**Pb**
1.78	23.31	0.29	1.14	0.31

Sample ID	Hand Sample Description	Interval (m)	DDH ID
505	Fine grained galena with euhedral pyrite and minor pyrrhotite in an amphibole matrix.	1034.8	DUB210 (5600N)


Lithology				
Carbonate-Chlorite Schist				
Min. Style and Lens(es)				
Type 3 – Lens 25				
Au	**Ag**	**Cu**	**Zn**	**Pb**
2.19	38.74	0.08	0.01	0.41

506	Sample has three distinctive parts. The first (highest stratigraphically) is fine grained galena in a chlorite amphibole matrix. The middle is a thin line of well formed chalcopyrite and the bottom is similar to the top, without the amphibole, and disseminated pyrite in place of galena.		1038.6		DUB210 (5600N)	
	 		**Lithology**			
			Carbonate-Chlorite Schist			
			Min. Style and Lens(es)			
			Type 3 – Lens 25			
			Au	**Ag**	**Cu**	**Zn**	**Pb**
			50.13	359.3	0.53	0.02	2.63
507	Fine grained galena with an amphibole/fine grained muscovite matrix. Minor chalcopyrite locally.		1045.0		DUB210 (5600N)	
	 		**Lithology**			
			Carbonate-Chlorite Schist			
			Min. Style and Lens(es)			
			Type 3 – Lens 25			
			Au	**Ag**	**Cu**	**Zn**	**Pb**
			19.85	277.7	0.54	0.01	3.64
508	Coarse grained galena in an amphibole/fine grained muscovite matrix.		1048.5		DUB210 (5600N)	
	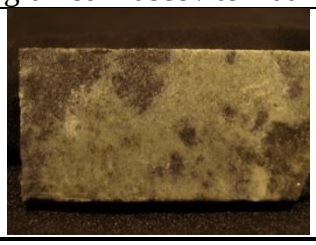 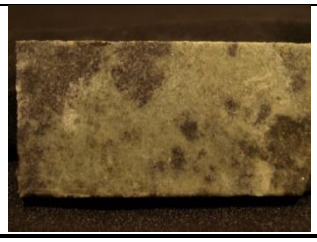		**Lithology**			
			Carbonate-Chlorite Schist			
			Min. Style and Lens(es)			
			Type 3 – Lens 25			
			Au	**Ag**	**Cu**	**Zn**	**Pb**
			8.85	211.9	0.29	0.09	2.36
509	Disseminated chalcopyrite with minor sphalerite in a matrix of amphibole/chlorite and fine grained galena.		1058.0		DUB210 (5600N)	
	 		**Lithology**			
			Carbonate-Chlorite Schist			
			Min. Style and Lens(es)			
			Type 3 – Lens 25			
			Au	**Ag**	**Cu**	**Zn**	**Pb**
			117.9	334.6	0.31	0.01	1.92

510	Bands of amphibole in a chlorite matrix. Large pyrite and pyrrhotite grains with minor chalcopyrite and magnetite.		1064.4		DUB210 (5600N)		
	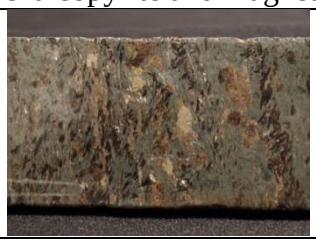		**Lithology**				
			Anthophyllite-Biotite-Cordierite Chlorite Schist				
			Min. Style and Lens(es)				
			Type 3 – Just below lens 25				
			Au	**Ag**	**Cu**	**Zn**	**Pb**
			0.58	9.26	0.07	0.04	0.11
511	Bands of pyrite and pyrrhotite with grains of sphalerite in an amphibole matrix; biotite may be present.		1067.9		DUB210 (5600N)		
			**Lithology**				
			Anthophyllite-Garnet-Staurolite-Biotite Cordierite Gneiss				
			Min. Style and Lens(es)				
			Type 3 – Below lens 25				
			Au	**Ag**	**Cu**	**Zn**	**Pb**
			0.31	5.83	0.04	0.01	0.05
512	Durchbewegung texture which consist of rounded pyrite grains with interstitial sphalerite and occasional dolomite. Minor chalcopyrite is also present.		815.6		DUB195 (5600N)		
	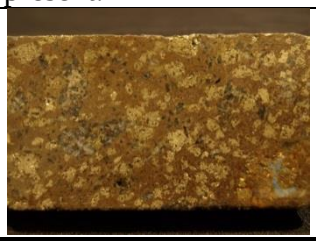		**Lithology**				
			Near Solid Sulfide				
			Min. Style and Lens(es)				
			Type 1 – Lens 21				
			Au	**Ag**	**Cu**	**Zn**	**Pb**
			1.37	4.46	0.19	0.79	0.06
513	Network of pyrite grains (>90%) with interstitial sphalerite.		821.1		DUB195 (5600N)		
			**Lithology**				
			Near Solid Sulfide				
			Min. Style and Lens(es)				
			Type 1 – Lens 21 and 20				
			Au	**Ag**	**Cu**	**Zn**	**Pb**
			4.01	88.8	1.91	10.15	0.01

	Euhedral pyrite, sphalerite, chalcopyrite and coarse grained dolomite with minor gahnite.		823.2		DUB195 (5600N)		
		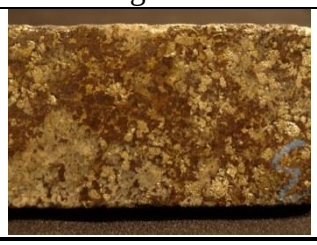	**Lithology**				
			Near Solid Sulfide				
			Min. Style and Lens(es)				
			Type 1 – Lenses 21 and 20				
			Au	**Ag**	**Cu**	**Zn**	**Pb**
			25.75	103.2	3.55	19.79	0.01
515	Sphalerite rich with euhedral chalcopyrite. Local pyrite, carbonate may be present.		824.3		DUB195 (5600N)		
			**Lithology**				
			Near Solid Sulfide				
			Min. Style and Lens(es)				
			Type 1 – Lenses 21 and 20				
			Au	**Ag**	**Cu**	**Zn**	**Pb**
			13.06	64.11	2.21	20.06	0.01
516	Disseminated pyrrhotite with some pyrite. Approaching massive sulfide zone.		786.4		DUB205 (5200N)		
	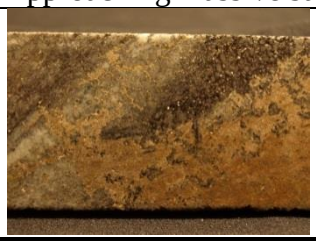		**Lithology**				
			Min. Sericite Schist				
			Min. Style and Lens(es)				
			Type 1 - Lens 10				
			Au	**Ag**	**Cu**	**Zn**	**Pb**
			0.27	7.54	0.34	3.31	0.11
517	Massive pyrite with trace amounts of sphalerite and minor quartz.		788.2		DUB205 (5200N)		
	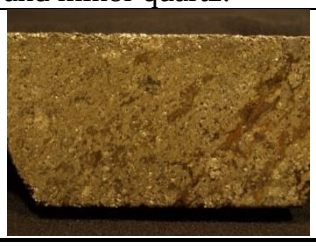	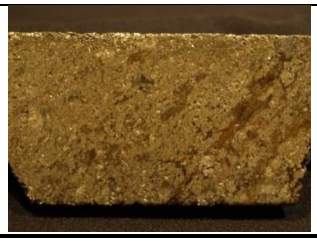	**Lithology**				
			Massive Sulfides				
			Min. Style and Lens(es)				
			Type 1 - Lens 10				
			Au	**Ag**	**Cu**	**Zn**	**Pb**
			0.14	2.06	0.11	3.37	0.02
518	Massive sphalerite with lesser pyrite and some quartz. Chalcopyrite may be present.		789.7		DUB205 (5200N)		
	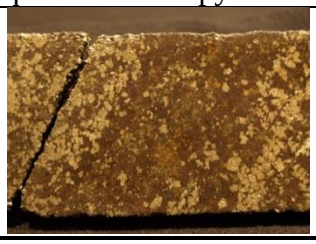		**Lithology**				
			Massive Sulfides				
			Min. Style and Lens(es)				
			Type 1- Lens 10				
			Au	**Ag**	**Cu**	**Zn**	**Pb**
			0.24	2.4	0.06	6.68	0.03

519	Massive pyrite and sphalerite with lesser chalcopyrite and minor interstitial quartz.	796.3		DUB205 (5200N)		
	 	**Lithology**				
		Massive Sulfides				
		Min. Style and Lens(es)				
		Type 1 - Lens 10				
		Au	**Ag**	**Cu**	**Zn**	**Pb**
		0.31	4.11	0.14	16.56	0.01
520	Massive pyrite with abundant chalcopyrite and lesser sphalerite. Large euhedral gahnite crystals are also present.	804.1		DUB205 (5200N)		
	 	**Lithology**				
		Massive Sulfides				
		Min. Style and Lens(es)				
		Type 1 - Lens 10				
		Au	**Ag**	**Cu**	**Zn**	**Pb**
		10.39	60.34	3.06	0.39	0.11
521	Chalcopyrite stringers with abundant pyrite and euhedral ghanite. This samples is directly below an igneous intrusion and contains some of the footwall material (mainly the amphibole matrix).	806.0		DUB205 (5200N)		
	 	**Lithology**				
		Min. Sericite Schist				
		Min. Style and Lens(es)				
		Type 1 - Lens 10				
		Au	**Ag**	**Cu**	**Zn**	**Pb**
		17.18	84.34	4.3	0.5	0.09
522	Discontinuous pyrrhotite and pyrite with trace chalcopyrite. Faded staurolite porphyroblasts are present. The matrix is composed of amphibole and quartz. This sample overlies a 12 m long quartz vein.	815.1		DUB205 (5200N)		
	 	**Lithology**				
		Min. Sericite Schist				
		Min. Style and Lens(es)				
		Type ? - Lens 10				
		Au	**Ag**	**Cu**	**Zn**	**Pb**
		3.84	17.83	0.86	0.07	0.02

523	Fine grained galena with small flakes of pyrite and pyrrhotite in a matrix of sericite and chlorite.	1015.3	DUB252W01 (5550N)			
	 	**Lithology**				
		Min. Chlorite Schist				
		Min. Style and Lens(es)				
		Type 3 - Above lens 25				
		Au	**Ag**	**Cu**	**Zn**	**Pb**
		22.83	317.8	1.22	0.01	2.7
524	Well formed grains of galena with minor pyrite and pyrrhotite in a matrix of quartz and chlorite.	1016.8	DUB252W01			
	 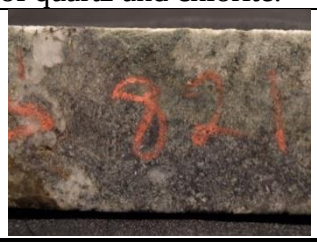	**Lithology**				
		Min. Chlorite Schist				
		Min. Style and Lens(es)				
		Type 3 - Above lens 25				
		Au	**Ag**	**Cu**	**Zn**	**Pb**
		15.43	314.7	0.37	0.01	2.61
525	Quartz rich with fine grained galena and minor chlorite and amphibole.	1017.6	DUB252W01 (5600N)			
	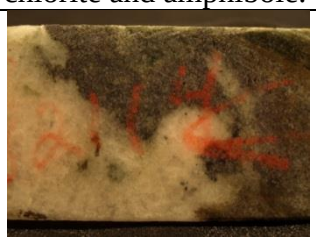 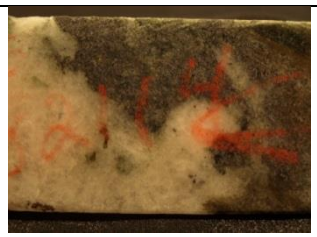	**Lithology**				
		Min. Chlorite Schist				
		Min. Style and Lens(es)				
		Type 3 – Lens 21				
		Au	**Ag**	**Cu**	**Zn**	**Pb**
		66.03	175.5	0.08	0.03	1.14
526	Disseminated chalcopyrite and sphalerite. Locally, sphalerite shows larger networked pattern. Pyrite is present in minor amounts.	1020.7	DUB252W01 (5600N)			
	 	**Lithology**				
		Min. Chlorite Schist				
		Min. Style and Lens(es)				
		Type 3 - Lens 21				
		Au	**Ag**	**Cu**	**Zn**	**Pb**
		11.93	130.3	2.23	0.33	0.25
527	Semi-massive sphalerite and pyrite with minor chalcopyrite in a carbonate rich matrix.	1023.0	DUB252W01 (5600N)			
	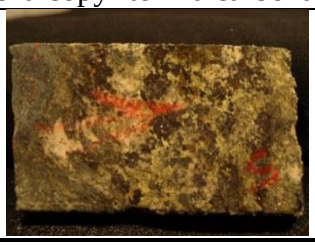 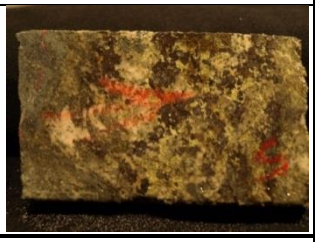	**Lithology**				
		Min. Chlorite Schist				
		Min. Style and Lens(es)				
		Type 3 - Lens 21				
		Au	**Ag**	**Cu**	**Zn**	**Pb**
		8.23	211.5	5.26	0.82	0.93

528	Chalcopyrite in a diffuse network with large flakes of pyrrhotite. Matrix is quartz and amphibole.		1024.8		DUB252W01 (5600N)		
		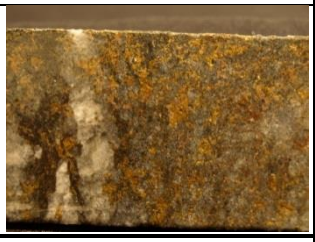	**Lithology**				
			Min. Chlorite Schist				
			Min. Style and Lens(es)				
			Type 3 - Lens 21				
			Au	**Ag**	**Cu**	**Zn**	**Pb**
			0.07	0.07	1.03	1.03	0.02
529	Diffuse chalcopyrite and pyrite in a matrix of quartz and amphibole.		1028.7		DUB252W01 (5600N)		
			**Lithology**				
			Quartz-Biotite-Garnet Gneiss				
			Min. Style and Lens(es)				
			Type 4 - Lens 21				
			Au	**Ag**	**Cu**	**Zn**	**Pb**
			5.42	68.91	1.01	0.01	0.49
530	Isolated chalcopyrite pyrite and chalcopyrite in a matrix of amphibole and chlorite with minor quartz.		1048.3		DUB252W01 (5600N)		
			**Lithology**				
			Quartz-Biotite-Garnet Gneiss				
			Min. Style and Lens(es)				
			Type 3 - Lens 21				
			Au	**Ag**	**Cu**	**Zn**	**Pb**
			14.95	120.3	0.14	0.01	0.36
531	Heterogenous sample with three distinct parts. The highest stratigraphically is fine grained galena with disseminated chalcopyrite in a matrix of chlorite.		1050.2		DUB252W01 (5600N)		
			**Lithology**				
			Kyanite-Quartz-Biotite Gneiss				
			Min. Style and Lens(es)				
			Type 3 – Lens 25				
			Au	**Ag**	**Cu**	**Zn**	**Pb**
			0.03	1.71	0.01	0.02	0.01
532	Pyrrhotite stringers with minor localized chalcopyrite in a transitional zone leaving the footwall. Matrix is quartz and amphibole.		1032.9		DUB252W01 (5600N)		
			**Lithology**				
			Quartz-Biotite-Garnet Gneiss				
			Min. Style and Lens(es)				
			Type ? - Far East of lens 21				
			Au	**Ag**	**Cu**	**Zn**	**Pb**
			2.3	41.83	0.35	0.04	0.01

533	Similar to 531; the upper part is a chalcopyrite network with fine grained galena, the middle is a channel of fine grained muscovite, the bottom is fine grained galena mixed with chlorite.	1060.9		DUB252**W01** (5600N)		
	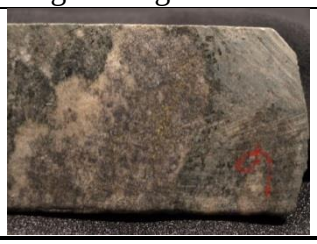 	**Lithology**				
		Chlorite-Biotite-Staurolite Schist				
		Min. Style and Lens(es)				
		Type 3 – Lens 25				
		Au	**Ag**	**Cu**	**Zn**	**Pb**
		0.01	0.01	0.01	0.01	0.01
534	Pyrrhotite stringers in footwall with chalcopyrite and sphalerite in a quartz chlorite matrix.	1007.8		DUB252**W01** (5600N)		
	 	**Lithology**				
		Min. Chlorite Schist				
		Min. Style and Lens(es)				
		Type 3 – Above lens 21				
		Au	**Ag**	**Cu**	**Zn**	**Pb**
		1.61	30.17	1.05	1.59	0.07
535	Well formed galena grains within a fracture/channel. Disseminated chalcopyrite and pyrrhotite within a quartz chlorite matrix.	1008.8		DUB252		
	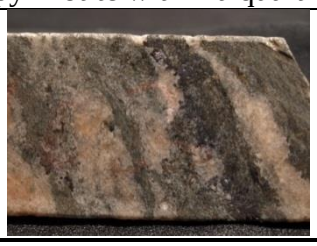 	**Lithology**				
		Min. Chlorite Schist				
		Min. Style and Lens(es)				
		Type 3 – Above lens 21				
		Au	**Ag**	**Cu**	**Zn**	**Pb**
		1.3	1.3	57.94	57.94	0.32
536	Networked sphalerite and disseminated chalcopyrite. Matrix is mostly quartz and kyanite.	1009.0		DUB252 (5550N)		
	 	**Lithology**				
		Min. Chlorite Schist				
		Min. Style and Lens(es)				
		Type 1 - Above lenses 25 and 21				
		Au	**Ag**	**Cu**	**Zn**	**Pb**
		0.03	0.69	0.01	0.01	0.01

<table>
<tr><td>537</td><td colspan="2">Sphalerite vein with pyrrhotite. Gahnite crystals with galena inside and minor chalcopyrite outside. This is a local feature; the section after this has exceptionally high Ag grades (but low Zn and Au).</td><td colspan="2">1012.1</td><td colspan="2">DUB252
(5550N)</td></tr>
<tr><td></td><td colspan="2">   </td><td colspan="4">Lithology
Min. Chlorite Schist
Min. Style and Lens(es)
Type 3 - Above lenses 25 and 21
Au | Ag | Cu | Zn | Pb
0.01 | 0.69 | 0.01 | 0.01 | 0.02</td></tr>
<tr><td>538</td><td colspan="2">Equal amounts of pyrrhotite and chalcopyrite dominate in a network; the two minerals do not mix together. Faded garnet porphyroblasts appear in an amphibole rich matrix with minor quartz.</td><td colspan="2">1141.5</td><td colspan="2">DUB252W01
(5600N)</td></tr>
<tr><td></td><td colspan="2">   </td><td colspan="4">Lithology
Min. Qtz-Anth-Cord Gneiss
Min. Style and Lens(es)
Type 4 – Lens 27
Au | Ag | Cu | Zn | Pb
0.07 | 0.07 | 0.69 | 0.69 | 0.02</td></tr>
<tr><td>539</td><td colspan="2">Chalcopyrite network with minor pyrrhotite in an amphibole quartz matrix. Faded garnet porphyroblasts are present. This sample is adjacent to a quartz vein.</td><td colspan="2">1148.7</td><td colspan="2">DUB252W01
(5600N)</td></tr>
<tr><td></td><td colspan="2">   </td><td colspan="4">Lithology
Chlor-Cord-Gnt-Anth Schist
Min. Style and Lens(es)
Type 2 – Lens 27
Au | Ag | Cu | Zn | Pb
0.01 | 0.01 | 0.01 | 0.01 | 0.01</td></tr>
<tr><td>540</td><td colspan="2">Chalcopyrite disseminated-network with minor pyrrhotite. Matrix has epidote, amphibole and some quartz.</td><td colspan="2">1165.4</td><td colspan="2">DUB252W01
(5600N)</td></tr>
<tr><td></td><td colspan="2">   </td><td colspan="4">Lithology
Qtz-Cord-Antho-Staur-Garnt Gneiss
Min. Style and Lens(es)
Type 2 - Lens 27
Au | Ag | Cu | Zn | Pb</td></tr>
<tr><td></td><td colspan="2"></td><td>27.84</td><td>45.6</td><td>5.82</td><td>0.28</td><td>0.01</td></tr>
<tr><td></td><td colspan="2"></td><td colspan="4"></td></tr>
</table>

541	Network of chalcopyrite with minor pyrrhotite in a quartz amphibole matrix.	1165.6		DUB252**W01** (5600N)		
	 	**Lithology**				
		Qtz-Cord-Antho-Staur-Garnet Gneiss				
		Min. Style and Lens(es)				
		Type 2 – Lens 27				
		Au	**Ag**	**Cu**	**Zn**	**Pb**
		27.84	45.6	5.82	0.28	0.01
542	Quartz amphibole matrix with trace garnet cordierite matrix. Chalcopyrite crystals are present in a disseminated network, often with a rim of gahnite. Minor pyrrhotite is present.	1177.1		DUB252**W01** (5600N)		
	 	**Lithology**				
		Qtz-Cord-Antho-Staur-Garnt Gneiss				
		Min. Style and Lens(es)				
		Type 2 – Lens 27				
		Au	**Ag**	**Cu**	**Zn**	**Pb**
		22.29	49.37	4.37	0.26	0.01
543	Semi-massive sulfides dominated by chalcopyrite. Matrix is quartz and amphibole with small garnet pophyroblasts.	1179.1		DUB252**W01** (5600N)		
	 	**Lithology**				
		Qtz-Cord-Antho-Staur-Garnt Gneiss				
		Min. Style and Lens(es)				
		Type 2 - Lens 27				
		Au	**Ag**	**Cu**	**Zn**	**Pb**
		42.75	49.71	4.98	0.15	0.02
544	Networked chalcopyrite with lesser pyrrhotite and minor sphalerite, ghanite and quartz. This sample is located below the ore zone.	1184.3		DUB252**W01** (5600N)		
	 	**Lithology**				
		Qtz-Cord-Antho-Staur-Garnt Gneiss				
		Min. Style and Lens(es)				
		Type 2 – Lens 27				
		Au	**Ag**	**Cu**	**Zn**	**Pb**
		54.82	56.23	6.24	0.47	0.01

545	Well formed pyrite cubes with amorphous sphalerite and minor pyrrhotite in a matrix of chlorite and minor quartz.		865.7		DUB198 (5100N)	
	 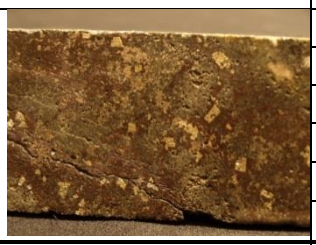		**Lithology**			
			Intermediate Gneissic Tuff			
			Min. Style and Lens(es)			
			Type 1 – Above lens 10			
			Au	**Ag**	**Cu**	**Zn**	**Pb**
			N/A	N/A	N/A	N/A	N/A
546	Discontinuous pyrite zone directly below the hanging wall in a chlorite-amphibole matrix with minor quartz.		862.6		DUB198 (5100N)	
	 		**Lithology**			
			Intermediate Gneissic Tuff			
			Min. Style and Lens(es)			
			Type 4 - Above lens 10			
			Au	**Ag**	**Cu**	**Zn**	**Pb**
			N/A	N/A	N/A	N/A	N/A
547	Network of chalcopyrite with lesser sphalerite and pyrrhotite as well as minor arsenopyrite in a matrix of quartz-chlorite, possibly with some amphiboles.		869.1		DUB198 (5100N)	
	 		**Lithology**			
			Intermediate Gneissic Tuff			
			Min. Style and Lens(es)			
			Type 4 - Above lens 10			
			Au	**Ag**	**Cu**	**Zn**	**Pb**
			N/A	N/A	N/A	N/A	N/A
548	Continuous pyrite and pyrrhotite zone with minor chalcopyrite. Matrix is chlorite and amphibole; small garnet grains are present as well.		874.9		DUB198 (5100N)	
	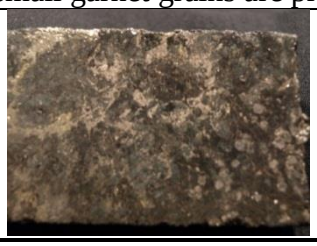 		**Lithology**			
			Quartz Biotite Actinolite Chlorite Schist			
			Min. Style and Lens(es)			
			Type 4 – Above lens 10			
			Au	**Ag**	**Cu**	**Zn**	**Pb**
			N/A	N/A	N/A	N/A	N/A

<table>
<tr><td>549</td><td colspan="2">Network of chalcopyrite with minor pyrrhotite and arsenopyrite. Faded porphyroblasts of garnet are present within the matrix of amphibole and chlorite.</td><td>881.0</td><td colspan="5">DUB198
(5100N)</td></tr>
<tr><td></td><td colspan="2">  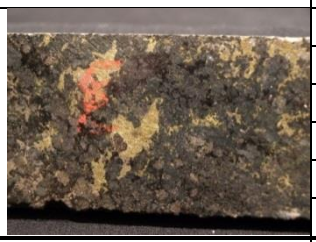 </td><td colspan="6">Lithology
Quartz Sericite Cordierite Schist
Min. Style and Lens(es)
Type 4 – Lens 10
Au Ag Cu Zn Pb
N/A N/A N/A N/A N/A</td></tr>
<tr><td>550</td><td colspan="2">Directly below highly deformed zone which contains folded muscovite. Staurolite porphyroblasts within an amphibole-quartz matrix.</td><td>891.6</td><td colspan="5">DUB198
(5100N)</td></tr>
<tr><td></td><td colspan="2">   </td><td colspan="6">Lithology
Quartz Sericite Kyanite Biotite Schist
Min. Style and Lens(es)
Type 4 - Lens 10
Au Ag Cu Zn Pb
0.1 5.14 0.02 0.01 0.01</td></tr>
<tr><td>551</td><td colspan="2">Directly below highly deformed zone which contains folded muscovite. Staurolite porphyroblasts within an amphibole-quartz matrix.</td><td>891.6</td><td colspan="5">DUB198
(5100N)</td></tr>
<tr><td></td><td colspan="2">   </td><td colspan="6">Lithology
Quartz Sericite Kyanite Biotite Staurolite Schist
Min. Style and Lens(es)
Type43 - Lens 10
Au Ag Cu Zn Pb
0.1 5.14 0.02 0.01 0.01</td></tr>
<tr><td>552</td><td colspan="2">Local quartz vein with euhedral chalcopyrite and pyrite. These veins are normally surrounded by gahnite; however, this is not the case here. Outside the vein is large garnet porphyroblasts with lesser staurolite in a matrix of quartz-amphibole.</td><td>1169.2</td><td colspan="5">DUB210
(5600N)</td></tr>
<tr><td></td><td colspan="2">   </td><td colspan="6">Lithology
Staurolite-Garnet-Anthophyllite Cordierite Gneiss
Min. Style and Lens(es)
Type ? - Below lens 27
Au Ag Cu Zn Pb
1.44 20.91 0.72 0.61 0.02</td></tr>
<tr><td>553</td><td colspan="2">Matrix is very siliceous and contains quartz and sericite with minor amphibole and disseminated</td><td>921.5</td><td colspan="5">DUB252W01
(5600N)</td></tr>
</table>

	pyrite. This sample is out of the ore zone.						
			**Lithology**				
			Sericite Altered Biotite-Quartz Schist				
			Min. Style and Lens(es)				
			Weak min. - Far above lens 27				
			Au	**Ag**	**Cu**	**Zn**	**Pb**
			0.07	0.07	2.06	2.06	0.02
554	Pinhead garnets in a quartz amphibole matrix, with possible chlorite. Euhedral pyrite is present with lesser pyrrhotite. This sample is outside of the ore zone.		926.6		DUB252W01 (5600N)		
			**Lithology**				
			Sericite Altered Biotite-Quartz Schist				
			Min. Style and Lens(es)				
			Weak min. - Far above lens 27				
			Au	**Ag**	**Cu**	**Zn**	**Pb**
			0.07	0.07	2.06	2.06	0.02
555	Gahnite and pyrite rich vein in a quartz amphibole matrix. Small staurolite porphyroblasts are present.		983.9		DUB252W01 (5600N)		
			**Lithology**				
			Cordierite-Staurolite-Biotite Schist				
			Min. Style and Lens(es)				
			Type 1(?) - Above lens 27				
			Au	**Ag**	**Cu**	**Zn**	**Pb**
			0.07	7.54	0.12	0.13	0.08
556	Well formed arsenopyrite grains with pyrrhotite in a quartz amphibole matrix.		1003.4		DUB252W01 (5600N)		
			**Lithology**				
			Min. Chlorite Schist				
			Min. Style and Lens(es)				
			Type 1(?) - Above lens 27				
			Au	**Ag**	**Cu**	**Zn**	**Pb**
			1.44	1.44	0.01	0.01	0.02
557	Chlorite rich matrix with lesser amphibole. Elongated sphalerite grains are present with chalcopyrite, pyrite and pyrrhotite.		1008.2		DUB252W01 (5600N)		
			**Lithology**				
			Min. Chlorite Schist				
			Min. Style and Lens(es)				
			Type 3(?) - Lens 27				
			Au	**Ag**	**Cu**	**Zn**	**Pb**
			1.61	30.17	1.05	1.59	0.07

558	Copper-Gold rich zone with networked pyrite and chalcopyrite, and lesser pyrrhotite. The surrounding matrix is quartz and biotite.		1214.8		DUB252W01 (5600N)		
			**Lithology**				
			Qtz-Cord-Antho-Staur-Garnt Gneiss				
			Min. Style and Lens(es)				
			Type 2 - Lens 27				
			Au	**Ag**	**Cu**	**Zn**	**Pb**
			6.75	141.9	6.68	0.32	0.02
559	Sphalerite in long grains with euhedral pyrite and lesser chalcopyrite in a matrix with mostly chlorite and minor quartz.		966.9		DUB245 (5600N)		
			**Lithology**				
			Mineralized Rhyodacite				
			Min. Style and Lens(es)				
			Type 3 – Lens 21				
			Au	**Ag**	**Cu**	**Zn**	**Pb**
			0.31	15.43	0.46	5.04	0.16
560	Euhedral galena mixed in with cordierite in a chlorite rich matrix.		969.1		DUB245 (5600N)		
			**Lithology**				
			Talc Altered Schist with Galena				
			Min. Style and Lens(es)				
			Type 3 – Lens 21				
			Au	**Ag**	**Cu**	**Zn**	**Pb**
			0.65	62.06	0.08	0.02	1.41
561	Patches of sphalerite with gahnite inside, hosted in a quartz-ankerite matrix.		980.8		DUB245 (5600N)		
			**Lithology**				
			Mineralized Alt. Felsic Volcanic Fr				
			Min. Style and Lens(es)				
			Type ? - Lens 21				
			Au	**Ag**	**Cu**	**Zn**	**Pb**
			0.17	7.89	0.14	0.24	0.01
562	Massive sphalerite in a matrix of quartz and biotite.		1025.6		DUB245 (5600N)		
	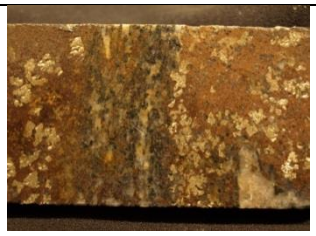	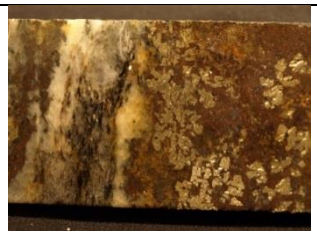	**Lithology**				
			Wkly Min. Alt. Felsic Vol. Fragmtnl				
			Min. Style and Lens(es)				
			Type 1 – Lens 25				
			Au	**Ag**	**Cu**	**Zn**	**Pb**
			0.79	1.03	0.03	0.03	0.01
563	Pyrite and chalcopyrite in euhedral flakes. Matrix		1078.5		DUB245		

	is quartz, biotite and ankerite. Large gahnite crystals are also present.				(5600N)	
			**Lithology**			
			Antho/Quartz/Bio/Chl/Gahnite Gneiss			
			Min. Style and Lens(es)			
			Type 2 - Lens 26			
			Au	**Ag**	**Cu**	**Zn**	**Pb**
			9.53	27.09	0.57	0.06	0.01
564	Chalcopyrite, pyrite and pyrrhotite in a quartz biotite matrix.		1085.9		DUB245 (5600N)		
			**Lithology**			
			Silicified Qtz/Amph/Bio/Ser/Chl Gne			
			Min. Style and Lens(es)			
			Type 2 - Lens 26			
			Au	**Ag**	**Cu**	**Zn**	**Pb**
			6.82	44.91	0.64	0.05	0.01
565	Gahnite rich zone with minor chalcopyrite in a matrix of chlorite and anthophyllite.		1129.3		DUB245 (5600N)		
			**Lithology**			
			Silicified Qtz/Amph/Cord/Staur/Gah			
			Min. Style and Lens(es)			
			Type 3-4 – Lens 26			
			Au	**Ag**	**Cu**	**Zn**	**Pb**
			2.3	9.26	0.22	0.05	0.02
566	Pyrrhotite and chalcopyrite in a vein with matrix of quartz and biotite. Gahnite is also present.		1142.5		DUB245 (5600N)		
			**Lithology**			
			Silicified Qtz/Amph/Cord/Staur/Gah			
			Min. Style and Lens(es)			
			Type 4 - Lens 28			
			Au	**Ag**	**Cu**	**Zn**	**Pb**
			1.75	16.46	0.32	0.09	0.01
567	Network of chalcopyrite in a quartz biotite matrix with some staurolite.		1146.5		DUB245 (5600N)		
			**Lithology**			
			Silicified Qtz/Amph/Cord/Staur/Gah			
			Min. Style and Lens(es)			
			Type 2 - Lens 27			
			Au	**Ag**	**Cu**	**Zn**	**Pb**
			12.3	73.37	2.4	0.17	0.01
568	Plagioclase and chlorite matrix with a network of pyrrhotite and lesser sphalerite and chalcopyrite.		906.5		DUB221 (5600N)		
			**Lithology**			

			WMN QFP Chl Gneiss				
			Min. Style and Lens(es)				
			Type 3(?) – Lens 20				
			Au	**Ag**	**Cu**	**Zn**	**Pb**
			3.84	68.23	2.47	0.96	0.68
569	Network of pyrrhotite, chalcopyrite and sphalerite in a quartz-chlorite matrix. This sample is in a heavily silicified zone.		909.1		DUB221 (5600N)		
			**Lithology**				
			Near Solid Sulphide				
			Min. Style and Lens(es)				
			Type 3(?) – Lens 20				
			Au	**Ag**	**Cu**	**Zn**	**Pb**
			0.31	38.06	0.56	13.99	0.8
570	Chalcopyrite rich with minor pyrhhotite in a matrix of quartz-amphibole and chlorite.		915.0		DUB221 (5600N)		
			**Lithology**				
			MN Amph-Bt-Crd Qtz Gneiss				
			Min. Style and Lens(es)				
			Type 3(?) – Lens 21				
			Au	**Ag**	**Cu**	**Zn**	**Pb**
			1.44	19.89	0.71	0.25	0.16
571	Two veins of pyrrhotite with lesser chalcopyrite and sphalerite separated by a zone of quartz-biotite-amphibole and chlorite. This assemblage is contained within a heavily silicified unit.		914.1		DUB221		
			**Lithology**				
			MN Amph-Bt-Crd Qtz Gneiss				
			Min. Style and Lens(es)				
			Type 2 - Lens 21				
			Au	**Ag**	**Cu**	**Zn**	**Pb**
			3.67	44.91	2.01	2.58	0.09
572	Coarse grained biotite and anthophyllite with the only sulfide being rare pyrite, this sample is part of the gold rich zone. Cordierite is also present with an unknown brown mineral.		965.8		DUB221 (5600N)		
			**Lithology**				
			Str-Crd-Chl-Act Qtz Gneiss				
			Min. Style and Lens(es)				
			Type 2 – Lens 25				
			Au	**Ag**	**Cu**	**Zn**	**Pb**
			12.89	9.94	0.01	0.01	0.01
573	Staurolite, chlorite, quartz, chlorite, biotite and		972.2		DUB221		

	amphibole matrix with rare pyrite. This sample also has high gold values, even with the few sulfides present.					(5600N)	
			**Lithology**				
			Str-Crd-Chl-Act Qtz Gneiss				
			Min. Style and Lens(es)				
			Type 2 – Lens 25				
			Au	**Ag**	**Cu**	**Zn**	**Pb**
			24.41	30.17	0.02	0.02	0.09
574	Network of pyrrhotite with lesser chalcopyrite and pyrite. Matrix is quartz, biotite with some chlorite and subhedral staurolite.			972.5		DUB221 (5600N)	
			**Lithology**				
			Str-Crd-Chl-Act Qtz Gneiss				
			Min. Style and Lens(es)				
			Type 2 – Lens 25				
			Au	**Ag**	**Cu**	**Zn**	**Pb**
			77.28	73.71	0.18	0.03	0.07
575	Chlorite dominated with pyrite and pyrrhotite in euhedral flakes with lesser sphalerite and galena, which are mostly concentrated in bands.			1014.3		DUB221 (5600N)	
			**Lithology**				
			Actinolite Chlorite Gneiss				
			Min. Style and Lens(es)				
			Type 3 - Below lens 25 above lens 26				
			Au	**Ag**	**Cu**	**Zn**	**Pb**
			N/A	N/A	N/A	N/A	N/A

Sample ID	Hand Sample Description		Interval (m)			DDH ID	
576	Local chalcopyrite and pyrrhotite grains associated with sphalerite and gahnite in a quartz biotite matrix. Carbonates may be present in nearby fracture veins.		1044.1			DUB221 (5600N)	
	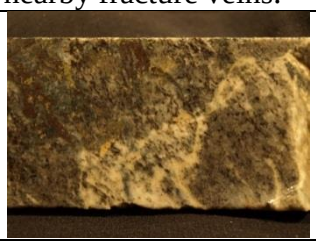		**Lithology**				
			Highly Altered Felsic Volcanic				
			Min. Style and Lens(es)				
			Weak mineralization - Below lens 25 above 26				
			Au	**Ag**	**Cu**	**Zn**	**Pb**
			0.82	2.74	0.05	0.43	0.01
577	Deformed grains of pyrite, pyrrhotite and chalcopyrite in a biotite-chlorite gneissic matrix. This segment, although representative of the surrounding 1 m interval, is the richest in sulfides.		1094.4			DUB221 (5600N)	

			**Lithology**				
			Ky-Bt-Chl Crd Gneiss				
			Min. Style and Lens(es)				
			Type 2 – Lens 27				
			Au	**Ag**	**Cu**	**Zn**	**Pb**
			7.89	41.83	0.95	0.14	0.01
578	Pyrrhotite and pyrite with minor chalcopyrite in a silicified matrix with minor chlorite. This sample is in a stringer zone.		1100.6		DUB221 (5600N)		
			**Lithology**				
			Chl-Amph Qtz Gneiss				
			Min. Style and Lens(es)				
			Type 2 – Lens 27				
			Au	**Ag**	**Cu**	**Zn**	**Pb**
			49.51	131.0	3.86	0.45	0.02
579	Quartz rich with minor chlorite and possibly biotite. This is another sample from a stringer zone with mostly pyrite and lesser chalcopyrite and pyrrhotite in euhedral grains.		1102.3		DUB221 (5600N)		
			**Lithology**				
			Chl-Amph Qtz Gneiss				
			Min. Style and Lens(es)				
			Type 2 – Lens 27				
			Au	**Ag**	**Cu**	**Zn**	**Pb**
			5.55	38.4	1.23	0.13	0.01
580	Stringers of pyrrhotite, pyrite and chalcopyrite bounded by biotite in a quartz biotite matrix.		1135.8		DUB221 (5600N)		
			**Lithology**				
			Chl-Amph Qtz Gneiss				
			Min. Style and Lens(es)				
			Type 2 – Lens 27				
			Au	**Ag**	**Cu**	**Zn**	**Pb**
			0.14	4.46	0.59	0.06	0.01
581	12 cm thick vein that consists of mostly pyrrhotite, pyrite and galena with minor chalcopyrite. The vein is bounded by epidote in a tuffaceous matrix of quartz, biotite, actinolite/tremolite and pinhead garnets. There are 2 other thick veins nearby this sample that consist mainly of pyrrhotite (i.e. feature is not entirely localized).		803.7		DUB258W01 (5700N)		
		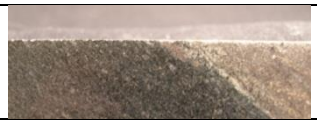	**Lithology**				
			Altered Silicified Mineralized Zone				
			Min. Style and Lens(es)				

			Weak mineralization – No lens				
			Au	**Ag**	**Cu**	**Zn**	**Pb**
			0.46	10	0.05	0.73	0.37
582	Pyrite and sphalerite with lesser galena and chalcopyrite; galena is always found associated with sphalerite in this section.		822.9		DUB258W01 (5700N)		
			**Lithology**				
			Altered Silicified Mineralized Zone				
			Min. Style and Lens(es)				
			Type 1-3 – No lens				
			Au	**Ag**	**Cu**	**Zn**	**Pb**
			0.3	30	0.23	4.53	0.76
583	Network of pyrrhotite, pyrite and sphalerite with minor chalcopyrite in a matrix of chlorite. This area is a semi-massive sulfide zone located above and below a chlorite-cordierite rich zone.		906.5		DUB258W01 (5650N)		
			**Lithology**				
			Mineralized Chlorite Bio +/- Ky Schist				
			Min. Style and Lens(es)				
			Type 1-3 – Lens 21				
			Au	**Ag**	**Cu**	**Zn**	**Pb**
			16.48	59	1.63	10.8	0.06
584	Galena with accessory pyrite and pyrrhotite in a quartz-biotite-chlorite matrix. This sample has exceptionally high Au values which may be associated with the galena.		946.5		DUB258W01 (5650N)		
			**Lithology**				
			Cordierite Biotite Anth Garnet Gneiss				
			Min. Style and Lens(es)				
			Type 3 – Lens 25				
			Au	**Ag**	**Cu**	**Zn**	**Pb**
			127.5	0.01	0.43	0.19	0.62
585	Sphalerite and pyrite in a sliicifed semi-massive zone with a mainly quartz matrix with minor chlorite.		946.7		DUB258W01 (5650N)		
			**Lithology**				
			Cordierite Biotite Anth Garnet Gneiss				
			Min. Style and Lens(es)				
			Type 3 – Lens 25				
			Au	**Ag**	**Cu**	**Zn**	**Pb**
			43.9	60	0.37	7.2	0.23
586	Galena and sphalerite with trace pyrite in a quartz rich matrix with minor chlorite. This sample has		949.3		DUB258W01 (5650N)		

	similar mineralization to 584; however, substantially lower Au and Ag values.						
	 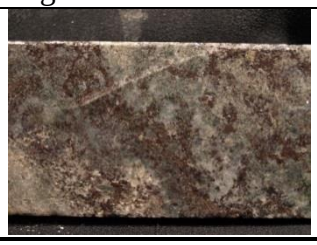	**Lithology**					
		Cordierite Biotite Anth Garnet Gneiss					
		Min. Style and Lens(es)					
		Type 3 – Lens 25					
		Au	**Ag**	**Cu**	**Zn**	**Pb**	
		1.12	38	0.21	5.15	1.55	
587	Massive sulfide zone with large pyrite grains and interstitial sphalerite and calcite.	956.0		DUB258W01 (5650N)			
	 	**Lithology**					
		Near Solid to Solid Sulphide Zone					
		Min. Style and Lens(es)					
		Type 3 – Lens 25					
		Au	**Ag**	**Cu**	**Zn**	**Pb**	
		0.6	13	0.25	17.56	0.36	
588	Pyrrhotite and pyrite with minor sphalerite in a quartz-biotite matrix. This is part of a stringer zone.	768.5		DUB230 (5600N)			
	 	**Lithology**					
		Garnet Biotite Gneiss					
		Min. Style and Lens(es)					
		Type 1 – Above lens 21					
		Au	**Ag**	**Cu**	**Zn**	**Pb**	
		0.1	15.77	0.11	2.2	0.33	
589	Pyrrhotite and sphalerite with minor chalcopyrite in a biotite-epidote matrix.	787.0		DUB230 (5600N)			
	 	**Lithology**					
		Disseminated Sulphides					
		Min. Style and Lens(es)					
		Type 1 - Above lens 21					
		Au	**Ag**	**Cu**	**Zn**	**Pb**	
		1.1	63.77	1.4	3.62	0.63	
590	Pyrite and sphalerite in a zone of Ca-alteration with a calcite-epidote matrix.	778.5		DUB230 (5600N)			
	 	**Lithology**					
		Well Mineralized Felsic Volcanics					
		Min. Style and Lens(es)					
		Type 1 – Above lens 21					
		Au	**Ag**	**Cu**	**Zn**	**Pb**	
		0.17	6.17	0.05	1.44	0.01	
591	Silicified matrix with minor biotite and abundant sphalerite and chalcopyrite.	855.2		DUB230 (5600N)			
	 	**Lithology**					

			Chlorite Kyanite Sericite Gahnite Gniess				
			Min. Style and Lens(es)				
			Type 1(?) – Above lens 21				
			Au	**Ag**	**Cu**	**Zn**	**Pb**
			1.75	82.97	0.18	16.52	3.74
592	Sphalerite and pyrite with lesser pyrrhotite in elongate disordered grains in a sericite chlorite matrix.		858.5		DUB230 (5600N)		
			**Lithology**				
			Chlorite Kyanite Sericite Gahnite Gniess				
			Min. Style and Lens(es)				
			Type 1 – Lens 21				
			Au	**Ag**	**Cu**	**Zn**	**Pb**
			11.59	80.23	1.47	2.56	0.18
593	Abundant chalcopyrite with lesser pyrrhotite in a quartz-biotite matrix. This sample is in a small Au-rich zone, outside of the main ore zone.		861.9		DUB230 (5600N)		
			**Lithology**				
			Chlorite Kyanite Sericite Gahnite Gniess				
			Min. Style and Lens(es)				
			Type 4 – Above lens 21				
			Au	**Ag**	**Cu**	**Zn**	**Pb**
			64.29	109.8	0.99	0.07	0.03
594	Abundant chalcopyrite, similar to 593 but with less pyrrhotite. Matrix is quartz biotite and sericite.		863.5		DUB230 (5600N)		
			**Lithology**				
			Chlorite Kyanite Sericite Gahnite Gniess				
			Min. Style and Lens(es)				
			Type 4 – Directly above lens 21				
			Au	**Ag**	**Cu**	**Zn**	**Pb**
			102.0	435.1	3.56	0.31	0.06
595	Network of chalcopyrite with euhedral pyrite and interstitial sphalerite. Minor calcite is present as well.		881.5		DUB230 (5600N)		
	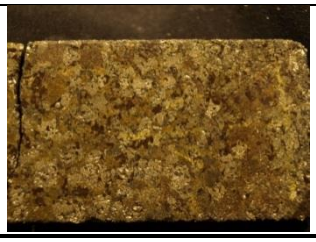	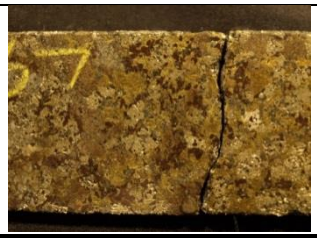	**Lithology**				
			Near Solid Sulphide				
			Min. Style and Lens(es)				
			Type 1 – Lens 21				
			Au	**Ag**	**Cu**	**Zn**	**Pb**
			20.4	116.6	3.34	10.64	0.57
596	Pyrite and sphalerite with interstitial calcite. This		884.5		DUB230		

	is from the same ore zone as 595.				(5600N)	
	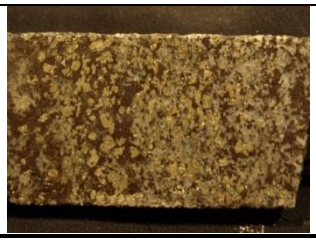 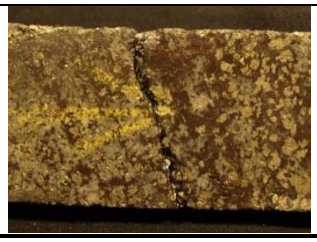	**Lithology**				
		Near Solid Sulphide				
		Min. Style and Lens(es)				
		Type 1 – Lens 21				
		Au	**Ag**	**Cu**	**Zn**	**Pb**
		0.65	39.09	0.24	14.04	1.61
597	Network of sphalerite and pyrrhotite in a quartz-biotite matrix. This well mineralized, zinc-rich sample is outside of the main ore zone.	733.5		DUB216		
	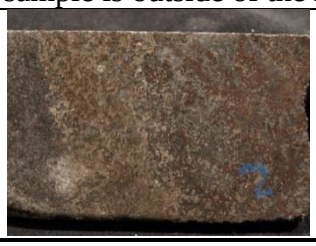 	**Lithology**				
		Amphibolitized Rhyolite				
		Min. Style and Lens(es)				
		Type 1 – Above 21 and 20				
		Au	**Ag**	**Cu**	**Zn**	**Pb**
		0.17	19.54	0.15	11.4	0.18
598	Coarse pyrite grains are at the top of this sample with interstitial sphalerite. The center is almost completely sphalerite with minor quartz. This sample is part of a discontinuous massive sulfide which alternates with intervals of footwall material.	740.6		DUB216		
	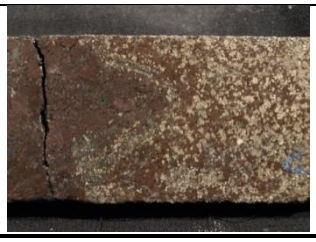 	**Lithology**				
		Near-Solid to Solid Sulphides				
		Min. Style and Lens(es)				
		Type 1 – Lens 21 (above 20)				
		Au	**Ag**	**Cu**	**Zn**	**Pb**
		0.34	39.43	0.05	12.6	0.72
599	Coarse grained pyrite with minor sphalerite and trace chalcopyrite in a quartz-biotite matrix. This is from the same ore zone as 598. Immediately below this sample, aggregates of quartz-calcite begin to appear. The matrix of this sample may be carbonaceous.	741.8		DUB216		
	 	**Lithology**				
		Near-Solid to Solid Sulphides				
		Min. Style and Lens(es)				
		Type 1 – Lens 21 (above 20)				
		Au	**Ag**	**Cu**	**Zn**	**Pb**
		1.89	47.66	0.75	7.01	0.56
600	Silicified zone with whispy grains of pyrite and chalcopyrite. This zone is Au-rich but roughly 10 m below the main ore zone. The surrounding area is weakly mineralized.	751.9		DUB216		
	 	**Lithology**				

			Mineralized Kyanite-Biotite-Sericite Quartz Schist				
			Min. Style and Lens(es)				
			Type 2 – Below lenses 21 and 20				
			Au	**Ag**	**Cu**	**Zn**	**Pb**
			22.11	78.17	2.18	0.63	0.09

Sample ID	Hand Sample Description	Interval (m)	DDH ID
601	Disseminated pyrite and pyrrhotite in a matrix of quartz and biotite.	980.5	DUB262W01 (5600N)
		**Lithology**	
		Mineralized biot+ser+graph schist	
		Min. Style and Lens(es)	
		Weak mineralization - No lens	
		Au / 0.02	**Ag** / 6
		Cu / 0.05	**Zn** / 3.9
		Pb / 0.02	
602	Well mineralized pyrite and sphalerite with minor chalcopyrite in a quartz biotite matrix.	989.2	DUB262W01 (5600N)
		**Lithology**	
		Mineralized biot+ser+graph schist	
		Min. Style and Lens(es)	
		Type 4 – No lens	
		Au / 0.04	**Ag** / 3
		Cu / 0.33	**Zn** / 8.52
		Pb / 0.01	
603	Networked pyrrhotite and chalcopyrite in a matrix of coarse grained biotite.	995.4	DUB262W01 (5600N)
		**Lithology**	
		MN cord+ant±stau±chl±gar±kya gneiss	
		Min. Style and Lens(es)	
		Type 2 – No lens	
		Au / 1.2	**Ag** / 9
		Cu / 2.36	**Zn** / 0.03
		Pb / 0.01	
604	Chlorite rich matrix with chalcopyrite grains in a quartz rich matrix with minor amphibole.	1030.5	DUB262W01 (5600N)
		**Lithology**	
		MN cord+gar±chl±biot±anth±stau gneiss	
		Min. Style and Lens(es)	
		Type 3 – No lens	
		Au / 8.67	**Ag** / 9
		Cu / 2.09	**Zn** / 0.02
		Pb / 0.01	
605	Chalcopyrite stringers with gahnite in a matrix of	1241.4	DUB262W01

	quartz-biotite. Staurolite is present with trace garnet. These chalcopyrite stringers are the only sulfides in the area, there are others like it but they are separated by around 5 m each.			(5600N)		
	 	**Lithology**				
		MN qtz/cord+biot+anth gneiss				
		Min. Style and Lens(es)				
		Type 2 - Far West of lens 27				
		Au	**Ag**	**Cu**	**Zn**	**Pb**
		1.78	48	4.13	0.72	0.07
606	Lightly fractured zone with ankerite veins, anthophyllite and quartz with grains of chalcopyrite, sphalerite and gahnite.	1321.1		DUB262W01 (5600N)		
	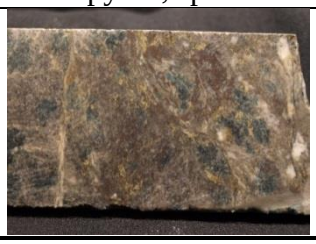 	**Lithology**				
		MN qtz/cord+biot+anth gneiss				
		Min. Style and Lens(es)				
		Type 4 – No lens				
		Au	**Ag**	**Cu**	**Zn**	**Pb**
		1.12	25	1.97	0.39	0.01
607	Network of chalcopyrite with lesser pyrrhotite in a matrix of quartz, biotite with minor anthophyllite. This sample is from a discontinuous chalcopyrite stringer zone; it shows the strongest mineralization and lies about 0.5 m above an amphibolite dike.	1321.6		DUB262W01 (5600N)		
	 	**Lithology**				
		MN qtz/cord+biot+anth gneiss				
		Min. Style and Lens(es)				
		Type 2 – No lens				
		Au	**Ag**	**Cu**	**Zn**	**Pb**
		2	43	2.84	0.51	0.01
608	Semi-massive pyrite with lesser sphalerite and pyrrhotite. Matrix is quartz with dark green amphiboles (actinolite/tremolite).	828.7		DUB169 (5600N)		
	 	**Lithology**				
		Mineralized Altered Rhyodacite				
		Min. Style and Lens(es)				
		Type 3 - Above lenses 21 and 20				
		Au	**Ag**	**Cu**	**Zn**	**Pb**
		0.48	44.57	0.28	4.88	1.06
609	Pyrrhotite and sphalerite with minor pyrite and chalcopyrite in a quartz-biotite-chlorite matrix. This sample is below the semi-massive zone and is part of a “stringer” zone.	831.3		DUB169 (5600N)		
	 	**Lithology**				

			Mineralized Altered Rhyodacite				
			Min. Style and Lens(es)				
			Type 3 - Above lenses 21 and 20				
			Au	**Ag**	**Cu**	**Zn**	**Pb**
			0.31	28.8	0.18	3.64	0.44
610	Euhedral pyrite and pyrrhotite with minor chalcopyrite and sphalerite. The matrix is chlorite-biotite-quartz. The area surrounding this sample is rich in calcite.		893.1		DUB169 (5600N)		
			**Lithology**				
			Chlorite Altered Rhyodacite				
			Min. Style and Lens(es)				
			Type 3 - Top of 21 and West of 20				
			Au	**Ag**	**Cu**	**Zn**	**Pb**
			3.43	44.91	0.98	1.9	0.44
611	Vein of sphalerite and galena with minor chalcopyrite in a quartz-sericite-gahnite-biotite matrix. These galena-sphalerite veins are common throughout this quartz sericite assemblage.		900.5		DUB169 (5600N)		
			**Lithology**				
			Chlorite Altered Rhyodacite				
			Min. Style and Lens(es)				
			Type 3 - Lens 21				
			Au	**Ag**	**Cu**	**Zn**	**Pb**
			1.27	42.51	0.14	7.13	8.2
612	Network of chalcopyrite and pyrrhotite in a matrix of quartz-biotite with minor chlorite. This vein in total is roughly 15 cm and is below a chlorite rich zone and above a quartz-sericite zone.		903.2		DUB169 (5600N)		
			**Lithology**				
			Chlorite Altered Rhyodacite				
			Min. Style and Lens(es)				
			Type 3 - Lens 21				
			Au	**Ag**	**Cu**	**Zn**	**Pb**
			1.71	10.97	0.43	0.88	0.02
613	Small chalcopyrite crystals (~5 mm) in a quartz-biotite matrix with sericite and possibly cordierite. This zone has high Au values but a very small amount of sulfides.		904.5		DUB169 (5600N)		
			**Lithology**				
			Chlorite Altered Rhyodacite				
			Min. Style and Lens(es)				
			Type 4 – Lens 21				
			Au	**Ag**	**Cu**	**Zn**	**Pb**

			55.95	165.6	1.91	0.25	0.08
614	Pyrrhotite with lesser chalcopyrite and minor pyrite in a network with a matrix of quartz and biotite. This sample is a vein within a biotite-quartz-garnet-staurolite assemblage.		908.2		DUB169 (5600N)		
			**Lithology**				
			Chlorite Altered Rhyodacite				
			Min. Style and Lens(es)				
			Type 2 - Lens 21				
			Au	**Ag**	**Cu**	**Zn**	**Pb**
			46.49	132	1.65	0.19	0.02
615	Pyrrhotite and chalcopyrite in a quartz-biotite matrix. This assemblage is Au-rich but relatively poor in sulfides; however, the interval chosen has roughly 20% sulfides compared to the matrix with roughly 5% sulfides.		914.2		DUB169 (5600N)		
			**Lithology**				
			Rhyodacite Fragmental				
			Min. Style and Lens(es)				
			Type 4 - Lens 21				
			Au	**Ag**	**Cu**	**Zn**	**Pb**
			17.25	57.26	1.47	0.1	0.01
616	This sample is only slightly down core from 615; with a bit over 5% sulfides (pyrite, pyrrhotite and chalcopyrite) it is slightly more enriched than the surrounding area but not by much. Once again, this area is Au-rich . Garnet is also present in this quartz-biotite matrix.		914.8		DUB169 (5600N)		
			**Lithology**				
			Rhyodacite Fragmental				
			Min. Style and Lens(es)				
			Type 2 - Lens 21				
			Au	**Ag**	**Cu**	**Zn**	**Pb**
			12.48	4.8	0.06	0.01	0.01
617	Sulfide poor zone with a small 3 cm interval of pyrrhotite with minor chalcopyrite and pyrite. The surrounding matrix is quartz-biotite-actinolite/tremolite with disseminated chalcopyrite and pyrrhotite. Once again, this sample is Au-rich with few sulfides.		922.8		DUB169 (5600N)		
			**Lithology**				
			Rhyodacite Fragmental				
			Min. Style and Lens(es)				
			Type 2 - Lens 21				
			Au	**Ag**	**Cu**	**Zn**	**Pb**

<table>
<tr><td></td><td colspan="2"></td><td>12.41</td><td>100.1</td><td>1.43</td><td>0.17</td><td>0.29</td></tr>
<tr><td>618</td><td colspan="2">Durchbewegung texture with euhedral pyrite and interstitial sphalerite and quartz-calcite. This massive sulfide interval is only about 40 cm long and constitutes the only major sulfide rich zone encountered in this hole.</td><td colspan="2">929.6</td><td colspan="3">DUB169
(5600N)</td></tr>
<tr><td></td><td colspan="2">   </td><td colspan="5">Lithology
Rhyodacite Fragmental
Min. Style and Lens(es)
Type 1 - Between lens 21 and 25
Au | Ag | Cu | Zn | Pb
0.62 | 32.57 | 0.76 | 11.8 | 0.98</td></tr>
<tr><td>619</td><td colspan="2">Pyrrhotite with lesser pyrite in a lightly foliated network. Matrix is very fine grained biotite and quartz. This zone is barren (low Au-Cu-Zn)</td><td colspan="2">1039.6</td><td colspan="3">DUB169DPN
(5600N)</td></tr>
<tr><td></td><td colspan="2">   </td><td colspan="5">Lithology
Weak Mineralized Rhy
Min. Style and Lens(es)
Weak mineralization - Below lens 25
Au | Ag | Cu | Zn | Pb
0.10 | 1.03 | 0.06 | 0.02 | 0.00</td></tr>
<tr><td>620</td><td colspan="2">Barren sulfide zone; euhedral pyrite with trace chalcopyrite in a biotite-cordierite-quartz matrix with kyanite porphyroblasts. This sample was collected for a compare and contrast with Au-Cu-Zn rich zones.</td><td colspan="2">1050.9</td><td colspan="3">DUB246W02**
(5750N)
**DUB246W01 was the only hole found.</td></tr>
<tr><td></td><td colspan="2">   </td><td colspan="5">Lithology
Quartz Biotite Gneiss
Min. Style and Lens(es)
Weak mineralization – Unknown lens
Au | Ag | Cu | Zn | Pb
0.02 | 0.01 | 0.02 | 0.02 | 0.01</td></tr>
<tr><td>621</td><td colspan="2">Gahnite, sphalerite, pyrite and pyrrhotite in a matrix of quartz-anthophyllite-biotite. This sample is near the top of the ore horizon.</td><td colspan="2">1075.1</td><td colspan="3">DUB246W02**
(5750N)</td></tr>
<tr><td></td><td colspan="2">   </td><td colspan="5">Lithology
Quartz Biotite Gneiss
Min. Style and Lens(es)
Weak mineralization – Unknown lens
Au | Ag | Cu | Zn | Pb
0.65 | 4 | 0.1 | 0.01 | 0.01</td></tr>
<tr><td>622</td><td colspan="2">Networked chalcopyrite and pyrite with minor pyrrhotite in a chlorite-biotite matrix with minor staurolite. This sample is the only sulfides for a roughly 1 m either way and it has the highest Au</td><td colspan="2">1077.3</td><td colspan="3">DUB246W02**
(5750N)</td></tr>
</table>

	grade in the vicinity.					
	 	**Lithology**				
		Quartz Biotite Gneiss				
		Min. Style and Lens(es)				
		Type 2 – Unknown lens				
		Au	**Ag**	**Cu**	**Zn**	**Pb**
		10.1	60	0.84	0.08	0.01
623	Euhedral chalcopyrite grains in a chlorite-cordierite-anthophyllite matrix. Partially retrograded staurolites are also present. This sample is above the Cu-Au zone.	1173.0		DUB246W02** (5750N)		
	 	**Lithology**				
		Quartz Chlorite Gneiss				
		Min. Style and Lens(es)				
		Type 3 – Unknown lens				
		Au	**Ag**	**Cu**	**Zn**	**Pb**
		0.28	3	0.41	0.05	0.01
624	Chalcopyrite and pyrrhotite rich with large gahnite crystals in a quartz-anthophyllite matrix.	1175.3		DUB246W02** (5750N)		
	 	**Lithology**				
		Quartz Chlorite Gneiss				
		Min. Style and Lens(es)				
		Type 4 – Unknown lens				
		Au	**Ag**	**Cu**	**Zn**	**Pb**
		7.91	52	3.96	0.78	0.01
625	This sample is at the base of the Cu-Au zone where silicification has increased. Chalcopyrite and pyrrhotite are present with large gahnite crystals in a silica rich matrix. Partially retrograded staurolites are still present.	1177.2		DUB246W02** (5750N)		
	 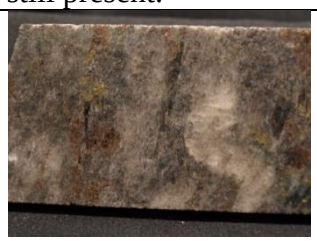	**Lithology**				
		Quartz Chlorite Gneiss				
		Min. Style and Lens(es)				
		Type 4 - Unknown lens				
		Au	**Ag**	**Cu**	**Zn**	**Pb**
		1.66	7	0.52	0.03	0.01

Sample ID	Hand Sample Description	Interval (m)	DDH ID
626	Folded chalcopyrite vein in a quartz-rich matrix with minor amphibole and well formed garnet porphyroblasts. There is no nearby significant mineralization in this area.	1228.3	DUB246W02** (5750N)
	 	**Lithology**	

			Quartz Amphibole Gneiss				
			Min. Style and Lens(es)				
			Type 4 – Unknown lens				
			Au	**Ag**	**Cu**	**Zn**	**Pb**
			5.94	35	3.54	0.12	0.01
627	Heavy quartz-ankerite fracturing with a small amount of chalcopyrite above, below and in the middle of the fracturing. This is from a quartz-amphibole section where garnet and staurolite are common. This sample represent a local feature as fractures are generally minor in this area and could be an indication of a shear zone.		1246.3		DUB246W02** (5750N)		
			**Lithology**				
			Quartz Amphibole Gneiss				
			Min. Style and Lens(es)				
			Type 4 – Unknown lens				
			Au	**Ag**	**Cu**	**Zn**	**Pb**
			1.96	9	0.48	0.01	0.01
628	Dominant chalcopyrite with minor pyrrhotite and pyrite in a quartz-rich vein with minor garnets. This vein is part of a larger (1.5 m) quartz-ankerite fracture vein. The fracturing overprints the original textures and mineralogy.		1293.6		DUB246W02** (5750N)		
			**Lithology**				
			Quartz Biotite Gneiss				
			Min. Style and Lens(es)				
			Type 4 – Unknown lens				
			Au	**Ag**	**Cu**	**Zn**	**Pb**
			4.59	36	3.81	0.16	0.01
629	Small disseminated chalcopyrite crystals in a fine grained quartz-biotite-amphibole matrix. This sample is from a small isolated chalcopyrite zone from 1365.4 – 1368.0 m. There are no sulfides in either direction for several meters.		1367.3		DUB246W02** (5750N)		
			**Lithology**				
			Quartz Anthophyllite Gneiss				
			Min. Style and Lens(es)				
			Type 4 – Unknown lens				
			Au	**Ag**	**Cu**	**Zn**	**Pb**
			0.38	3	0.14	0.01	0.01
630	Network of sphalerite with lesser pyrite and trace chalcopyrite and galena in a chlorite-carbonate		1019.0		DUB210 (5600N)		

	matrix. The surrounding area is poor in sulfides.							
			**Lithology**					
			Carbonate-Chlorite Schist					
			Min. Style and Lens(es)					
			Type 3					
			Au	**Ag**	**Cu**	**Zn**	**Pb**	
			4.59	65.49	0.19	0.35	0.62	
631	Coarse well formed garnet porphyroblasts with minor staurolites in a dominantly chlorite matrix with minor biotite. Chalcopyrite with minor pyrrhotite generally wrap around the garnets. This sample was collected as it shows how sulfides are remobilized. Sulfides are discontinuous in the area.		1210.6		DUB273** (5600N) **This drill hole has not been plotted on the most current drill plan			
			**Lithology**					
			Qtz Feld Gt Amph Gneiss					
			Min. Style and Lens(es)					
			Type 2 – Unknown lens					
			Au	**Ag**	**Cu**	**Zn**	**Pb**	
			1.26	6	2.35	0.01	0.01	
632	Stringers of pyrrhotite and pyrite with minor chalcopyrite in a quartz-biotite matrix with minor garnets. Calcic alteration is present (anhydrite, calcite, epidote) and associated with the sulfides. This sample was selected as to examine the relative timing of the calcic alteration and sulfide precipitation (and/or remobilization). This is part of a larger (~9m) stringer zone.		841.3		DUB191 (5400N)			
			**Lithology**					
			Mafic Crystal Wacke					
			Min. Style and Lens(es)					
			Type 1 - Above lens 10					
			Au	**Ag**	**Cu**	**Zn**	**Pb**	
			0.34	28.11	0.28	0.02	0.23	
633	Networked pyrite, pyrrhotite, sphalerite with some durchbawergung texture. Matrix is quartz and biotite. This sample is representative of the same sulfide zone as 632.		843.6		DUB191 (5400N)			
		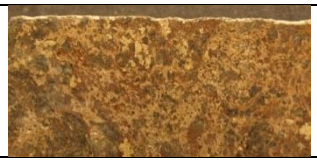	**Lithology**					
			Stringer to Near Solid Sulphide Zone					
			Min. Style and Lens(es)					
			Type 1 – Lens 10					

			Au	Ag	Cu	Zn	Pb
			0.17	20.57	0.5	4.64	0.02
634	Networked pyrite, pyrrhotite, sphalerite and minor chalcopyrite in a matrix of biotite and quartz. This sample is representative of its contained ore zone.		877.9		DUB191 (5400N)		
			**Lithology**				
			Solid to Near Solid Sulphide Zone				
			Min. Style and Lens(es)				
			Type 1 – Lens 10				
			Au	**Ag**	**Cu**	**Zn**	**Pb**
			0.69	19.54	0.68	12.33	0.03
635	Sphalerite and quartz-biotite matrix showing durchbawergung texture with euhedral pyrite grains.		879.4		DUB191 (5400N)		
			**Lithology**				
			Solid to Near Solid Sulphide Zone				
			Min. Style and Lens(es)				
			Type 1 – Lens 10				
			Au	**Ag**	**Cu**	**Zn**	**Pb**
			1.78	18.86	0.42	17.12	0.04
636	Networked pyrrhotite, pyrite and chalcopyrite in a matrix of quartz and biotite. This sample is in the same ore zones as 634 and 635 and is also representative of the highly variable mineralization.		881.7		DUB191 (5400N)		
			**Lithology**				
			Stringer Sulphide Zone				
			Min. Style and Lens(es)				
			Type 1 – Lens 10				
			Au	**Ag**	**Cu**	**Zn**	**Pb**
			0.55	17.83	0.75	0.1	0.03
637	Massive pyrite in a quartz-biotite matrix with kyanite being present in local clusters. This sample is representative of the contained sulfide rich zone.		911.5		DUB191 (5400N)		
			**Lithology**				
			Near Solid Sulphide Zone				
			Min. Style and Lens(es)				
			Type 1 – Lens 10				
			Au	**Ag**	**Cu**	**Zn**	**Pb**

			0.14	14.06	0.02	0.07	0.22
638	Gahnite-anthophyllite-biotite rich matrix with minor pyrite and pyrrhotite. This sample lies directly on top of the zinc rich zone.		1153.6		DUB191		
			**Lithology**				
			Epidote Altered Cordierite Staurolite Anthophyllite Gneiss				
			Min. Style and Lens(es)				
			Type 1 – Above lens 40				
			Au	**Ag**	**Cu**	**Zn**	**Pb**
			34.59	59.31	0.23	7.87	0.08
639	Massive sphalerite and pyrite. This sample is directly within the zinc rich zone.		1154.8		DUB191		
			**Lithology**				
			Mineralized Zone Solid to Near Solid Sulphide				
			Min. Style and Lens(es)				
			Type 1 – Lens 40				
			Au	**Ag**	**Cu**	**Zn**	**Pb**
			8.74	18.51	0.62	37.23	0.01
640	Gahnite-anthophyllite-quartz with minor biotite and minor ankerite fracture veins. This sample is directly below the ore zone.		1156.1		DUB191		
	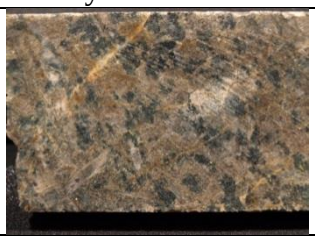		**Lithology**				
			Mixed Mineralized Zones and NSS				
			Min. Style and Lens(es)				
			Type 1 – Below lens 40				
			Au	**Ag**	**Cu**	**Zn**	**Pb**
			1.1	8.57	0.26	24.36	0.01
641	Bands of pyrite in a quartz-biotite matrix. This sample is representative of the assemblage leading up to the massive sulfide zone; it is directly below a sericite-pyrite rich zone (see Antoine for sample 339 right next to this one).		883.3		DUB198 (5100N)		
			**Lithology**				
			Quartz Sericite Kyanite Biotite Schist				
			Min. Style and Lens(es)				
			Type 1 – Lens 10				
			Au	**Ag**	**Cu**	**Zn**	**Pb**
			0.27	9.94	0.07	0.01	0.02
642	Durchbewegung texture (difficult to see due to rusting) with massive pyrite and sphalerite (and minor chalcopyrite with possible calcite as		902.3		DUB198 (5100N)		

	weathered out pockets). This is the uppermost interval of the massive sulfide zone.						
			**Lithology**				
			Mineralized Sericite Kyanite Quartz Biotite Gneiss				
			Min. Style and Lens(es)				
			Type 1 – Lens 10				
			Au	**Ag**	**Cu**	**Zn**	**Pb**
			0.27	27.43	0.79	8.66	0.23
643	Massive pyrite and sphalerite after a 20 cm intrusion. Calcite may be present as well. This sample is from the base of the massive sulfide zone.		905.7		DUB198 (5100N)		
			**Lithology**				
			Sulphide Zone				
			Min. Style and Lens(es)				
			Type 1 – Lens 10				
			Au	**Ag**	**Cu**	**Zn**	**Pb**
			0.14	7.2	0.23	12.78	0.01
644	Euhedral galena with pyrite in a matrix of actinolite-tremolite-quartz and biotite. This sample is roughly 7 m below the massive pyrite and sphalerite.		913.4		DUB198 (5100N)		
			**Lithology**				
			Biotite Chlorite Kyanite Schist				
			Min. Style and Lens(es)				
			Type 3(?) – Lens 10				
			Au	**Ag**	**Cu**	**Zn**	**Pb**
			18.48	294.9	0.09	0.01	1.97
645	Chalcopyrite vein above the near-solid chalcopyrite zone. Surrounding matrix is medium grained quartz and biotite.		1358.4		DUB265W01 (5900N)		
			**Lithology**				
			Quartz Anthophylite Gneiss				
			Min. Style and Lens(es)				
			Type 2 – No lens				
			Au	**Ag**	**Cu**	**Zn**	**Pb**
			7.51	76	9.54	6.22	0.01
646	Quartz veins with gahnite and chalcopyrite in a surrounding matrix of quartz-amphibole-biotite. Minor garnets are present as well; however, they are highly deformed and may be present as both		1364.7		DUB265W01 (5900N)		

	almandine and grossular (based on colour only as textures are destroyed).							
			**Lithology**					
			Quartz Anthophylite Gneiss					
			Min. Style and Lens(es)					
			Type 2 – No lens					
			Au	**Ag**	**Cu**	**Zn**	**Pb**	
			1.7	10	3.26	0.18	0.01	
647	Semi-massive chalcopyrite and gahnite adjacent to a quartz vein. Surrounding matrix is quartz-biotite.		1367.1		DUB265W01 (5900N)			
			**Lithology**					
			Quartz Anthophylite Gneiss					
			Min. Style and Lens(es)					
			Type 3 – No lens					
			Au	**Ag**	**Cu**	**Zn**	**Pb**	
			31.98	53	6.1	0.38	0.01	
648	Semi-massive networked chalcopyrite with minor pyrrhotite in a quartz-biotite matrix with common garnets. This sample is within the Au-Cu ore zone.		1368.5		DUB265W01 (5900N)			
			**Lithology**					
			Near Solid Sulfide					
			Min. Style and Lens(es)					
			Type 1 – No lens					
			Au	**Ag**	**Cu**	**Zn**	**Pb**	
			6.63	78	15.13	0.82	0.02	
649	Chalcopyrite within a quartz vein surrounded by a matrix of garnet-amphibole-biotite-quartz. This is well below the Au-Cu ore zone.		1390.3		DUB265W01 (5900N)			
			**Lithology**					
			Quartz Anthophylite Gneiss					
			Min. Style and Lens(es)					
			Type 2 – No lens					
			Au	**Ag**	**Cu**	**Zn**	**Pb**	
			0.1	0.01	0.16	0.02	0.01	
650								
			Lithology					
			Min. Style and Lens(es)					

			Au	Ag	Cu	Zn	Pb
			N/A	N/A	N/A	N/A	N/A

Sample ID	Hand Sample Description	Interval (m)	DDH ID
651	Pyrrhotite and gahnite with lesser pyrite in a matrix of chlorite, biotite and calcite. This sample was collected to evaluate the potential for de-sulfidation of pyrite and sphalerite to give pyrrhotite and gahnite as seen in this sample.	876.3	DUB255W01
	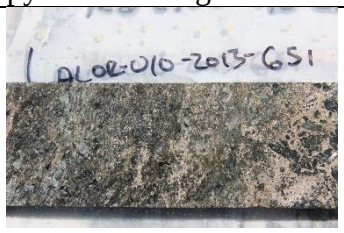 	**Lithology**	
		Min. Style and Lens(es)	
		Type 1 - Lens 10	

Au	Ag	Cu	Zn	Pb
0.274	9.26	0.66	0.15	0.00

Sample ID	Hand Sample Description	Interval (m)	DDH ID
652	Coarse grains of pyrite and sphalerite with lesser galena (best seen on the sides) in a matrix with calcium, actinolite-tremolite and epidote.	909.2	DUB211
	 	**Lithology**	
		Min. Style and Lens(es)	
		Type 3 - Above 10	

Au	Ag	Cu	Zn	Pb
4.56	282.5	0.12	1.36	16.70

Sample ID	Hand Sample Description	Interval (m)	DDH ID
653	Quartz-biotite gneiss with pyrite and chalcopyrite following the foliation. This sample is part of an Au-Cu zone.	1005.1	DUB185W01
	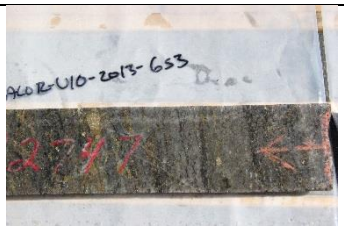 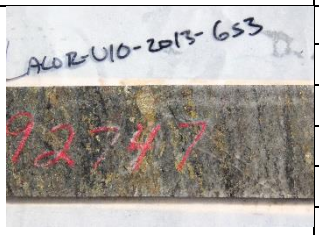	**Lithology**	
		Min. Style and Lens(es)	
		Type 2 - Lens 10	

Au	Ag	Cu	Zn	Pb
8.115	65.49	2.49	0.15	0.00

Sample ID	Hand Sample Description	Interval (m)	DDH ID
654	Coarse pyrite and galena with interstitial sphalerite in a matrix of almost entirely carbonates.	877.8	DUB174
	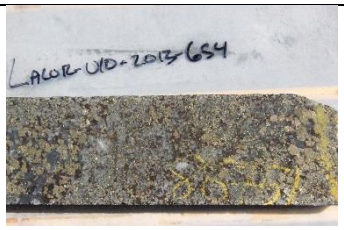 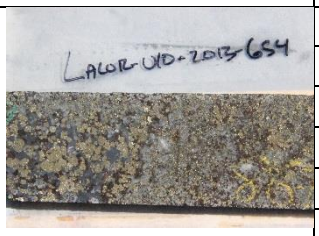	**Lithology**	
		Min. Style and Lens(es)	
		Type 1 – Lens 31	

Au	Ag	Cu	Zn	Pb
2.023	99.77	0.26	10.23	7.43

Sample ID	Hand Sample Description	Interval (m)	DDH ID
655	Weakly mineralized fine grained quartz-biotite-	89.5	LD0013

	actinolite/tremolite. This sample is right in the 10 lens but has low sulfides and very high Au and Ag.						
	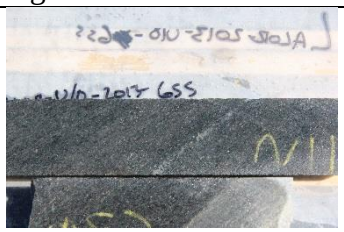	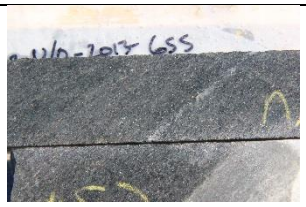	**Lithology**				
			NSS_SS				
			Min. Style and Lens(es)				
			Type X - Lens 10				
			Au	**Ag**	**Cu**	**Zn**	**Pb**
			7.749	117.5	0.21	0.15	0.7
656	Weakly mineralized pyrite and pyrrhotite in a quartz-biotite-diopside matrix.		206.4		LP00011		
	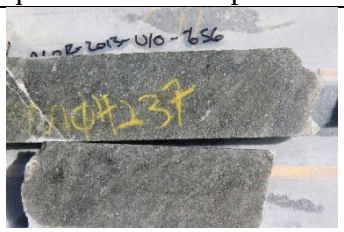		**Lithology**				
			NSS				
			Min. Style and Lens(es)				
			Type 4 - Lens 40				
			Au	**Ag**	**Cu**	**Zn**	**Pb**
			28.87	53.93	0.33	0.09	0.35
657	Strong galena mineralization with accessory pyrite in a chlorite dominated matrix with lesser calcite, anhydrite and actinolite-tremolite.		57.6		LP00011		
	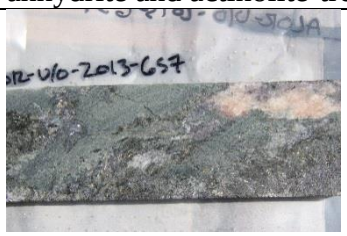	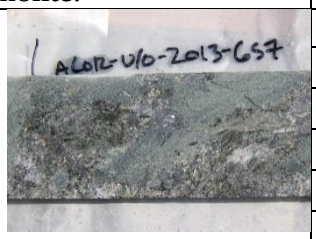	**Lithology**				
			Chlorite Schist				
			Min. Style and Lens(es)				
			Lens 21 – Type 3				
			Au	**Ag**	**Cu**	**Zn**	**Pb**
			1.41	172.8	0.24	0.15	2.7
658	Quartz-actinolite vein with strong galena mineralization. The assemblage this is contained within is a quartz-biotite assemblage. Samples Cate-437 and 438 are below and above this vein and represent variations of the assemblage.		789.9		DUB236		
	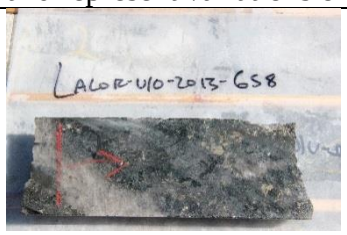		**Lithology**				
			Min. Style and Lens(es)				
			Type 3 – Above 10				
			Au	**Ag**	**Cu**	**Zn**	**Pb**
			1.47	90.86	0.13	0.08	5.58
659	Mafic intrusion with strong arsenopyrite mineralization. Matrix is Ca-amphiboles with biotite-garnet and rare plagioclase phenocrysts.		720.4		DUB174		
	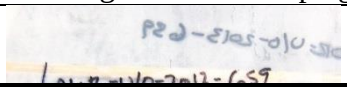	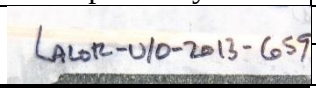	**Lithology**				

<table>
<tr><td></td><td></td><td></td><td colspan="5">Min. Style and Lens(es)</td></tr>
<tr><td></td><td></td><td></td><td colspan="5">Type X – Above 10</td></tr>
<tr><td></td><td></td><td></td><td>Au</td><td>Ag</td><td>Cu</td><td>Zn</td><td>Pb</td></tr>
<tr><td></td><td></td><td></td><td>4.83</td><td>288.3</td><td>0.40</td><td>0.04</td><td>2.44</td></tr>
<tr><td>660</td><td colspan="3">Strong calcium alteration with disseminated galena in a carbonate-diopside-actinolite/tremolite matrix.</td><td colspan="3"></td><td colspan="2"></td></tr>
<tr><td></td><td colspan="2">  </td><td colspan="5">Lithology</td></tr>
<tr><td></td><td colspan="2"></td><td colspan="5">N/A</td></tr>
<tr><td></td><td colspan="2"></td><td colspan="5">Min. Style and Lens(es)</td></tr>
<tr><td></td><td colspan="2"></td><td colspan="5">Type 3 – No lens</td></tr>
<tr><td></td><td colspan="2"></td><td>Au</td><td>Ag</td><td>Cu</td><td>Zn</td><td>Pb</td></tr>
<tr><td></td><td colspan="2"></td><td>N/A</td><td>N/A</td><td>N/A</td><td>N/A</td><td>N/A</td></tr>
<tr><td>661</td><td colspan="3">Stringer chalcopyrite and pyrrhotite with minor pyrite in a matrix of quartz-biotite-anthophyllite with minor gahnite. This sample is part of the stringer zone in lens 10.</td><td colspan="3">88.7</td><td colspan="2">LD0030</td></tr>
<tr><td></td><td colspan="2">  </td><td colspan="5">Lithology</td></tr>
<tr><td></td><td colspan="2"></td><td colspan="5">Felsic Schist</td></tr>
<tr><td></td><td colspan="2"></td><td colspan="5">Min. Style and Lens(es)</td></tr>
<tr><td></td><td colspan="2"></td><td colspan="5">Type 2 – Lens 10</td></tr>
<tr><td></td><td colspan="2"></td><td>Au</td><td>Ag</td><td>Cu</td><td>Zn</td><td>Pb</td></tr>
<tr><td></td><td colspan="2"></td><td>0.27</td><td>20.30</td><td>0.85</td><td>0.08</td><td>0.43</td></tr>
</table>